Title
Human Trophoblast Differentiation and Invasion During Normal Pregnancy and Preeclampsia

Author
Hunkapiller, Nathan Michael

Publication Date
2011

Peer reviewed|Thesis/dissertation

Human Trophoblast Differentiation and Invasion During Normal Pregnancy and Preeclampsia

by

Nathan Hunkapiller

DISSERTATION

Submitted in partial satisfaction of the requirements for the degree of

DOCTOR OF PHILOSOPHY

in

Biomedical Sciences

in the

GRADUATE DIVISION

of the

UNIVERSITY OF CALIFORNIA, SAN FRANCISCO

Acknowledgments

The success of my graduate work at UCSF is the result of an amazing network of people who have supported me throughout my time here. First, I would like to acknowledge all the members of Fisher lab who have been teachers, collaborators, and friends. Given the large size of our lab, the majority of my scientific training has come from our most experienced members; I recognize that I would never have come half as far as I have in this lab without learning techniques from and sharing ideas with Yan Zhou, Aka Prakobphol, Olga Genbacev, Kristy Red-Horse, and Miko Kapidzic. Because the leaps and bounds of scientific research tend to be few and far between, I am grateful to have worked with such personalities that lifted my spirits no matter the day. Kit Nazor, Matt Donne, and Gabe Goldfien were always in the mood to either talk science or just have a good time, whichever the situation required.

My thesis committee members, Zena Werb and Rong Wang, were very generous to offer me their time and energy. I am thankful for their insightful project guidance and willingness to speak with me whenever I needed help.

I doubt I would be a scientist if it were not for my family. There are many Hunkapillers that are thriving in science and, fortunately, I have always had them to look up to and emulate as models of how successful I wanted to be. I hope my Dad, Mike, knows how proud I am of his accomplishments and also that his career in science has had everything to do with mine. My big sister, Kathryn, was also clearly someone I wanted to take after, given that I followed her through every step of my education until now (elementary school, middle school, high school, college, and even working at Applied Biosystems after graduating college). As the only non-scientist in my immediate family, my mom, Beth, is responsible, among many other great things, for nurturing my

social development in addition to my scientific development. I am grateful for such an amazing and generous family, unwavering in their support of me.

I can't say where I would be in life without my wife, Julie. No other person is more responsible for my happiness and my desire to be successful. As she is also a graduate student as UCSF, we have bolstered each other through the daily ups and downs of research. I am thankful that I can share every aspect of my life, including work, with her.

Finally, I am thrilled to have chosen Susan Fisher as my graduate advisor (and that she let me join her lab!). Her warmth and passion for science struck me the first time I met her and has always been uplifting. As a former graduate student in the lab once said, "Susan may not have much time to meet with you, but when you need her help, everything she tells you is scientific gold." Nothing could have been more true. If I ever felt lost in my work, I need only go talk with Susan and soon I was back on track. I could not imagine a more brilliant, kind, generous, and encouraging science and life coach, and Susan knows how to have a good time, too! I am sure that we will maintain a great relationship throughout my career.

Human Trophoblast Differentiation and Invasion During Normal Pregnancy and Preeclampsia

By Nathan Hunkapiller

Graduate Advisor: Susan J. Fisher, Ph.D.

This work stems from our group's interest in identifying the mechanisms that govern placental function in normal human pregnancy and in pregnancy complications. Cytotrophoblasts (CTBs) carry out many of the placenta's most important functions. CTBs in contact with the uterus differentiate and subsequently invade the uterine stroma and blood vessels, a process that anchors the placenta to the uterus and redirects maternal blood toward the embryo/fetus. During differentiation/invasion, CTBs undergo phenotypic changes that result in vascular mimicry and display a marked arterial tropism. However, in preeclampsia (PE) CTB differentiation goes awry, and CTB invasion, particularly the arterial component, is shallow.

First, we theorized that molecules involved in arterial differentiation/function might play a role during vascular invasion. We found that expression of Notch family members, which play important roles during arterial differentiation, was extensively modulated during human CTB invasion. Inhibition reduced CTB invasion and expression of an arterial marker. Using mouse models, we confirmed that Notch activity was highest in artery-associated trophoblasts. Analysis of mouse trophoblast stem cell differentiation *in vitro* suggested that *Notch2* played an important role in remodeling the uterine arterioles in this species. Conditional deletion of *Notch2* in invasive trophoblast lineages highlighted its central importance in coordinating increases in utero-placental blood flow; trophoblast invasion of maternal arterioles failed, the blood canals that supply the placenta were smaller, and placental perfusion was decreased. Lastly, we asked whether defects in CTB expression of Notch family members were evident in PE. An

absence of endovascular TB expression of the Notch ligand, JAG1, was frequently observed, suggesting that failures in Notch signaling are an important part of the pathogenesis of this condition.

Second, we theorized that dysregulated CTB differentiation underlies preeclampsia. To test this hypothesis, we compared gene expression in differentiating CTBs derived from normal and PE placentas. Molecules known to be dysregulated in PE as well as novel candidate regulators were differentially expressed. Of these targets, we performed an expanded functional analysis on *SEMA3B*. The results helped to explain alterations in CTB and endothelial cell (EC) phenotypes that are commonly observed in PE.

Last, we designed and tested high throughput methods to profile miRNA expression. These were applied in studies we initiated to probe the molecular mechanisms involved trophoblast differentiation and to identify novel serum biomarkers associated with PE. First, we performed experiments to optimize our experimental workflow, in which we measured the quantitative sensitivity of the Taqman miRNA expression assays in a variety of experimental conditions. Next, we identified miRNAs expressed by differentiating CTBs from normal and preeclamptic pregnancies. Lastly, we found many miRNAs that were differentially expressed in serum samples from women who experienced normal pregnancies or those complicated by PE. We believe that the results of the aforementioned experiments will enable many new research directions in the study of the maternal-fetal vascular interactions that occur during normal placentation and in pathological pregnancies.

Table of Contents

Page

List of Tables and Figures

Tables **Page**

Figures **Page**

Chapter 1: Introduction

Early Embryonic Development and Uterine Attachment

Human pregnancy begins in the oviduct when a single sperm cell fertilizes an oocyte (Figure 1). For descriptive purposes, this event defines the first day postcoitus (the first 24 hours following conception). DNA fusion between these two cells and the subsequent mitotic cell division of the fertilized zygote initiates the cleavage stage of the embryo as it continually migrates down the fallopian tube toward the uterus. The first 3 cell divisions are symmetric and occur in the absence of growth at ~12-24 hour intervals. However, additional cleavages necessarily create an outside/inside polarity after the 8-cell stage. Restricted by geometry, the dividing blastomeres at this phase must undergo one of two types of division that either asymmetrically allocate cells to both the inside and outside of the embryo or that symmetrically maintain both daughter cells' positions within the inside or outside regions. Likely a result of both positional and molecular cues, the first embryonic differentiation event occurs at the 32-cell blastocyst stage when most of the descendents of the outside cells become trophectoderm, which gives rise to the fetal portion of the placenta, and the remaining inside cells become the pluripotent inner cell mass (ICM), which contributes to the embryo. The mechanisms that control whether blastomeres undergo symmetric or asymmetric division are not fully understood but may be influenced by the establishment of apical-basal cell polarity, which occurs at the 8-cell stage in the mouse (Ducibella *et al.,* 1977). For instance, the apical membranes of blastomeres at the 8-cell stage accumulate PKC, PAR6, and EZRIN, molecules involved in cell polarity (Pauken and Capco, 2000; Vinot *et al.,* 2005; Louvet *et al.,* 1996). A cell's propensity to become either trophectoderm or ICM is thought to

result from inheritance of apical and basolateral cellular contents, respectively, in the individual daughter cells that divide assymetrically. A portion of this cell fate specification program may be mediated by the CDX2 transcription factor, which becomes developmentally restricted to the trophectoderm by the blastocyst stage (Strumpf *et al.,* 2005), and the POU51F and NANOG transcription factors, which, in the mouse, are only found in the ICM (Avilion *et al.,* 2003; Niwa *et al.,* 2005). Interestingly, POU51F is expressed by human trophectoderm cells of the blastocyst stage, suggesting that there are species-specific differences in early fate specification (Genbacev *et al.,* unpublished results).

Uterine attachment, which occurs between days 6 and 7 postcoitus, is the next step that must occur in order for the pregnancy to be successful and requires the synchronized development of both the embryo and the endometrial lining to an implantation competent state. Throughout its migration toward the uterus, the embryo is surrounded by the zona pellucida, a protective lipid/glycoprotein shell that prevents premature adhesion in the fallopian tube. Once in the uterus, the embryo hatches from the zona pellucida around days 5-6 and elongates along its embryonic/abembryonic axis. Apposition, the physical joining of the blastocyst and uterine wall in close proximity, is aided by two mechanisms. Physically, closure of the uterine lumen, which occurs as a result of normal endometrial thickening that precedes conception during the luteal phase, brings the blastocyst and uterine lining side by side (Enders, 2000). Molecularly, the uterine luminal epithelium and trophectoderm simultaneously acquire adhesive properties during a short period of time that has been described as the "window of implantation" (Psychoyos, 1973). On the embryonic side, the trophectoderm upregulates adhesion receptors that mediate its interactions with the uterine wall, including members of the integrin and selectin families (Sutherland et al, 1993; Bazer *et*

al., 2010; Genbacev *et al.,* 2003) and perhaps utilizes adhesion mechanisms similar to leukocyte rolling and tethering. On the uterine side, LIF (Stewart *et al.,* 1992), HOX10 (Benson *et al.,* 1996), and HBEGF (Rabb *et al.,* 1996) are critical mediators of uterine-trophectoderm interactions that are coordinately upregulated by the uterine luminal epithelial cells during the window of receptivity. Ovarian progesterone and estrogen are fundamental upstream regulators of this process (Psychoyos, 1973). Interestingly, the described molecular events that contribute to uterine receptivity take place in the absence of fertilization. However, while an embryo can mature to the blastocyst state *ex vivo*, it cannot become implantation competent in that context. Taken together, these findings suggest that blastocyst apposition and the subsequent steps of implantation result from a combination of pre-programmed developmental steps and from blastocyst-endometrial communication.

Implantation and Placental Morphogenesis

Highlighting both the importance and the associated challenges of uterine implantation, an estimated 30-70% of human embryos fail to progress beyond this developmental stage (Cooke, 1988). Humans are dramatically less efficient than many other species in this regard. While the developmental significance is unknown, it is interesting to note that human preimplantation blastocysts adhere to uterus with their ICM oriented antimesometrially (toward the uterine wall), while mouse blastocysts orient their ICM mesometrially (Smith, 1985). Implantation in both species requires the placenta's specialized epithelial cells, trophoblasts, to acquire the ability to aggressively invade maternal tissues (Fisher *et al.,* 1989; Librach *et al.,* 1991). Much of what we understand about this process in humans (Figure 2) comes from a limited number of

studies that utilized rare human tissue samples or has been extrapolated from observations made in other species (Hertig *et al.,* 1956; Knoth and Larson, 1972; Hertig and Rock, 1945; Boyd and Hamilton, 1970).

Although it has never been observed in humans, the first step of implantation, which occurs around day 6-7, is thought to involve uterine epithelial penetration by trophoblast infiltration through the luminal intracellular junctions (Figure 2A; Enders, 2000). In other primate species, trophectoderm cells situated at the face of uterine contact fuse to form a layer of multinucleated syncytium (syncytiotrophoblasts; STBs). Events immediately following epithelial displacement have been observed in humans; between days 7 and 8, the STBs dramatically invade outward from the embryo, thickening and penetrating the uterine tissue and extracellular matrix (ECM) with cone-like projections (Figure 2B). Concomitantly, the blastocyst as a whole progressively embeds itself into the uterine wall via invasion, an interstitial-type implantation underneath the uterine lining and within the stroma. The STB layer of the newly embedded surface expands upon contact with the uterine surface, but not as dramatically as that located near the embryonic pole, which invades first and sets the orientation of the deepest placental invasion. As the syncytium expands, fluid-filled clefts, or lacunae, form behind the invasion front (Figure 2C). These vacuolar cavities continually enlarge and fuse together to form an interconnected space allocated inside the syncytium. The remaining STBs in this region now become oriented into thick columns separated by lacunar space, referred to as trabeculae, that bridges the gap between the uterus and embryo. During its continued expansion, between days 8-13, the syncytium also envelopes maternal blood vessels and glands. The STBs forms junctions with endothelial cells (ECs) in the vessels, thereby linking the maternal vessels and lacunae and incorporating the placenta into the maternal circulation.

Because STBs do not proliferate, their dramatic expansion during the initial wave of invasion is fueled by additional fusion of mononuclear cytotrophoblasts (CTBs). CTBs are the only other trophoblast population and at day 8-9 are localized in a nearly uniform epithelial layer of cells beneath STBs. In this position, these cells are in direct contact with the blastocoel cavity and ICM. This layer of CTBs forms the primary chorionic plate, the structural basis for what later becomes the floor of the placenta. At day 12, the cores of syncytial trabeculae are invaded by projections of CTBs from the primary chorionic plate, creating new structures referred to as primary villi (Figure 2D). As the CTBs move through the syncytial trabeculae, extraembryonic mesenchyme spreads at the base of the chorionic plate and soon follows through the cores of the CTB projections (Figure 2E; day 15). The result of this morphogenesis is a trilaminar structure, now termed secondary villi, with STBs on the exterior, a single layer of CTBs in the middle, and extraembryonic mesenchyme as the core. The final maturation of these structures into tertiary villi involves extensive branching throughout their length and the formation of a fetal circulation within their mesenchymal cores by vasculogenesis and angiogenesis (Figure 2F). Branches that terminate within the intervillous space are referred to as floating villi. Bathed in maternal blood, floating villi mediate nutrient and gas exchange between the maternal and fetal circulations. Those branches that terminate within the superficial endometrium are called anchoring villi and perform very unique functions as described next. The end result of placental morphogenesis is the creation of a vascular interface that juxtaposes the maternal and fetal circulations across a trophoblastic barrier.

Interstitial and Endovascular Invasion at the Maternal-Fetal Interface

The mature placenta is commonly depicted as a simple, disc-shaped structure connecting the embryo/fetus to the uterus (Figure 3A). Before birth this portion of the placenta carries out many metabolic and transport activities, but some of the placenta's most novel and interesting functions lie in a part of this organ that rarely appears in diagrams. Here, at the maternal-fetal interface (Figure 3B) CTBs of the anchoring villi are attached peripherally to the uterine wall. These cells differentiate and invade both the uterine stroma (interstitial invasion) and maternal blood vessels (endovascular invasion). Their progenitor stem cells form a polarized epithelium that is attached to the basement membrane surrounding the mesenchymal cores of chorionic villi. During invasion, CTBs leave this basement membrane to form columns of unpolarized cells that attach to and then penetrate the uterine wall. The ends of the columns terminate within the superficial endometrium, where they give rise to invasive (extravillous) CTBs.

During interstitial invasion, a subset of these cells, either individually or in small clusters, commingles with resident decidual, myometrial and immune cells. During endovascular invasion, masses of CTBs breach and plug the vessels (likened to dripping candle wax [Ramsey *et al.,* 1976]). In the first 10-12 weeks of pregnancy, CTBs remain in the luminal spaces, which significantly limits placental perfusion and keeps the placenta/fetus in a state of physiological hypoxia. CTB progenitors proliferate under hypoxic conditions; thus, vascular plugging by endovascular CTBs in the first trimester may support the expansion of the CTB progenitor population and enable rapid growth of the placenta in the 2nd and 3rd trimesters (Genbacev *et al.,* 1997). Beginning around 10-12 weeks of gestation, the CTBs of endovascular plugs disperse and subsequently replace the resident maternal endothelium and portions of the smooth muscle wall. The result is a novel chimeric vasculature composed of both maternal and fetal cells, which is maintained for the duration of pregnancy. Loss of arterial smooth muscle dramatically

increases the size of spiral arterioles at the maternal-fetal interface and, through the absence of responses to systemic signals that regulate vascular contractility, maintains steady and high rates of blood flow to the placenta (Burton *et al.,* 1999). It has been estimated that utero-placental blood flow rates increase to 500 milliliters/minute by term (Metcalfe *et al.,* 1955). Normally, the endovascular invasion process encompasses the portions of uterine arterioles that span the decidua and the inner third of the myometrium. In contrast, only the termini of uterine veins are breached (Zhou *et al.,* 1997a). Together, interstitial and endovascular CTB invasion anchor the placenta to the uterus and permit a consistent increase in the supply of maternal blood that is delivered to the growing embryo/fetus.

Cellular and Molecular Aspects of CTB Differentiation and Invasion

Some of the key molecular aspects of human CTB differentiation and invasion are known. The cells' expression of several classes of functionally relevant molecules is precisely modulated as they invade either *in situ* (the uterine wall) or *in vitro* (ECM). For example, work from our group and other investigators has produced a detailed picture of how invading CTBs modulate the expression of molecules that facilitate both interstitial and endovascular invasion. Interestingly, CTB differentiation/invasion is accompanied by unusual changes in fundamental aspects of the cells' phenotypic characteristics, which have the net effect of mimicking many aspects of arterial ECs (Damsky and Fisher, 1998). For example, they switch on the expression of vascular-type adhesion molecules (Zhou *et al.,* 1997a), vasculogenic/angiogenic factors such as the VEGF and angiopoietin family members (Zhou *et al.,* 2002; Zhou *et al.,* 2003), and Ephrin family members that play a role in arterial function and identity (Red-Horse *et al.,* 2005). Our

lab has shown that CTB modulation of Ephs/ephrins directs their migration through the uterus. Specifically, as CTBs begin to differentiate toward an invasive phenotype, they downregulate expression of *EPHB4* mRNA and upregulate expression of *EFRNB2* mRNA (Red-Horse *et al.,* 2005). Due to repulsive interactions induced by EFRNB2/EPHB4 ligation, EFRNB2-expressing CTBs are directed away from their EPHB4-expressing progenitors and toward EFRNB2-expressing arteries, where permissive interactions take place (Red-Horse *et al.,* 2005). As the aforementioned molecules all play important roles in the vascular endothelium, our group has proposed that CTBs utilize vascular mimicry to carry out many of their most important functions (Zhou *et al.,* 1997a)

With regard to adhesion molecules, the onset of CTB differentiation/invasion is characterized by reduced staining for receptors characteristic of polarized CTB epithelial stem cells—*e.g*., integrin α6β4 and E-cadherin—and the onset of expression of adhesion receptors characteristic of endothelium—*e.g.*, VE-cadherin, Ig family members VCAM-1 and PECAM-1, and integrins αVβ3 and α1β1 (Damsky *et al.,* 1992; Vicovac *et al.,* 1995; Blankenship and Enders, 1997; Zhou *et al.,* 1997a). CTBs also express L-selectin, a leukocyte cell surface receptor that promotes adhesion under shear stress (Genbacev *et al.,* 2003). Similarly, Cadherin-11 is upregulated on extravillous CTBs and on decidualizing endometrial stroma (MacCalman *et al.,* 1996; MacCalman *et al.,* 1998). Whether this interaction promotes or restrains interstitial CTB invasion is not yet clear. All CTBs in this pathway, regardless of location, stain for Mel-CAM, a melanoma-associated Ig family receptor also expressed on endothelium (Shih and Kurman, 1996). Finally, CTBs within the maternal blood vessels turn on neural cell adhesion molecule (NCAM, CD56) (Blankenship and King, 1996), an adhesion receptor that is also

expressed by maternal natural killer cells that home to the pregnant uterus (Starkey *et al.,* 1988).

Changes in the CTB adhesion molecule repertoire take place in the context of the cells' equally dramatic modulation of their proteinase and proteinase inhibitor expression. Some aspects of this phenotypic transformation are undoubtedly linked to CTB acquisition of an invasive phenotype. For example, expression and activation of matrix metalloproteinase (MMP)-9 is required for invasion *in vitro* (Librach *et al.,* 1991). We speculate that CTBs upregulate the expression of other proteinases/inhibitors to present a nonthrombogenic surface to maternal blood. The urokinase plasminogen activators uPA (Queenan *et al.,* 1987) and PAI-1 (Feinberg *et al.,* 1989), as well as the thrombin receptor (Even-Ram *et al.,* 1998), might function in this manner. Invading CTBs also upregulate the expression of immune molecules that likely enable them to escape maternal rejection. Mechanisms used for this purpose include their expression of HLA-G, a unique major histocompatibility class Ib antigen with limited polymorphism (Ellis *et al.,* 1990; Kovats *et al.,* 1990), and IL10, a potent immunosuppressive cytokine (Roth *et al.,* 1996). Altogether, the regulated expression of the aforementioned molecules provides insights into how CTBs perform many of their most remarkable functions. The significance of CTB differentiation/invasion is illustrated by the fact that this process largely fails in preeclampsia (PE).

Preeclampsia, a Placental Pathology Associated with Faulty CTB Differentiation/Invasion.

PE is a serious complication that affects ~7% of first-time pregnancies in the U.S. (Levine *et al.,* 1997; Redman and Sargent, 2005). The mother shows signs of

widespread alterations in EC function, such as high blood pressure, proteinuria, and edema (Roberts and Lain, 2002). In some cases, the fetus stops growing, resulting in intra-uterine growth restriction. Compounding the dangers of this condition is the fact that the maternal and fetal signs can appear suddenly—hence the name preeclampsia (derived from the Greek eklampsis, sudden flash or development).

The PE syndrome reveals the significance of the process whereby CTBs differentiate as they invade the uterine wall. Floating chorionic villi in PE placentas are relatively unaffected. However, anchoring villi and the invasive CTBs they spawn show distinct anomalies. The extent of interstitial invasion by CTBs is variable, but frequently shallow. Endovascular invasion is consistently rudimentary, making it extremely difficult to find any maternal vessels that contain CTBs (Brosens *et al.,* 1972; Zhou *et al.,* 1993, 1997b; reviewed in Pijnenborg *et al.,* 2006). These anatomical defects suggested to us that in PE, CTB differentiation along the invasive pathway is abnormal. Biopsies of the uterine wall of women with this syndrome showed that invasive CTBs retain expression of adhesion receptors characteristic of the progenitor population and fail to turn on receptors that promote invasion and/or assumption of an EC phenotype (Zhou *et al.,* 1997b).

Placental production of VEGF family members is also abnormal in PE. Immunolocalization on tissue sections of the placenta showed that CTB VEGF-A and VEGFR-1 staining decreased; however, staining for placental growth factor (PlGF) was unaffected. CTB secretion of sFlt-1 *in vitro* also increased (Zhou *et al.,* 2002), an observation that gains additional importance in light of the discovery that excess sFlt-1 produces a PE-like syndrome in rats (Maynard *et al.,* 2003). Together, these results suggested that PE might involve specific failures in vascular mimicry, which makes the study of molecules involved in arterial development particularly relevant.

Notch Signaling, Vascular Development, and Disease-Associated Defects.

First described in mutant Drosophila fruit flies with incompletely formed, "notched" wings, the Notch signaling pathway governs differentiation and function during cell-cell contact in a wide variety of tissues and organs (reviewed in Miele, 2006; Bianchi *et al.,* 2006) with especially interesting functions in the vasculature (Shawber and Kitajewski, 2004). Consistent with the central importance of this signaling system, the Notch family shows striking genetic conservation, with orthologs appearing in all metazoan species studied thus far (Lai, 2004). Interestingly, Notch molecules can maintain an undifferentiated cell state as well as specify differentiation toward committed cell types, referred to as "inhibitory" and "inductive" signaling, respectively. These contextually dependent, seemingly opposing functions of Notch family members are consistent with the fact that they are ancient molecules that have evolved the ability to modulate expression of varying combinations of transcriptional activators and repressors.

Mechanistically, the Notch receptors are distinct from other signaling molecules in that they operate both on the cell surface to receive activating signals and within the nucleus as transcriptional modulators (Figure 4; Alva and Iruela-Arispe, 2004). The core pathway comprises a conserved family of four transmembrane receptors (NOTCH1-4) and five ligands (DLL1, -3, -4, JAG1 and -2). It is interesting to note the unique aspects of this signaling system in terms of the proteolytic steps and other posttranslational modifications (reviewed in Bianchi *et al.,* 2006; Miele, 2006). Specifically, Notch receptors, which are synthesized as precursors, are cleaved by a furin-like convertase in the trans-Golgi compartment. The extracellular (NEC) and transmembrane (NTM)

portions, which are linked noncovalently, are transported to the plasma membrane as heterodimers. Binding of a receptor on one cell to a ligand on another is mediated by epidermal growth factor repeats in the NEC (Rebay *et al.,* 1991). Receptor-ligand interactions trigger metalloproteinase ADAM (a disintegrin and metalloproteinase) -10 or -17 cleavage of the NEC and gamma secretase-mediated generation of the Notch intracellular domain (NICD) from the NTM (Schroeter *et al.,* 1998). Subsequently, cleaved NICD translocates to the nucleus, where it binds to CBF1/Su(H)/LAG1 family transcription factors (Lai, 2004). In general, Notch binding converts a CBF1/Su(H)/LAG1 family member from a transcriptional repressor to a transcriptional activator, inducing multiple downstream targets such as the basic helix-loop-helix factors *Hes* and *Hey* (Weinmaster, 1998). Notch signaling can be regulated at several points along this pathway. For example, the affinity of receptor–ligand interactions is modulated by Fringe proteins, β1,3 N-acetylglucosaminyltransferases that modify O-linked fucose moieties on the NEC (Shao and Haltiwanger, 2003), and phosphorylation of the NICD by GSKβ (Foltz *et al.,* 2002) or CDK8 (Fryer *et al.,* 2004) regulates its half-life; E3 ligases ubiquinate Notch, triggering degradation (Oberg *et al.,* 2001). Outside the core pathway, other modes of Notch signaling have been identified but are poorly understood (Hu *et al.,* 2003; Langdon *et al.,* 2006).

As to functions, mice with targeted deletions of Notch family genes exhibit a variety of vascular defects. *Notch1* is the most extreme case. The null mice die between embryonic days (E) 9.5 and 11.5 due to a profound failure in angiogenic vascular remodeling of both embryonic and extraembryonic tissues. The mice form a primary vascular plexus, indicating that *Notch1* is not required for vasculogenesis; however, they are unable to remodel this plexus into an organized network of larger and smaller vessels (Krebs *et al.,* 2000). Mice with hypomorphic alleles of *Notch2* exhibit

milder vascular defects than those lacking *Notch1*, although embryonic lethality is still observed by E11.5. These animals have vascular anomalies such as widespread hemorrhages, edema, myocardial hypoplasia, and malformation of the hyaloid vasculature of the eye (Hamada *et al.,* 1999; McCright *et al.,* 2001). *Notch3*-null animals are viable and fertile (Krebs *et al.,* 2003), although arteries fail to form properly due to errors in vascular smooth muscle differentiation and maturation (Domenga *et al.,* 2004). Mice lacking the *Notch4* gene develop normally with no obvious vascular defects during embryogenesis. However, in ~50% of cases, *Notch1/Notch4* double mutants show more severe vascular defects than mice lacking only *Notch1*, suggesting that *Notch1* and *Notch4* have partially redundant functions (Krebs *et al.,* 2000). In support of this theory, mice with an activated allele of *Notch4* (INT3) die in utero by E10 and display severe vascular anomalies reminiscent of those seen in *Notch1*-null mice (Uyttendaele *et al.,* 2001). Similarly, targeted EC expression of INT3 produces reversible arteriovenous defects in adult mice (Carlson *et al.,* 2005). Loss of several Notch ligands also produces significant failures in vessel form and function. *Dll1* homozygous mutant embryos die by E12 with widespread hemorrhaging (Hrabe de Angelis *et al.,*1997). *Jag1* deletion also results in lethality from E11.5 to E12.5 due to hemorrhage, with failures in angiogenic remodeling clearly evident (Xue *et al.,* 1999). In support of its role as the primary EC Notch ligand, removal of *Dll4* results in haploinsufficiency. Vascular defects in *Dll4* mutants include arteriovenous malformations, a lack of vascular remodeling, and collapse or incomplete formation of the major vessels (Krebs *et al.,* 2004; Duarte *et al.,* 2004).

A role for Notch family members has also been described in differentiation of the arterial and venous portions of the circulation. As early as E9.5 to E11.5 of murine development, when the primary vascular plexus begins to remodel into a hierarchical

network of arteries and veins, *Notch1*, *Notch4*, and *Dll4* are expressed within and around the developing vasculature (Alva and Iruela-Arispe, 2004). However, by E13.5, expression of these molecules is largely confined to the arterial endothelium (Villa *et al.,* 2001). Concurrently, *Efrnb2* and *Ephb4* emerge as markers of arterial and venous identity, respectively (Wang *et al.,* 1998). In zebra fish, loss of Notch signaling reduced EC expression of the arterial marker *efrnb2*, with simultaneous enhancement of the venous marker *ephb4*—evidence that Notch functions upstream of both molecules in specifying vessel identity (Zhong *et al.,* 2001; Lawson *et al.,* 2001). Growing evidence suggests that this hierarchy also exists in mammals (Shawber *et al.,* 2003; Carlson *et al.,* 2005; Iso *et al.,* 2006). These findings indicate that Notch signaling regulates the differentiation of the arterial vasculature from more primitive, undefined networks. Thus, it appears that from their genesis, arterial and venous ECs have different molecular characteristics and that cross talk between the two segments is crucial for vascular patterning.

In addition to their role in vascular biology, Notch family members have been implicated in the pathogenesis of a wide variety of cancers, although the mechanisms of transformation often differ. In most cases, including mammary (reviewed Yin *et al.,* 2009 and originally described in Gallahan and R. Callahan *et al.,* 1987), pancreatic (Mullendor *et al.*, 2009), prostate (Wang *et al.,* 2010), and lymphoid (Weng *et al.,* 2004) cancers, Notch activation drives malignant progression. Less often, *e.g.*, in skin (Liu *et al.,* 2006) and liver (Wang *et al.,* 2009; Qi *et al.,* 2003) cancer, Notch can act as a tumor suppressor, with both oncogenic and tumor suppressor activity in lung cancer (Chen *et al.,* 2007; Zheng *et al.*, 2007). Over 50% of T-cell acute lymphoblastic leukemias have activating mutations in *NOTCH1* (Weng *et al.,* 2004). Interestingly, Notch can either suppress or enhance the activity of p53, a well-established tumor suppressor, in a

context dependent manner (Dotto, 2009). In melanomas, Notch enhances cell survival and proliferation through the MAPK and AKT signaling pathways while simultaneously enhancing tumor cell adhesion through upregulation of N-cadherin (Liu *et al.,* 2006). Downregulation of Notch in pancreatic cancer can serve to block tumor invasion by downregulating VEGF, NF-κB, and MMP-9 (Wang *et al.,* 2006).

Mouse Placentation

As compared to the human placenta, the mature mouse placenta arises from developmental mechanisms that are both highly similar and uniquely divergent. For instance, rather than penetrating the uterine epithelium with an intrusive-type invasion, the mouse trophectoderm initiates the first steps of invasion by inducing epithelial degeneration and subsequent displacement (Schlafke and Enders, 1975). Furthermore, penetration of the epithelial basement membrane in the human occurs by trophectoderm-mediated degradation, but in the mouse this occurs by the actions of maternal decidual cells (Benirschke *et al.,* 1995). Implantation in this species begins at E4.5 and, like the human, is classified as interstitial. Differing from the primary syncytial invasion observed following implantation in humans, syncytial differentiation in the mouse takes place well after implantation and plays no part in the invasion process. Rather, murine trophectoderm invasion is initiated by a primary wave of mononuclear polyploid trophoblast giant cells (TGCs), which differentiate from the surface of the trophectoderm. TGCs mediate the implantation/invasion process and line the outermost surface of the placenta throughout pregnancy. The mechanism of TGC invasion through the uterus involves uterine epithelial phagocytosis, remodeling of the ECM, and cell migration (Cross *et al.,* 1994). Because TGCs exit the cell cycle upon terminal

differentiation, further expansion of the placenta's surface area is supported by secondary TGC differentiation from the ectoplacental cone (EPC), a trophoblastic region that forms underneath the outermost TGC layer at the embryonic pole around E5.5. By E7.5-E8.5, the outer regions of the EPC that are associated with the TGC layer can be distinguished by mRNA expression of Trophoblast Specific Protein (*Tpbpa*) while those remaining at the core lack *Tpbpa* expression. This early marker distinguishes those cells that will contribute to the invasive trophoblast lineages from those that form the labyrinthian portion of the placenta, which are discussed next.

By midgestation, the mouse placenta is composed of 3 layers: the labyrinth, the junctional zone, and the decidua (Figure 5A). The labyrinth fills the innermost region where gas and nutrient exchange takes place. Here, the maternal and fetal circulations spread into interlaced sinusoidal networks and are separated by a thin trichorial structure, which is composed of one layer of sinusoidsal TGCs (S-TGCs) in contact with maternal blood and 2 underlying layers of STBs lined by fetal endothelium. Labyrinthian development results from a complex interaction between cells of the ectoplacental cone, chorion, and allantois (Simmons *et al.,* 2008). This process begins around E8.0 when the EPC and chorion fuse. S-TGCs are thought to arise from the innermost EPC layer but may also derive from the chorion. Both syncytium layers, on the other hand, are generated from the chorion. The presence of markers that delineate these cell types in the EPC and chorion just prior to EPC-chorion fusion support this hypothesis. Specifically, *Hand1* is expressed by cells of the EPC but not chorion and later, at E12.5, marks mature S-TGCs along with *Ctsq*. Reciprocally, chorion but not EPC cells express *Gcm1, Cebpa*, and *Synb*, which later serve as markers of mature STBs. At E8.5 the chorion fuses with the allantois from which the fetal vasculature begins to infiltrate the chorion. Protrusion of the allantoic mesoderm into the chorion initiates villous

morphogenesis and subsequent branching produces dense fetal vascular sinusoids. At the same time, the invasive trophoblast lineages in the junctional zone and decidual layers recruit a maternal blood supply to this region.

The junctional zone layer lies at the border between the largely maternal decidua and the fetal labyrinth. The cells that populate this region are primarily comprised of the descendents of outermost EPC cells that expressed *Tpbpa*. The spongiotrophoblast makes up the majority of this layer and is a significant source of endocrine production. Parietal TGCs (P-TGCs) in a near continuous layer line the surface of the junctional zone and maintain the maternal-fetal interface during the first half of pregnancy. The EPC gives rise to at least four types of TGCs that have been identified by their unique localization, developmental origins, and lineage specific markers (Simmons *et al.,* 2007). Specifically, P-TGCs express *Plf, Pl1, Pl2* in the absence *Ctsq*. S-TGCs express *Pl2* and *Ctsq* but not *Pl1* or *Plf*. Canal-associated TGCs (C-TGCs) express *Plf, Pl2*, and *Ctsq* but not *Pl1*. Lastly, spiral artery-associated TGCs (SpA-TGCs) can be identified by their expression of *Plf* in the absence of the other markers. Prior to E12.5 few fetal cells are observed in the placenta's outer layer, the decidua. However, around this time some SpA-TGCs and glycogen trophoblast cells (GlyTCs; *Pcdh12*-positive), both of which are derived from the EPC, begin to invade the decidual stroma and spiral arterioles. The role of the GlyTCs is not well understood, but the SpA-TGCs carry out many of the same functions that endovascular CTBs perform in the human placenta. SpA-TGCs invade and remodel maternal arterioles in the mouse decidua and account for a portion of their physiological change during pregnancy through degradation of the elastic smooth muscle that encircles these vessels. This vascular degradation is facilitated by the cells' expression of placenta-specific cathepsins, *Cts7* and in particular *Cts8*, (Screen *et al.,* 2008). Despite significant changes in the structure of maternal spiral arterioles along

their entire course through the decidua, TGC endovascular invasion progresses only ~150-300 microns beyond the junctional zone (Adamson *et al.,* 2002), suggesting the involvement of other factors in this process.

The vascular structure of the mouse placenta varies considerably from that of the human (Figure 5B). Because pregnant female mice often have multiple gestates in each uterine horn, the uterine blood supply is organized serially, in which the radial arteries that supply each placental unit branch off the main uterine artery. An important implication of this anatomical organization is that each placenta's vascular physiology is influenced by its position in the uterine horn and hemodynamic effects from other placentas. Upon entering each placenta, the radial arteries further branch into 8-12 interconnected spiral arteries that pass through the spongiotrophoblast layer and reconverge into 1-4 trophoblast-lined canals. Rather than emptying into an intervillous space as in the human placenta, maternal blood enters the placenta through trophoblast-lined canals that traverse the labyrinth and open into sinusoidal networks near the base of the placenta at the chorionic plate. The sinusoids are drained by veins at the maternal side of the placenta. The fetal sinusoidal circulation runs countercurrent to the direction of maternal blood flow, which maximizes the rate of fetal-maternal gas exchange. As respiratory exchange is one of the placenta's most important functions, proper control of placental vascular morphogenesis is a prerequisite to successful pregnancy. The molecular drivers of this process and their functions in normal pregnancy and in pregnancy complications are the focus of this dissertation.

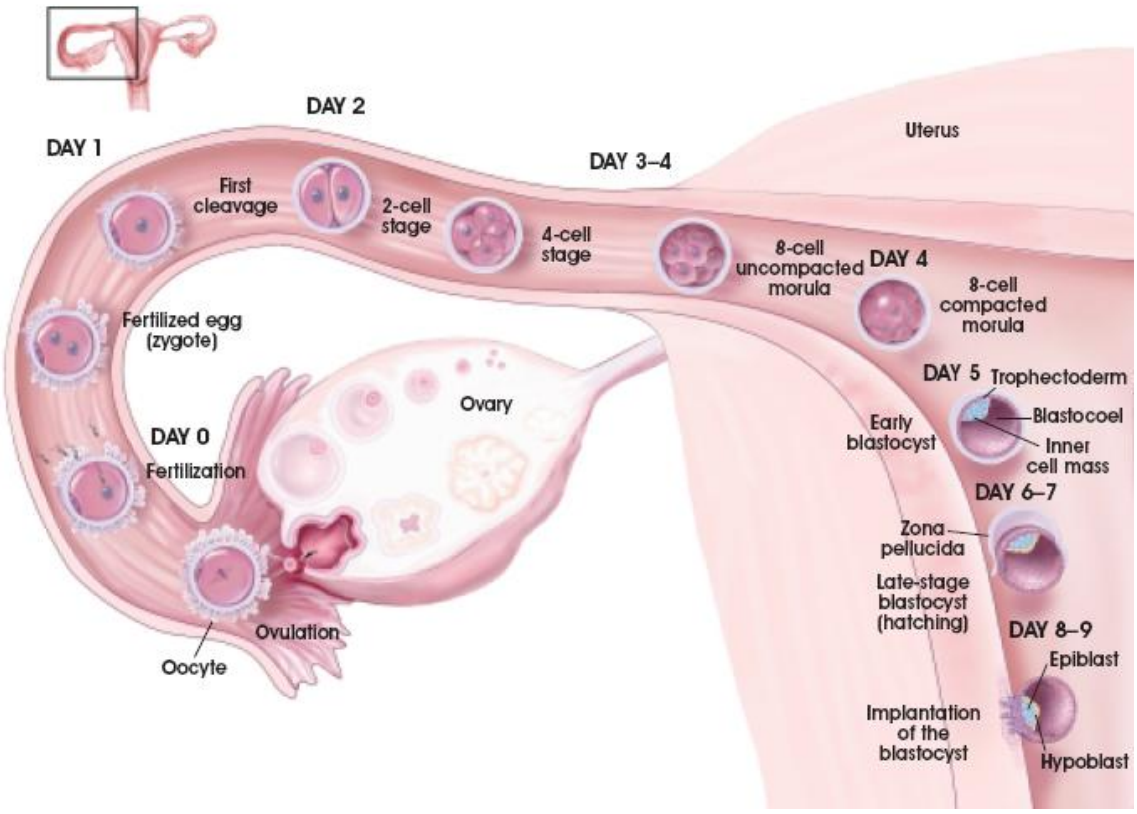

Figure 1. (Adapted from Winslow, 2009) *Preimplantion Development of the Human Blastocyst.*

The oocyte is ovulated into the fallopian tubule by the ovary and successful fertilization occurs at day zero when the oocyte is penetrated by a single sperm cell. As the fertilized zygote travels down the fallopian tubule, it undergoes several rounds of cell division during the cleavage stage with the first 3 divisions taking place every 12-24 hours. At the 8-cell stage, the individual blastomeres of the embryo develop tight junctions with each other to form a compacted morula. The first differentiation event occurs during subsequent cell divisions as the zygote matures into a blastocyst with an outer layer of trophectoderm surrounding both the fluid-filled blastocoel cavity and the pluripotent inner cell mass. Between days 6 and 7, the blastocyst hatches from the zona pellucida, a thick glycoprotein shell that prevents premature adhesion to the uterine wall. Apposition of the trophectoderm layer of the blastocyst to the uterine wall initiates the implantation process during the window of receptivity.

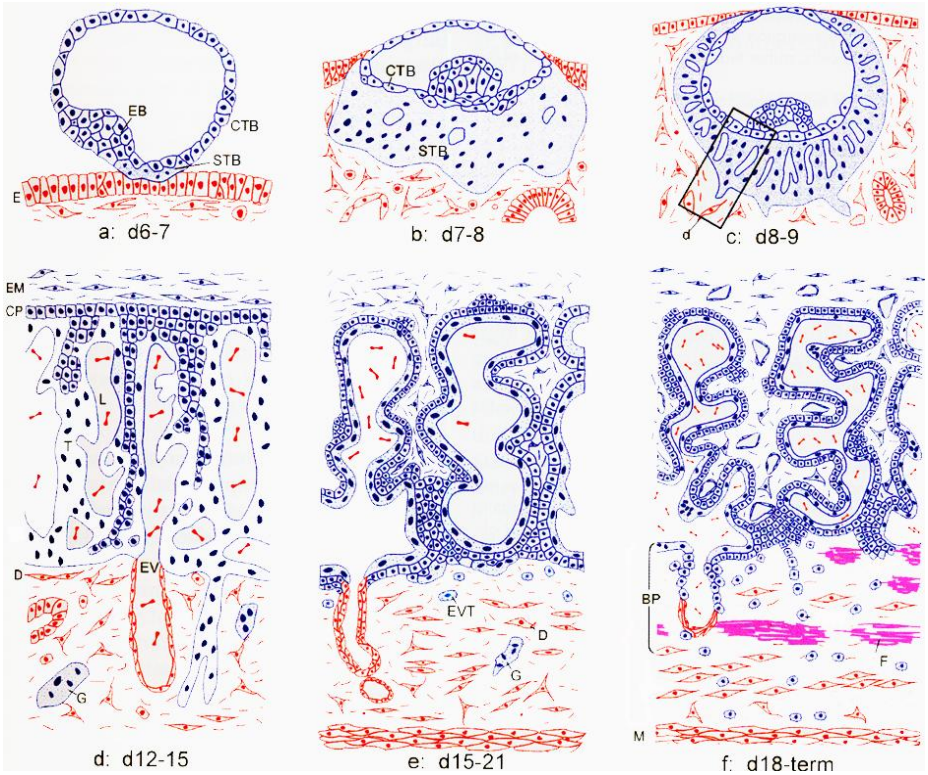

Figure 2. (Adapted from Benirschke *et al.,* 1995) *Stages of Implantation and Early Placental Morphogenesis.*

(A) The first phase of implantation takes place between days 6-7 post coitus, when the trophectoderm layer of the blastocyst initiates adhesive interactions with the uterine wall. Trophoblast cells in contact with the uterine luminal epithelium fuse and differentiate into syncytiotrophoblasts (STBs), which infiltrate the uterine epithelium (E). (B) Between days 7-8, the STBs expand and invade through the decidua (D), drawing the blastocyst deeper into the uterine wall. Cytotrophoblast (CTB) cells line the innermost layer of STBs and fuel their expansion through proliferation and fusion. (C) The lacunar phase of implantation occurs between days 8-9 when fluid-filled lacunae (L) form inside the STB mass. The embryo becomes almost completely embedded in the uterine wall at this phase as the luminal epithelium begins to close over the implantation site. (D) In the trabecular phase (days 12-15), the lacunae merge together as the STBs orient into long columns (Trabeculae; T) that extend between the chorionic plate (CP) and decidua. Endometrial blood vessels (EV) are degraded as they become enveloped by the STBs, which causes maternal blood to flow into the lacunar spaces. Extraembryonic mesoderm (EM) spreads over the floor of the chorionic plate and CTBs from this region begin to invade through the cores of the trabeculae, which are now referred to as primary villi. (E) Secondary villi generation occurs between days 15-21 as EM moves into the villi underneath the CTB layer. Concomitantly, CTBs pass through the STB layer and reach the uterine wall, where they differentiate and invade the decidua and EVs. (F) Chorionic villi mature into tertiary villi after day 18 as they continue to branch into tree-like structures, increase their surface area, and become populated by fetal vessels. EB, Embryoblast; G, Gland; BP, Basal Plate; M, Myometrium; F, Fibrinoid.

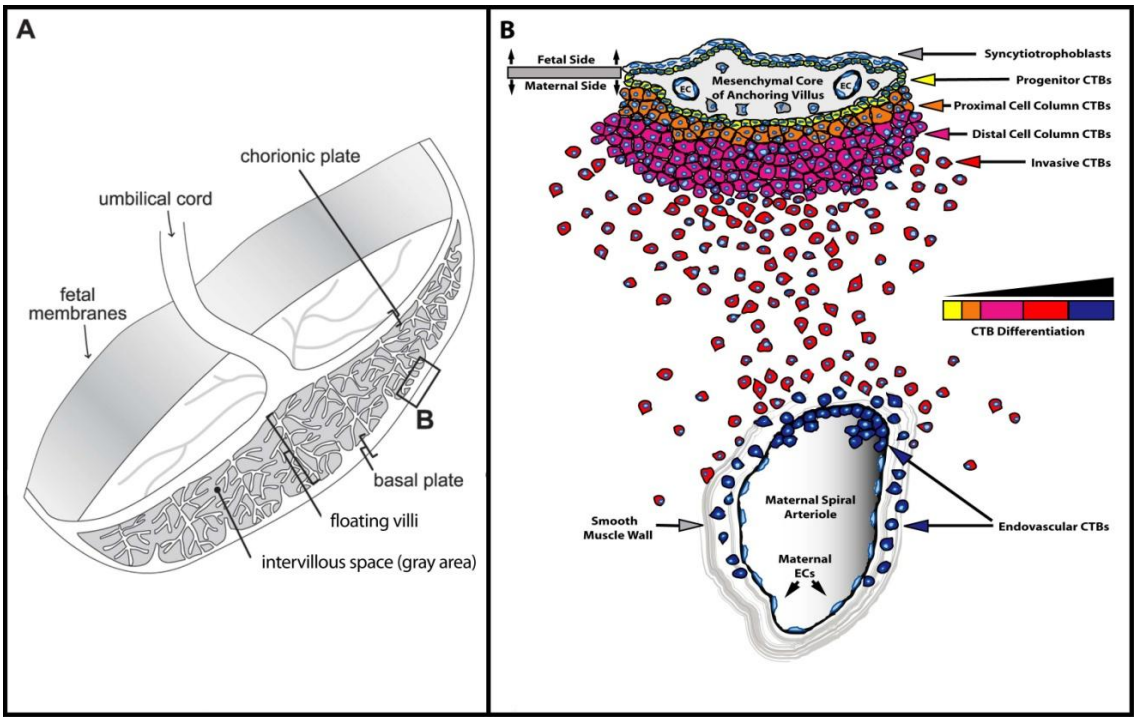

Figure 3. (Hunkapiller and Fisher, 2008) *Placental Structure and Representation of CTB Differentiation/Invasion in the Basal Plate.*

(A) The mature placenta is a disc shaped organ that connects the fetus to the maternal uterine wall. Chorionic villi stem from the chorionic plate and lie within the intervillous space, where they are bathed in maternal blood. The fetal circulation enters the placenta through the umbilical cord and circulates through capillaries in the placental chorionic villi. Villi that terminate within the intervillous space are referred to as floating villi while those that terminate within the superficial endometrium are called anchoring villi. The point of attachment between anchoring villi and the underlying maternal tissue is referred to as the basal plate (box B). (B) Enlargement of the area in box B. CTBs of anchoring chorionic villi differentiate as they invade the maternal uterus. Undifferentiated CTB progenitors (yellow) surround the mesenchymal cores of anchoring villi (av). These progenitors differentiate as they move into the proximal and distal regions of the cell columns (cc; orange and purple). Invasive CTBs (red) leave the columns and migrate through the uterine interstitium. Endovascular CTBs (blue) go on to disrupt the smooth muscle layer of maternal blood vessels (bv) where they also replace the ECs.

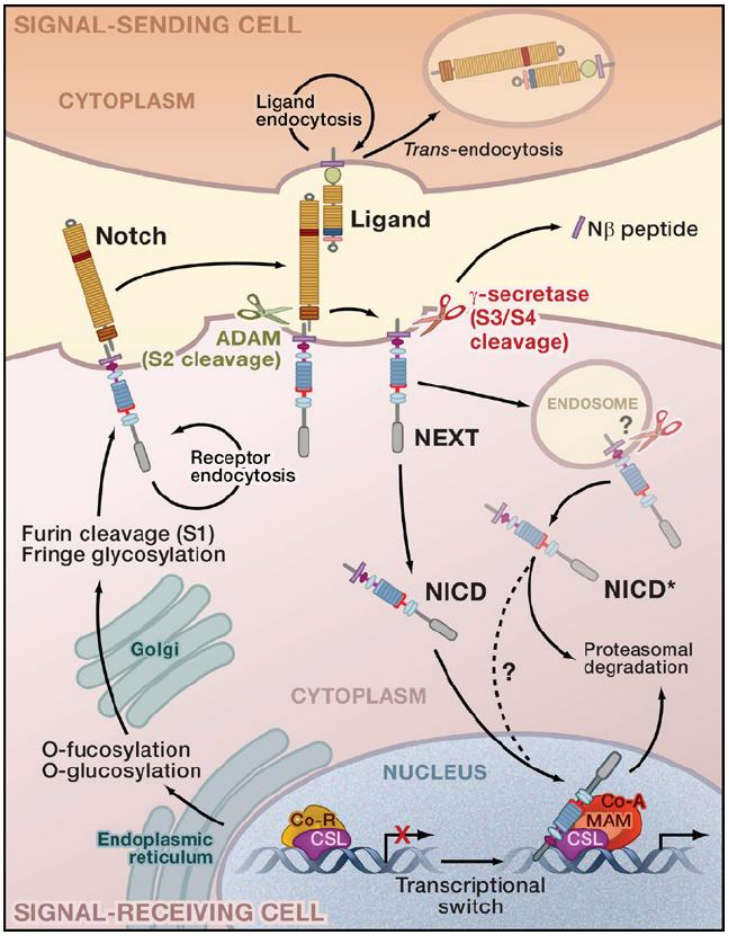

Figure 4. (Adapted from Kopan and Ilagan, 2009) *The Notch Signaling Pathway.*

The core pathway comprises a conserved family of four transmembrane receptors (NOTCH1-4) and five ligands (DLL1, -3, -4, JAG1 and -2). Notch receptors, which are synthesized as precursors in the endoplasmic reticulum, are cleaved by a furin-like convertase in the trans-Golgi compartment (S1 cleavage). The extracellular (NEC) and transmembrane (NTM) portions, which are linked noncovalently, are transported to the plasma membrane as heterodimers. Receptor endocytosis and trafficking regulate both ligand and receptor concentration in the plasma membrane. Binding of a receptor on one cell to a ligand on another cell is mediated by epidermal growth factor repeats in the NEC. Receptor-ligand interactions trigger ligand endocytosis in the signal-sending cell and ADAM (a disintegrin and metalloproteinase) cleavage (S2) of the NEC in the signal-receiving cell, which produces the Notch extracellular truncation (NEXT) fragment. Gamma secretase-mediated activity produces the Notch intracellular domain (NICD) from the NEXT fragment and releases the Nβ peptide, the result of two processive intramembrane proteolysis events (S3/S4). Subsequently, the NICD translocates to the nucleus, where it binds to CBF1/Su(H)/LAG1 (CSL) family DNA binding factors. In the absence of the NICD, CSL molecules may bind to transcriptional Co-repressors (Co-R). However, NICD binding induces CSL molecules to exchange Co-R for Co-activators (Co-A), which recruit Mastermind (MAM) and induce downstream expression of Notch targets.

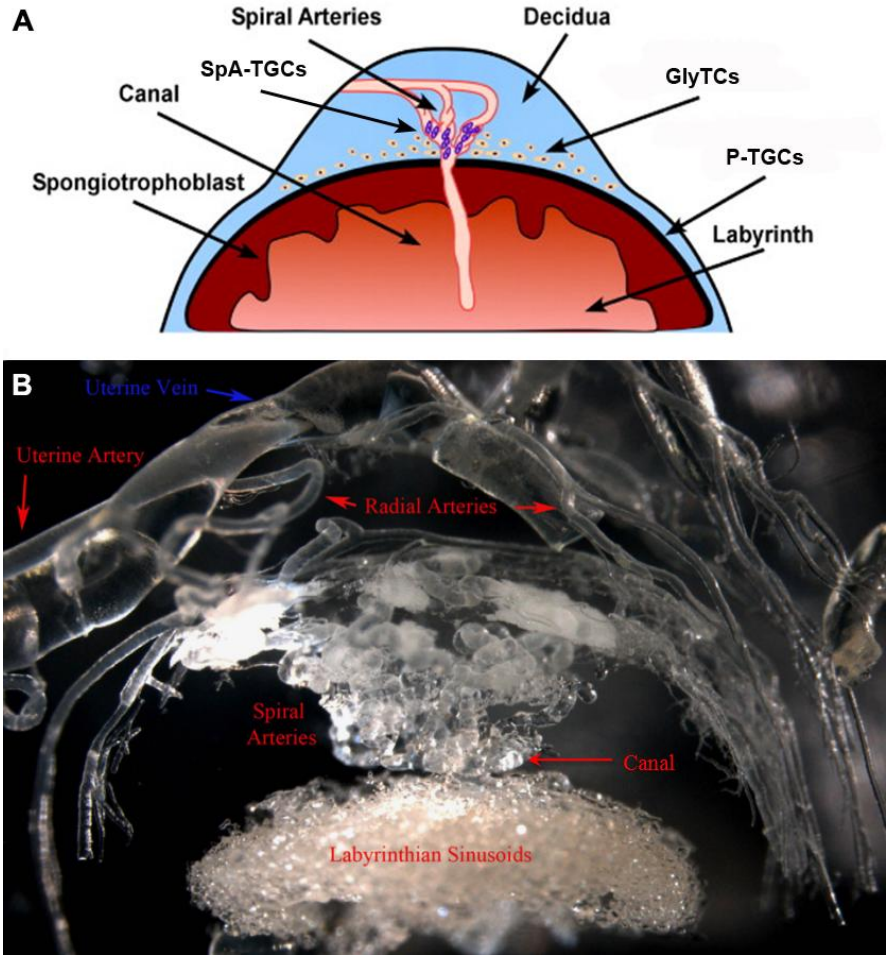

Figure 5. *Anatomy of the Mouse Placenta and its Arterial Vasculature.*

(A) (Adapted from Simmons *et al.,* 2008) Cartoon of the mouse placenta at embryonic day 14.5. The mouse placenta is organized into 3 layers. The labyrinth (pink) lies at the base of the placenta and is where maternal -fetal exchange takes place. The junctional zone is the middle layer, which is made up of the spongiotrophoblast (red) and a near continuous layer of parietal trophoblast giant cells (P-TGCs; black) that encircle the fetal portion of the placenta. The decidua (blue) is the outermost layer and is mainly composed of maternal decidual cells, although fetal glycogen trophoblast cells (GlyTCs) and a small population of spiral artery-associated trophoblast giant cells (SpA-TGCs) also invades this region. (B) Vascular corrosion cast of the maternal arterial network in mouse placenta at embryonic day 14.5. Maternal blood reaches the placenta through radial arteries that stem from the uterine artery. Upon entering each placenta, the radial arteries further branch into ~8-12 interconnected spiral arteries that pass through the decidua and reconverge into ~1-4 trophoblast-lined canals at the junctional zone. These trophoblast-lined canals empty into sinusoidal networks at the base of the labyrinth. After maternal blood percolates upward through the sinusoids it is drained by veins at the maternal side of the placenta. These veins have been dissected away to highlight only the arterial circulation.

Chapter 2: Review of Methods Useful in the Study of Cytotrophoblast Endovascular Invasion

Hunkapiller, N.M., and Fisher, S.J. (2008). Chapter 12. Placental remodeling of the uterine vasculature. *Methods Enzymol* 445, 281-302.

Introduction

In the past, investigations of human CTB endovascular invasion have been limited to immunohistochemical examination of tissue sections. In this chapter, we will discuss the use of *in vitro* and *in vivo* techniques that have been adapted for the study of the complex events that occur during CTB endovascular invasion. As background, aspects of placental morphology and CTB differentiation/invasion were discussed in Chapter 1 and are not repeated in this introduction as originally published. Here, we present techniques used in the isolation and culture of primary CTBs and chorionic villous explants. Approaches for identifying trophoblast-modified blood vessels in placental tissue sections are also described. Next, we review methods used by other groups to study CTB/endothelial interactions in culture focusing on techniques that employ isolated cells and chorionic explants. Finally, we conclude with methods devised by our group and others to explore the complex heterotypic cell-cell interactions that occur as CTBs invade blood vessels *in vivo* in the nude mouse.

Isolation and Culture of Human Cytotrophoblasts

To study the cells' behavior in culture, we isolate CTBs from whole placental tissue collected after elective pregnancy termination or at term. CTBs reside within the villous tissue of the placenta (Figure 6A-B), which is also comprised of STBs, red blood cells, fibroblasts, endothelial cells, leukocytes, and other mesenchymal progeny. The major steps in the cell isolation procedure include removal the outer layer of syncytium, release of the underlying CTBs by sequential enzymatic digestions, and purification of the cells by Percoll density gradient centrifugation. Any remaining leukocytes are removed by virtue of their interactions with CD45-coated beads, which are then separated with a magnetic device. Using these methods for CTB isolation, we typically achieve greater than 95% purity. The viability and purity of the cells are subject to a number of factors including tissue quality, gestational age, and tissue handling during the procedure. Our methods have never been published in detail, and as such, we will describe the procedure that we have evolved over the past 20 years.

Cytotrophoblast Isolation Procedure

1. Working with human tissue requires approval by an institutional human subjects review board.
2. Obtain the placental tissue as soon as possible after elective termination/delivery and place immediately in cytowash medium (see table 1). If the tissue is exposed to water, the CTBs initiate apoptosis.
3. Keep the tissue on ice prior to dissection.
4. Perform all work in a biosafety hood using techniques appropriate for working with potentially biohazardous tissues.

5. Place the tissue in a petri dish and add fresh cytowash. Frequent exchange of the wash medium helps remove contaminating pathogens and maternal blood.
6. Remove fibrinoid, blood clots, amnion and basement membrane from the placental villi using vannas scissors and forceps. Dissect villi into approximately 2-4 mm pieces.
7. Filter the tissue through a mesh strainer (1 mm gaps) to remove small pieces of villi that would otherwise undergo digestion too quickly, which results in DNA breakdown, a process that entraps the cells in a viscous gel.
8. Wash the remaining tissue with 1 liter or more of cytowash to remove any remaining maternal blood.
9. Pour the dissected tissue into a 50 ml conical tube and fill with cytowash. Centrifuge the tube at 1300 rpm for 5 minutes at 4°C. This centrifugation speed corresponds to 365 rcf in a Sorvall Legend RT centrifuge.
10. Aspirate the supernatant and weigh the tissue pellet within the tube.
11. Prewarm the first enzyme dissociation solution by adding a volume of collagenase (see table 1) that is equal to six times the weight of the tissue to a sterile flask and place in a 37°C water bath shaker for approximately 10 minutes or until the desired temperature is reached.
12. Add the tissue to the warmed collagenase solution and shake in the water bath at 175 rpm for approximately 7 minutes. The amount of time necessary for digestion will depend heavily on the gestational age and health of the tissue. This step removes the syncytiotrophoblast layer (Figure 7A).
13. Transport the flask from the water bath to the biosafety hood and place it on ice at an angle to allow the tissue to settle at the bottom.
14. Aspirate and discard the supernatant.

15. During step 11, pre-warm the trypsin solution (see table 1) to 37°C.
16. Add a volume of trypsin solution equal to six times the weight of the tissue, return flask to the water bath, and shake at 175 rpm for approximately 10 minutes at 37°C. The exact length of this incubation will again depend greatly on tissue health and gestational age. This step releases the CTBs from the villous tissue (Figure 7B.).
17. Transport the flask from the water bath to the biosafety hood and place on ice at an angle that allows the tissue to settle at the bottom. Immediately after the remaining tissue settles, collect the supernatant and add an equal volume of cytowash.
18. Place 2 layers of sterile gauze over the mouth of a 50 ml conical tube that contains 5 ml of fetal bovine serum (Hyclone, SH30071.03). To halt enzymatic digestion, transfer 45 ml through the gauze. Note: this step will require multiple 50 ml tubes, with the exact number depending on the volume of dissociation buffer used.
19. Centrifuge the tubes at 1,300 rpm for 8 minutes at 4°C
20. Meanwhile, prepare the Percoll gradient (see table 1) that will be used later. Slowly layer 6 ml of each concentration in a 50 ml conical tube in the following order: 70%, 60%, 50%, 40%, 30% and 20%. Store at 4°C. Make one tube for each 7 grams of starting tissue.
21. Aspirate and discard the supernatant. Re-suspend and combine the cell pellets in one 50 ml conical tube with 50 ml of cytowash. Centrifuge again at 1,300 rpm for 8 minutes at 4°C.
22. Aspirate and discard the supernatant. Then, re-suspend the cell pellet in pre-warmed collagenase solution using 1 ml per gram of starting tissue.
23. Place the cell suspension in a sterile flask and transfer to the water bath. Shake the flask at 150 rpm for 3 minutes at 37°C. This second collagenase digestion dissociates clumps of CTBs into single cells (Figure 7C).

24. Add cytowash to the collagenase solution up to 50 ml. Pass the cell suspension through a 100 micron cell strainer into a 50 ml conical tube. Centrifuge at 1,300 rpm for 8 minutes at 4°C.
25. Aspirate and discard the supernatant. For every 7 grams of starting tissue, re-suspend the cell pellet in 4ml serum-free medium (see table 1). Very slowly add 4 ml of the cell suspension to the top of the Percoll gradient. Note: multiple Percoll tubes are usually required.
26. Centrifuge the tubes at 2,700 rpm for 25 minutes at 4°C. This centrifugation speed corresponds to 1573 rcf in a Sorvall Legend RT centrifuge. This step separates cells according to their individual densities.
27. Aspirate the top two bands of the Percoll gradient. Collect the CTB-containing layers between 20-28 ml. Combine the 8 ml harvested from each tube into a fresh 50 ml conical tube and fill with cytowash. Centrifuge at 1300 rpm for 8 minutes. The resulting semi-purified preparation will contain CTBs along with other cells of similar size (Figure 7D).
28. Aspirate and discard the supernatant, re-suspend the pellet in 50 ml cytowash, and centrifuge at 1300 rpm for 8 minutes at 4°C.
29. Aspirate and discard the supernatant, re-suspend the pellet in 10 ml serum-free medium.
30. Count cells using a hemocytometer.
31. Add cytowash to a final volume of 50 ml and centrifuge at 1300 rpm for 8 minutes at 4°C.
32. Aspirate the supernatant and re-suspend the pellet in serum-free medium at a concentration of 10^6 cells per ml. Ideally, the cells are approximately 80-90% pure at this stage. Greater than 95% purity can be achieved by negative selection using CD-

45 coated Miltenyi beads (Miltenyi Biotec, according to the manufacturer's directions).

33. Prior to plating cells, coat tissue culture wells with a 1:1 mixture of Matrigel (BD Biosciences, 354234) and serum-free medium. For each well of a six-well plate, use 50 microliters of the Matrigel:serum-free medium mixture. Allow the Matrigel to polymerize for 15 minutes at 37°C. Note: We use Matrigel lots prescreened for their ability to support CTB adhesion.
34. Plate 3-4 million cells per well.

Enzymatic Digestions, Time Considerations

First Collagenase Digestion: The gestational age and health of the tissue greatly affects the required digestion time period. For example, first trimester tissue between 6 and 10 weeks of gestation usually requires about 6-8 minutes of digestion, tissue aged 13 weeks needs about 12 minutes, and villi from a 20 week placenta need 18 minutes or more. A good rule of thumb is to digest one minute for every week in age. With regard to the health of the tissue, fibrinoid deposits and/or clotted blood will add to the digestion time. Collagenase digestion can be monitored in real-time by placing a drop of the reaction under a phase contrast microscope and checking whether the syncytium has lifted from the surface of the villi (Figure 7A). Clumps of syncytium should be visible in the enzymatic supernatant. The first appearance of large, single cells (CTBs) indicates that the collagenase reaction has reached completion and should be halted. Note that the exact times used in this and all the other digestion steps are recalculated for each new batch of enzyme, which we purchase in lots.

Trypsin Digestion: The time required also increases with gestational age. Most first trimester tissues will be adequately digested in about 10 minutes. Second trimester villi require about 14 minutes of incubation. As in the collagenase digestion, the enzymatic reaction progress can be monitored under the microscope. Clumps should be visible along with single large CTBs (Figure 7B). The larger clumps of CTBs will be dissociated in the second collagenase digestion (Figure 7C.). The presence of smaller fibroblast cells from the villous core indicates that the tissue has been over digested and the reaction must be stopped immediately.

Second Collagenase Digestion: This step is less subject to factors that change the required time. Digestion for 3 minutes is almost always sufficient and should never exceed 5 minutes.

Isolation and Culture of First Trimester Human Placental Villous Explants

Different culture conditions can be used to study a wide variety of CTB behaviors, including differentiation and invasion (reviewed in Miller *et al.,* 2005). We have used the techniques described, herein, to generate explants for analysis *in vitro* (Prakobphol *et al.,* 2006) and *in vivo* (Red-Horse *et al.,* 2006) using the nude mouse as a host. In general, explant culture requires careful selection of anchoring villous remnants with attached cell columns. Floating villi are not adequate in studies of invasion because the component CTBs are programmed to differentiate into syncytium rather than invasive cells. Under a phase microscope, cell columns extend well beyond the translucent villous core, appearing more opaque with an irregularly shaped border (see Figure 8A). Cell columns are most frequently observed in association with placentas up to 7 weeks of gestation. Placentas are collected and dissected under

stereomicroscopic visualization into explants between 2 and 5 millimeters in diameter. Depending on the application, the villous explants may be cultured in any number of conditions.

For illustrative purposes, the following is a description of one method for culturing anchoring villous explants that we have used in many different applications. Briefly, villi are transferred to Matrigel-coated 12-mm inserts that are placed in 24-well plates and completely submerged in several drops of medium (Ham's F-12/Dulbecco's modified Eagle's medium [1:1, vol/vol]) supplemented with an antibiotic/antimycotic mixture (100 U/ml penicillin, 100 µg/ml streptomycin, 50 µg/ml gentamycin) and 10% fetal calf serum. 8-24 hours later, when the cell columns have adhered to the matrix, additional medium is added. The cultures are incubated at 37°C under standard conditions (5% CO_2/95% air) for 72 to 96 hours. Medium is changed daily. The morphology of the villi and their CTB outgrowths should be monitored at regular intervals using an inverted-phase microscope (Figure 8B). Explants with similar growth patterns should be paired as experimental and control samples.

Identification of Cytotrophoblast-Modified Blood Vessels in Tissue Sections

Microscopic analysis of histological sections of the pregnant uterus that contain spiral arterioles is often the starting point for gathering information about molecules that are relevant to CTB endovascular invasion. While this approach offers only a snapshot of the invasion process, it is a necessary prerequisite in forming hypotheses about the molecules that are involved. To play a role, they must be expressed in a relevant location at the right time. By way of background, CTB invasion of maternal blood vessels occurs in several stages. The fetal CTBs breach the termini of both arteries and

veins. Within veins, invasion rarely progresses beyond the point of entry. In contrast, invasion within the spiral arterioles ultimately involves almost the entire intra-uterine course of these vessels, and normally goes as deep as the first third of the myometrium (Robertson *et al,* 1973; Brosens *et al.,* 1972). During much of the first trimester, these fetal cells plug uterine arterioles, an arrangement that is thought to maintain an hypoxic environment that favors CTB proliferation (Burton *et al.,* 1999). Starting at about 10 weeks of gestation, the cells begin to migrate in a retrograde fashion up the vessel lumina, which rapidly recanulate (Enders and Blankenship, 1997). Once the vessels are fully modified, which includes a 10-50 fold or larger increase in diameter, they can deliver liters of blood per minute to the intervillous space.

In these types of studies, several criteria should be considered, including the gestational age of the tissue and the site of placental insertion. Regarding gestational age, it should be noted that elective pregnancy termination in the first trimester is most commonly achieved by vacuum aspiration, a process that rarely, if ever, yields intact CTB-modified maternal blood vessels. In our experience, such vessels are best obtained following hysterectomies performed during the early gestation period. However, tissue acquired from terminations that are performed during the second trimester period by curettage, often contains intact maternal blood vessels, which are grossly visible on the surface of the basal plate (Figure 6A). These vessels are also found in association with placental tissue acquired after caesarian section. In addition, there are regional differences within the placenta. At the periphery, invasion is usually superficial as compared to the central region.

Although morphological analyses are very informative, the value of these studies can be vastly increased when they are performed in the context of immunolocalization experiments. In this case, samples of the basal plate that contain spiral arterioles are

collected and quickly processed following elective pregnancy termination to prevent degradation of the tissue. The vessels and the immediately adjacent decidua, 2-3 mm in diameter (Figure 9A), are dissected free of the remaining tissue and fixed in 3% paraformaldehyde for 30 minutes. Then, the tissue is washed three times in PBS (4°C), infiltrated with gradually increasing concentrations of sucrose (5–15%) followed by OCT compound and freezing in liquid nitrogen. Placental tissues are processed using immunolocalization protocols that we published previously (Zdravkovic *et al.,* 2006). Nonspecific antibody reactivity is blocked by incubation in 3% bovine serum albumin in PBS for 1 hour. Primary antibodies for identification of CTBs in the basal plate include a rat anti-human cytokeratin 8 and 18 produced in our laboratory and a mouse anti-human cytokeratin 7 (Dako). Tissue sections are incubated with primary antibodies overnight at 4°C, washed three times in PBS and incubated in the appropriate species-specific FITC- or rhodamine-conjugated secondary antibodies. Negative control sections are incubated in the absence of primary antibodies. After staining, antibody reactivity is photographed using a Leica DM 500B fluorescence microscope (Leica Microsystems, Wetzlar, GDR). The antibodies used for the identification of endothelial cells in incompletely remodeled blood vessels include a rabbit anti-human Von Willebrand Factor (Dako). CTB remodeling of large bore vessels often leaves no endothelial cells behind, and therefore, antibodies that recognize smooth muscle actin may help to visualize blood vessel remnants, although it should be noted that the muscular walls of the arterioles are also disrupted by endovascular invasion. Cytokeratin-positive glandular epithelial cells are often present in earlier samples from the 1st and 2nd trimester. In such cases, endovascular CTBs can be distinguished from glands by virtue of their HLA-G expression (McMaster *et al.,* 1995). Glands may also be distinguished morphologically by their columnar epithelial organization relative to the more stellate, disorganized

distribution of endovascular CTBs. An example of a CTB-remodeled uterine spiral arteriole is shown in Figure 9B. In this case, the tissue section was stained with an antibody that specifically reacted with cytokeratin 7 and nuclei were visualized by staining with DAPI.

Cytotrophoblast Migration and Induction of Endothelial Cell Apoptosis During Co-culture

Given the limited number of approaches available to study interactions between CTBs and host endothelial cells *in vivo*, several groups have attempted to model such behavior with co-culture systems. While the unique experimental conditions differed, for example, in the use of freshly isolated cells versus choriocarcinoma cell lines and 2-dimensional versus 3-dimensional culture conditions, several commonalities have emerged in the results. First, CTBs migrate toward and adhere to the endothelial cells. Second, the state of the endothelium, *e.g.*, activation or differentiation, influences CTB behavior. Third, CTBs can induce apoptosis of the cultured endothelial cells. The methods used in these studies will be described with results highlighting the CTB behaviors that were observed.

Co-culture of Jar choriocarcinoma cells with endothelial monolayers (Chen *et al.,* 2005; Chen *et al.,* 2007): Rather than using freshly isolated cells, which are costly to prepare and have a limited lifespan in culture, the authors utilized choriocarcinoma cells. As background, choriocarcinoma arises during or after pregnancy with the common feature that the abnormal cells are derived from CTB progenitors (reviewed in Benirschke et al., 1995; Shih and Kurman, 2002). This neoplasm is characterized by solid sheets of CTBs and syncytial trophoblasts with the distinctive features of aggressive vascular invasion (Benirschke et al., 1995), frequent metastases (Berkowitz

and Goldstein, 1996), and human chorionic gonadotropin (hCG) production. While it is certain that malignant choriocarcinoma cells do not replicate all the behaviors exhibited by primary CTBs in culture, they do share many of their properties, and therefore, are widely used as models in the study of CTB biology. As to the methods of this study, human umbilical vein endothelial cells (HUVECs) and human microvascular endothelial cells (HMECs) were stained with green cell tracker dye (CMFDA) and seeded ($5x10^4$cells/mL) onto plastic cover slips in 6-well plates. Once confluent, Jar cells ($2.5x10^4$ cells/mL) that had been labeled with a red cell tracker dye (SNARF) were added to the endothelial cultures. Interactions among the cells were characterized at multiple time points up to 48 hours. The Jar cells displaced the endothelial cells from the surface of the dish, a phenomenon that occurred progressively over time. Further investigation revealed that the choriocarcinoma cells induced apoptosis in the endothelial cells, which they phagocytosed. Interestingly, activation of the endothelial cells by addition of TNF alpha, interferon gamma, or necrotic cells prevented their displacement by Jar cells as well as their apoptotic cell death. These results suggest that the state of the endothelium regulates CTB-endothelial interactions, a novel observation.

Co-culture of first trimester CTBs with differentiated endometrial endothelial cells in a 3-dimensional model (Aldo *et al.,* 2007)*:* The authors tracked CTB migration in a 3-dimensional matrix environment that promoted endothelial differentiation and tube formation. Human endometrial endothelial cells (HEECs) were isolated from endometrium by virtue of their affinity for biotinylated *Ulex europaeus* lectin and grown in EMB-2 medium (Cambrex). The HEECs were immortalized by retroviral transfection of telomerase (Krikun *et al.,* 2004). For endothelial tube formation, 300 microliters of Matrigel were added to 24-well tissue culture plates and polymerized at 37°C for 30

minutes. HEECs were stained with a green fluorescent dye PKH67 (Sigma-Aldrich) and added to the Matrigel-coated wells at a concentration of 100,000 cells per well. Endothelial tube formation occurred over the next 4-8 hours in culture. First trimester CTBs, isolated as described above, were labeled with a red fluorescent dye, PKH26 (Sigma-Aldrich), and seeded onto the endothelial tubes, 80,000 cells per well. Over the next 24-96 hours, cell interactions were observed by fluorescence microscopy and photographed. CTBs migrated towards the endothelial tubes within 2 hours and were either positioned on top or had intercalated within the lumina after 8 hours. Interestingly, intercalation within the tubes was blocked by LPS activation of the endothelial cells prior to CTB addition.

Using similar methods as those described above, other investigators have shown by time lapse microscopy that both primary CTBs and CTB cell lines can induce endothelial cell and smooth muscle apoptosis through Fas/FasL signaling (Ashton *et al.,* 2004; Harris, *et al.,* 2006). A role for Tumor Necrosis Factor α-Related Apoptosis Inducing Ligand (TRAIL) signaling in this process has also been described (Keogh *et al.,* 2007)

In Vitro Models of CTB Endovascular Invasion Using Explanted Spiral Arterioles

While cell culture models of CTB/endothelial interactions are very useful, they fail to provide many elements that are present during endovascular invasion *in vivo* such as the stromal and extracellular matrix factors present in decidual tissue, the complex vessel architecture, and the variety of cell types that are present in this complex milieu. Additionally, endothelial and CTB cell lines used in the studies described above may not possess the same characteristics as their living equivalents. Therefore, several

investigators have attempted to model CTB invasion using explanted tissues. Three unique approaches will be presented. In the first, spiral arterioles were dissected from myometrial biopsies obtained at term and infused with CTBs (Cartwright, *et al.,* 2002; Ashton *et al.,* 2004; Crocker *et al.,* 2005). In the second, explanted spiral arterioles were denuded of endothelium to expose the smooth muscle lining (Harris, *et al.,* 2006; Keogh *et al.,* 2007). In the last, chorionic villous explants were co-cultured with explanted decidual tissue under conditions of hypoxia (Dunk *et al.,* 2004).

CTB invasion of term myometrial spiral artery segments in vitro (Cartwright, *et al.,* 2002; Ashton *et al.,* 2004; Crocker *et al.,* 2005)*:* Spiral arteries were dissected under sterile conditions from myometrial biopsies obtained following caesarian section. In choosing this approach, it is important to keep in mind that CTB invasion does not normally progress beyond the inner third of the myometrial segments of spiral arterioles. These arterial explants, which included adjacent decidua, allowed study of both the interstitial and endovascular components of CTB invasion. Either a CTB cell line (SGHPL-4) or primary CTBs, isolated from first trimester tissue, were fluorescently labeled with CellTracker Orange (Invitrogen, C2927). To assay interstitial invasion, the ends of the spiral arterioles were tied off to prevent CTB infiltration along a luminal path. Ligated arteries were embedded in fibrin gels. To prepare the gels, fibrinogen (Sigma) was suspended in PBS (2.5 mg/ml) with 200 Units/ml aprotinin (Trasylol, Bayer, Germany) in a 6-well plate. Polymerization of the gel was induced by the addition of thrombin (0.625 units/ml). $5x10^4$ fluorescently labeled CTBs were resuspended in EC growth medium (TCS Biologicals) at a concentration of 10^5 cells/ml and added to the top of the fibrin gel containing the arterial explant. Cultures were incubated for 5 days and the fresh unfixed explants were embedded in OCT and sections 5 and 10 microns were prepared. To assay endovascular invasion, spiral arterioles placed in a pressurized

perfusion chamber (Living Systems), cannulated, and the lumina were maintained by exerting low pressure. Control vessels were perfused with medium alone (10 microliters) and experimental vessels were exposed to medium containing fluorescently labeled CTBs ($5x10^4$ in 10 microliters). Then, the vessels ends were tied off and the explants were embedded in fibrin gels, incubated for 5 days, and analyzed as described above.

As to results, in the original publication describing this model (Cartwright *et al.,* 2002) the authors observed CTB endovascular invasion through both interstitial and lumenal routes, with CTBs intercalating within the vessel wall and lining the lumen, respectively. Invasion was accompanied by apoptosis and loss of the resident endothelial cells as revealed by TUNEL staining and the presence of cleaved PARP within the remaining endothelial cells (Ashton *et al.,* 2004). In later work, immunohistochemical analyses and electron microscopy (Crocker *et al.,* 2005) revealed that CTBs disrupted both the endothelial and smooth muscle compartments, although the overall integrity of the vessel was not compromised. Vessels perfused with CTBs often lacked endothelium and showed reduced staining for smooth muscle actin. CTBs adherent to the vessel wall occasionally exhibited cellular processes extending deep into the smooth muscle layer. Invasion, which depended on oxygen concentration, was reduced in hypoxia.

The same group studied interactions between CTBs and spiral arterioles that were denuded of endothelium by passing a column of air through the cannulated vessels (Harris, *et al.,* 2006; Keogh *et al.,* 2007). Perfusion of either CTBs or CTB conditioned medium induced apoptosis in the smooth muscle wall of these vessels. Additional experiments showed that this phenomenon depended of Fas/FasL signaling (Harris, *et al.,* 2006) and TRAIL signaling (Keogh *et al.,* 2007).

Chorionic villous CTBs invade first trimester decidual explants in vitro (Dunk *et al.,* 2004): The authors devised a novel model to study endovascular invasion. Chorionic villi were co-cultured with decidua parietalis explants from the same pregnancy. Experiments were conducted under conditions of physiological hypoxia, which were required for CTB invasion. This is in contrast to the experiments described above in which hypoxia inhibited CTB invasion of spiral arterioles. As to methods, tissue samples were collected following elective termination of pregnancies, 6-9 weeks of gestation. Chorionic villous explants were prepared as described above and co-cultured with decidual tissue that was dissected into cubes of approximately 2-3mm^3. Millicell-CM culture inserts with 0.4 micron pores (Millipore) were coated with 200 microliters of Matrigel (BD Biosciences) and incubated at 37°C until the Matrigel polymerized. Decidual explants were transferred to the culture insert, epithelial surface facing upwards, and placental villi added. Culture medium was changed every 48 hours and consisted of a 50/50 mix of DMEM/Ham's F12 medium supplemented with 10% FBS, 100 U/ml penicillin, 100 µg/ml streptomycin, and 0.25 µg/ml ascorbic acid (pH 7.4). Cultures were incubated under conditions of physiological hypoxia (3% oxygen) with 5% carbon dioxide and were maintained up to 6 days. Decidual cultures without villous explants served as controls. Following termination of the experiments, tissues were fixed in 4% paraformaldehyde and 5 micron sections were prepared.

Immunostaining for trophoblast, endothelial and smooth muscle markers revealed that CTBs invaded through the decidua (interstitial invasion) and colonized blood vessels (endovascular invasion), which lost most of their resident endothelial cells. Those remaining often appeared to be partially detached from the underlying basement membrane. In addition, CTB-modified vessels showed reduced staining for smooth muscle actin. In contrast, decidual explants cultured without placental villi contained

vessels with intact endothelial and smooth muscle layers. Interestingly, when experiments were carried out in a hyperoxic environment (17% oxygen) CTB invasion of the decidual explants was not observed.

In Vivo Models of Human Cytotrophoblast Vascular Remodeling

During human pregnancy, placental CTBs of fetal origin invade the uterine wall. This process has two components. In the first, CTBs invade the uterine parenchyma where they interact with the stromal compartment and a resident maternal immune population. In the second, a subpopulation of CTBs invades uterine blood vessels with subsequent colonization of the arterial side of the circulation. Although some information is known about the molecular bases of these unique processes, a great deal remains to be learned. One reason is the lack of *in vivo* models for studying these unique heterotypic cell-cell interactions. For example, the mechanisms whereby CTBs replace the maternal endothelial lining of uterine arterioles and intercalate within the surrounding smooth muscle layer are difficult to study *in vitro* and almost certainly do not recapitulate the complex series of events that occur *in vivo*. Thus, the mechanisms of CTB vascular remodeling are of considerable interest.

Placental xenograft of the murine mammary fat pad and kidney capsule: In a recent study, we devised a novel *in vivo* model to study CTB invasion in which human placental chorionic villi are implanted into the mammary fat pads or under the kidney capsules of SCID mice (Red-Horse *et al.,* 2006). These *in vivo* models were very successful as CTBs exhibited robust interstitial and endovascular invasion in both regions. Within the highly vascularized kidney capsule, CTBs invaded deeply, moving along the surfaces of capillaries. Xenograft in the mammary fat pad, which contains

large bore vessels, was more suited for the analysis of CTB interactions with arterioles. These experiments yielded a variety of interesting information such as the observation that CTB invasion of arterioles in this region was associated with endothelial apoptosis. The success of these experiments was not surprising given that CTBs exhibit invasive behavior in a variety of extrauterine sites. As examples, ectopic pregnancies can occur in the fallopian tube, abdominal wall, cervix and ovary (Molinaro and Barnhart, 2007). In addition, choriocarcinomas frequently metastasize to the lungs, brain, and liver (Cheung, 2003).

As to the methods, protocols involving animals and human fetal tissue were approved by the UCSF Committee on Animal Research and the UCSF Committee on Human Research, respectively. Homozygous C.B-17 *scid/scid* mice (Taconic) were the recipients. Anchoring placental villi were dissected into 2-5mm pieces. Prior to surgery, mice were anesthetized with isoflurane anesthesia or ketamine/zylazine for mammary or kidney capsule procedures, respectively. For transplantation to the mammary fat pad, placental villi were surgically placed within a small incision made below this region, which was subsequently sutured. For transplantation under the kidney capsule, a small incision was made through the skin covering the lumbar area and the organ was exteriorized. Placental villi were implanted under the capsular membrane using techniques that have been described previously (McCune *et al.,* 1988; Stoddart *et al.,* 2001). Following both mammary fat pad and kidney capsule surgeries, mice were maintained under pathogen-free conditions for one to three weeks, at which time the experiments were terminated and either whole kidneys containing implants or implants dissected from a portion of the fat pads were immediately placed in 3% paraformaldehyde. Tissues were fixed for three hours at 4°C before being passed through a sucrose gradient, snap-frozen in liquid nitrogen, and sectioned. Histological

analyses allowed quantitative estimates of invasion that were made by calculating the distance between the implanted villi and the outer perimeter of placental cells that had invaded murine tissues.

Choriocarcinoma xenograft of the murine skin: Another group reported an alternative model for investigating CTB invasive behavior (Grummer *et al.,* 1999). Rather than studying primary CTBs or explants isolated from placental tissue, this group utilized the tumorigenic properties of the Jeg-3 human choriocarcinoma cell line, which was injected subcutaneously in the murine flank. In this location, Jeg-3 cells established tumors that grew rapidly within 2 weeks. Regarding endovascular invasion, two primary observations were made. First, Jeg-3 tumors had lacunar blood spaces that appeared to be the result of tumor cells colonizing host vessels; Von Willebrand factor-positive endothelial cells and hCG-positive Jeg-3 tumor cells lined the blood-filled lacunae. Second, Jeg-3 cells replaced the host endothelium at junctional zones between the tumor and the host tissues. Taken together, these results indicate that Jeg-3 cells remodel the host vasculature.

As to methods, the experiments were carried out in athymic nude mice (Han:NMRI nu/nu) maintained under pathogen-free conditions. Prior to transfer into 10 week-old recipient mice, Jeg-3 cells were grown to 80–90% of confluence and detached with trypsin/EDTA. One million cells in a volume of 200 microliters were injected into the subcutaneous space of the flanks of male mice. To reduce the numbers of animals required, each mouse received injections on both sides of its body. Tumor tissue was collected at the termination of experiments 21 days following injection. For histological studies, tumor and adjacent host tissues were subject to one of the following fixation procedures. Some tissues were immediately embedded in OCT medium and frozen in liquid nitrogen. Others were fixed in 3% paraformaldehyde and processed in paraffin.

Alternatively, specimens were fixed in 2.5% glutaraldehyde and embedded in Epon/Araldite for fine structural analysis.

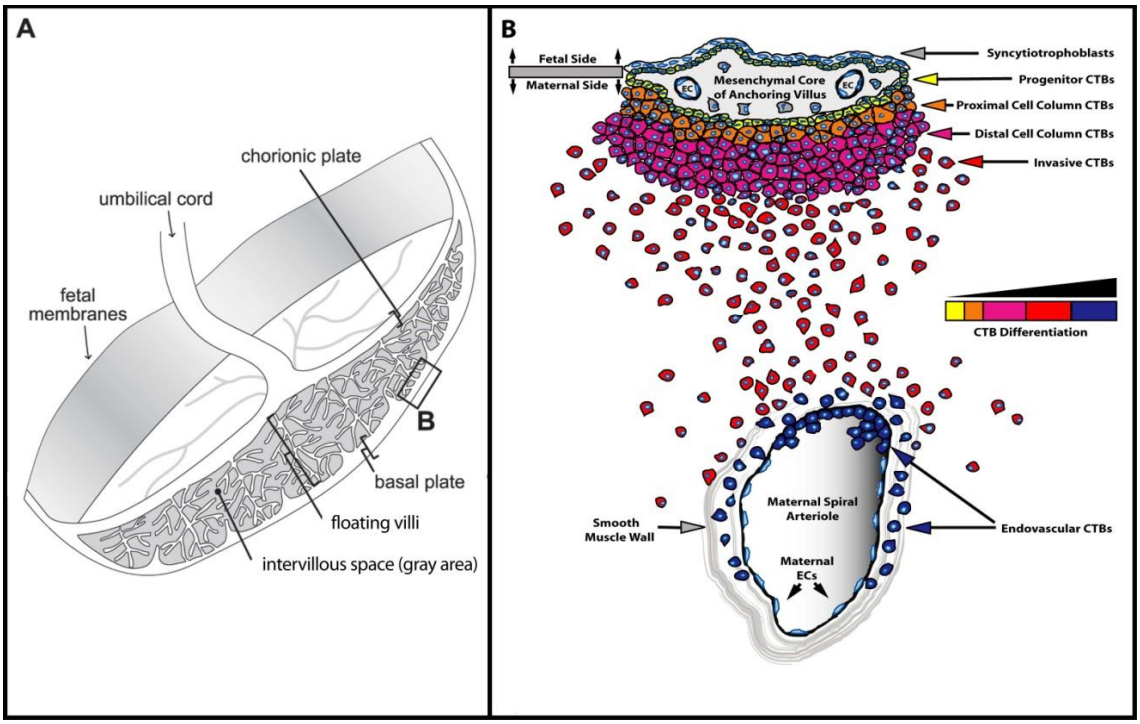

Figure 6. *Anatomy of the Maternal-Fetal Interface.*

Anchoring chorionic villi (B) attach the placenta to the uterus and give rise to invasive CTBs. (A) Placental chorionic villi stem from the chorionic plate and lie within the intervillous space. The point of attachment between anchoring villi and the underlying tissue is referred to as the basal plate (box B). (B) Enlargement of the area in box B. Undifferentiated CTB progenitors in the anchoring villi give rise to invasive CTBs that invade the uterine interstitium (interstitial invasion) and the maternal endothelium (endovascular invasion).

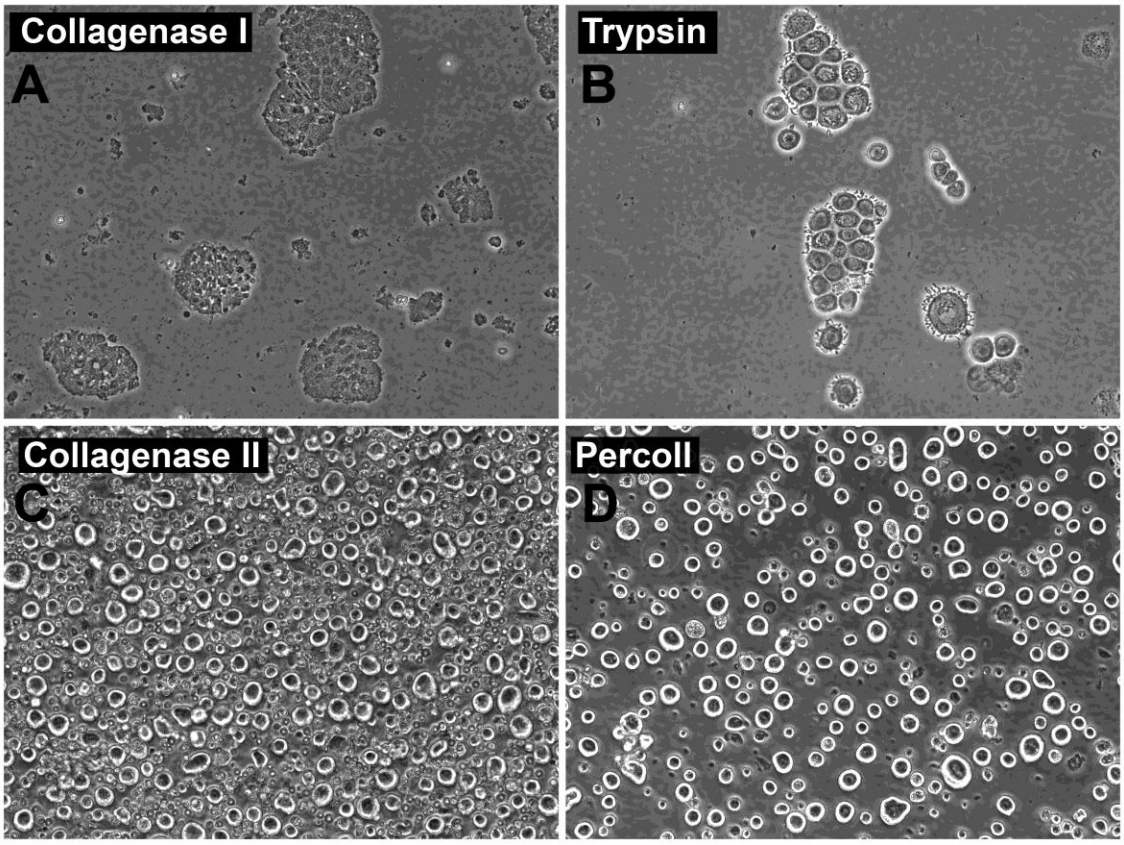

Figure 7. *Monitoring Enzymatic Digestions and Cell Purification During CTB Isolation.*

(A) The first collagenase digestion releases the syncytiotrophoblasts from the surface of placental villi, which appear as multinucleated flattened cells at 20x magnification. The presence of any CTBs in the supernatant from the first collagenase digestion indicates that this step is complete and must be stopped immediately (not shown). Trypsin digestion releases large clumps of CTBs (B), which are broken down into single cells during the second collagenase treatment (C). Also present at this stage are blood cells, fibroblasts, leukocytes, and other cell types. (D) CTBs are preferentially isolated by the Percoll density gradient centrifugation step.

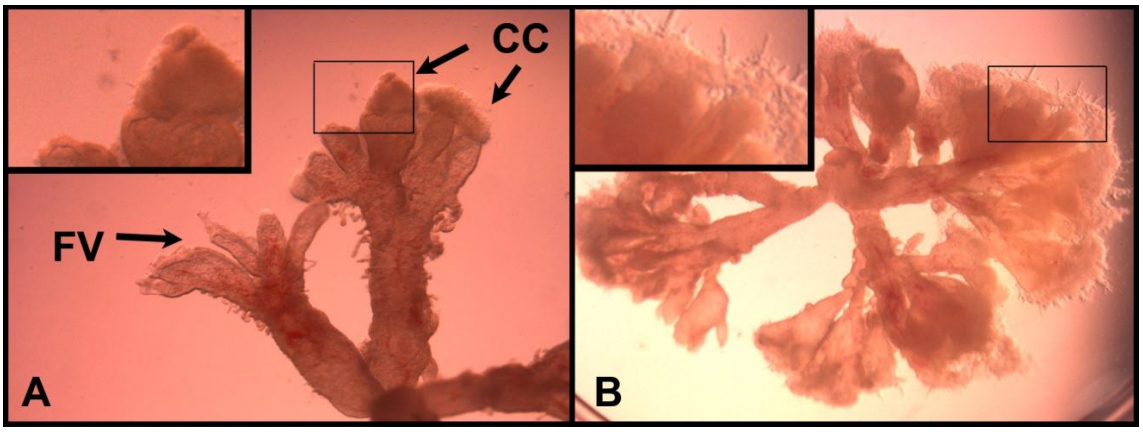

Figure 8. *Chorionic Villous Explants.*

(A) Remnants of anchoring villi containing CTB cell columns can be distinguished from floating villi by their irregular outlines and opaque caps that extend from their termini (inset). (B) Explant cultured on Matrigel showing CTB outgrowths (inset). Abbreviations used: CCs; cell columns, FV; floating villi.

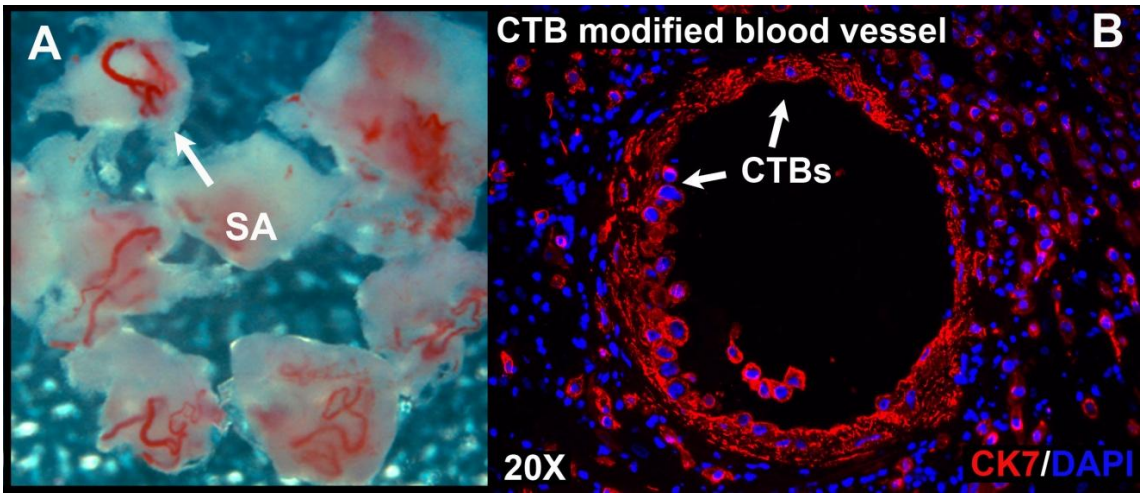

Figure 9. *Spiral Arterioles and a Histological Section of the Uterus that Contains a CTB-Modified Blood Vessel.*

(A) Spiral arterioles (SA) dissected from the decidua at 12 weeks of gestation. (B) Frozen section of an 18 week basal plate biopsy containing a CTB-modified blood vessel. CTBs were distinguished from other cell types by staining for cytokeratin 7 (CK7; red); nuclei were visualized by staining with DAPI (blue).

Serum-Free Medium	**500ml**
DME/H-21 Medium (Gibco, 11965-092)	469.5ml
Nutridoma (Roche, 11011375001)	10ml
Sodium Pyruvate (Sigma, S8636)	5ml
HEPES Buffer (Invitrogen, 15630-080)	5ml
Glutamine Plus (Atlanta Biologicals, B92010)	5ml
Penicillin/Streptomycin (Invitrogen, 15140-122)	5ml
Gentamycin (Invitrogen, 15750-060)	0.5ml
Cytowash	**500ml**
DME/H-21 Medium (Gibco, 11965-092)	477ml
Fetal Bovine Serum (Hyclone, SH30071.03)	12.5ml
Glutamine Plus (Atlanta Biologicals, B92010)	5ml
Penicillin/Streptomycin (Invitrogen, 15140-122)	5ml
Gentamycin (Invitrogen, 15750-060)	0.5ml
Trypsin Solution	**100ml**
1X PBS Mg^{2+} Ca^{2+} free (Gibco, 14190-144)	100ml
Trypsin (Sigma, T-8003)	0.0069g
DNase (Sigma, DN25)	0.0400g
EDTA (Sigma, ED2SC)	0.0200g
Collagenase Solution	**100ml**
1X PBS Mg^{2+} Ca^{2+} free (Gibco, 14190-144)	100ml
Collagense (Sigma, C-2674)	0.062g
DNase (Sigma, DN25)	0.040g

Hyaluronidase (Sigma, H-3506)		0.069g
BSA (Sigma, A7906)		0.100g
Percoll Gradient Reagents		
Percoll (Amersham, 17-0891-01)		
10x Hank's BSS without Phenol Red (Invitrogen, 14185)		
1x Hank's BSS without Phenol Red (Invitrogen, 14175)		
1x Hank's BSS with Phenol Red (Invitrogen, 14170)		
Percoll Stock Solutions	**90% Percoll***	**Hank's 1X**
70%	35.0 ml	10.0 ml (w/o Phenol Red)
60%	30.0 ml	15.0 ml (with Phenol Red)
50%	25.0 ml	20.0 ml (w/o Phenol Red)
40%	20.0 ml	25.0 ml (with Phenol Red)
30%	15.0 ml	30.0 ml (w/o Phenol Red)
20%	10.0 ml	35.0 ml (with Phenol Red)
* 90% Percoll (270 ml Percoll + 30 ml 10x Hanks BSS without Phenol Red)		

Table 1. *Preparation of Medium, Enzyme Solutions, and Percoll Density Gradient.*

Chapter 3: A Role for Notch Signaling in Trophoblast Endovascular Invasion and in the Pathogenesis of Preeclampsia

Hunkapiller, N.M., Gasperowicz, M., Kapidzic, M., Plaks, V., Maltepe, E., Kitajewski, J., Cross, J.C., and Fisher, S.J. (2011). A Role for Notch Signaling in Trophoblast Endovascular Invasion and in the Pathogenesis of Preeclampsia. (Submitted to *JCI*)

Abstract

Placental trophoblasts (TBs) invade and remodel uterine vessels with an arterial bias. This process, which involves vascular mimicry, reroutes maternal blood to the placenta, but fails in preeclampsia. We investigated Notch family members in both contexts, as they play important roles in arterial differentiation/function. Immunoanalyses of tissue sections showed step-wise modulation of Notch receptors/ligands during human TB invasion. Inhibition of Notch signaling reduced invasion of cultured human TBs and expression of the arterial marker *EFRNB2*. In mouse placentas, Notch activity was highest in endovascular TBs. Conditional deletion of *Notch2*, the only receptor upregulated during mouse TB invasion, reduced arterial invasion, the size of maternal blood canals 30-40%, and placental perfusion 23%. By E11.5 there was litter-wide lethality in proportion to the number of mutant offspring. In preeclampsia, expression of the Notch ligand JAG1 was absent in perivascular CTBs. We conclude that Notch signaling is critical for TB vascular invasion.

Introduction

Human placentation involves unique interactions between embryonic/fetal CTBs and maternal cells. For example, CTBs that arise from the placental surface colonize the uterine wall and resident maternal vessels (Figure 10A), a process that requires their aggressive invasion of maternal tissues (Fisher *et al.,* 1989; Librach *et al.,* 1991). During *interstitial* invasion, a subset of these cells commingle with decidual, myometrial and immune cells. During *endovascular* invasion, masses of CTBs breach and plug maternal spiral arterioles. Subsequently, these fetal cells replace the maternal endothelium and portions of the smooth muscle wall, creating a novel chimeric vasculature composed of both maternal and fetal cells, a process that greatly increases arteriole diameter. CTBs form only superficial connections with uterine veins. These remarkable cell-cell interactions are accompanied by equally unusual changes in fundamental aspects of the cells' phenotypic characteristics, which have the net effect of mimicking many aspects of endothelial cells (ECs). For example, they switch on the expression of vascular-type adhesion molecules (Damsky *et al.,* 1992; Zhou *et al.,* 1997a), vasculogenic/angiogenic factors (Zhou *et al.,* 2002; Zhou *et al.,* 2003), and Ephrin family members that play a role in arterial function and identity (Red-Horse *et al.,* 2005). The significance of CTB endovascular invasion is illustrated by the fact that this process largely fails in preeclampsia (PE).

PE is a serious complication that affects ~7% of first-time pregnancies (Levine *et al.,*1997; Redman and Sargent, 2005). The mother shows signs of widespread alterations in EC function such as high blood pressure, proteinuria, and edema (Roberts and Lain, 2002). In some cases, the fetus stops growing, resulting in intra-uterine growth restriction. In PE the extent of interstitial invasion by CTBs is variable, but frequently shallow. Endovascular invasion, on the other hand, is consistently rudimentary (Brosens *et al.,* 1972; Naicker *et al.,* 2003; Zhou *et al.,* 2007), resulting in

increased vascular resistance and decreased placental perfusion (Matijevic and Johnston, 1999). The PE syndrome reveals the significance of this differentiation process. Biopsies of the uterine wall of women with this syndrome showed that invasive CTBs fail to turn on receptors that promote invasion and/or assumption of an EC-like phenotype (Zhou *et al.,* 2002; Zhou *et al.,* 2003). The upstream regulatory mechanisms that are responsible for these defects remain enigmatic. In this context, ligands/receptors that play a role in vascular patterning would appear to be particularly relevant.

The Notch signaling pathway governs differentiation and function during cell-cell contact in a wide variety of tissues and organs (Bianchi *et al.,* 2006; Miele, 2006) with particularly important roles in vascular patterning (Roca and Adams, 2007; Swift and Weinstein, 2009). Mechanistically, the Notch receptors operate both on the cell surface to receive activating signals and within the nucleus as transcriptional modulators (Alva and Iruela-Arispe, 2004; Kopan and Ilagan, 2009). The core mammalian pathway is a conserved family of four transmembrane receptors (NOTCH1-4) and five ligands (DLL1, -3, -4, JAG1 and -2). Binding of receptors and ligands on adjacent cells triggers a series of proteolytic cleavages of the receptor, ultimately releasing the Notch intracellular domain (NICD) via gamma secretase-mediated processing (Schroeter *et al.,* 1998). Subsequently, cleaved NICD translocates to the nucleus, binds to CBF1/Su(H)/Lag2 family transcription factors, and induces multiple downstream targets such as *Hes* and *Hey* (Weinmaster, 1998).

Notch signaling regulates the differentiation of primitive undefined ECs into hierarchical networks by specifying arterial identity. By embryonic days (E) 9.5-11.5 of mouse development, when the primary vascular plexus begins to remodel into a network of arteries and veins, *Notch1, -3, -4, Jag1* and *Dll4* mRNAs are expressed within and

around the developing vasculature. However, by E13.5, their expression is largely confined to the arterial endothelium (Villa *et al.,* 2001). Concurrently, *Efrnb2* and *Ephb4* emerge as markers of arterial and venous identity, respectively (Wang *et al.,* 1998). In zebra fish, loss of Notch signaling reduced EC expression of *efrnb2* while simultaneously enhancing *ephb4*—evidence that *Notch* functions upstream of both molecules in specifying vessel identity (Lawson *et al.,* 2001; Zhong *et al.,* 2001). Targeted deletions of Notch family genes produce a variety of vascular defects, most of which result in embryonic lethality between E9.5 and E12.5 due to failed incorporation of the arterial vasculature into the circulation (Roca and Adams, 2007; Swift and Weinstein, 2009). In this context, it is plausible that Notch family members play a role in programming CTB arterial invasion.

In culture, undifferentiated mouse trophoblast stem (TS) cells express all members of the Notch family (Cormier *et al.,* 2004). *In vivo*, differentiated trophoblasts at the junctional zone (the placenta's maternal-fetal interface) express only *Notch2* and expression is restricted to a narrow temporal window at midgestation (Nakayama *et al.,* 1997) suggesting that trophoblast differentiation *in vivo* likely involves significant modulation of Notch expression. As to function, *Notch2*, *Hes2* and *Hes3* are co-expressed in trophoblast giant cells (TGCs) which, along with glycogen trophoblast cells (GlyTCs), carry out interstitial and endovascular invasion in this species. Tetraploid rescue experiments in *Notch2*-deficient mice revealed that placental defects involving the labyrinthian circulatory system are associated with the lethality in *Notch2*-deficient animals (Hamada *et al.,* 2007). However, the mechanisms involved remained elusive. We theorized that defects in trophoblast endovascular invasion, the process that is responsible for increases in placental perfusion during pregnancy and is dysregulated in PE, contributed to the observed phenotype. Here, we used a combination of mouse and

human models to prove this theory and to identify PE-associated aberrations in CTB expression of Notch family members.

Results

Human CTBs Modulated Expression of Notch Molecules as they Differentiated/Invaded In Vivo and In Vitro

We used an immunolocalization approach to survey Notch family members at the maternal-fetal interface (Figure 10A). The results showed that CTBs modulated the expression of Notch molecules in unique patterns as they invaded the uterine wall and the maternal blood vessels that traverse this region. As to receptor localization, staining for NOTCH2 (Figure 10B) was either absent or weak and sporadic in CTB progenitors that attached to the trophoblast basement membrane. However, NOTCH2 expression was dramatically upregulated in the CTB cell columns as invasion began. CTBs at all stages of differentiation stained for NOTCH3 (Figure 10C and 10D). NOTCH4 (Figure 10E) exhibited a unique and unexpected pattern. Initially high in CTB progenitors and cell columns, immunoreactivity abruptly declined with deeper invasion, particularly as the cells approached spiral arterioles. Maternal and fetal cells stained for several Notch ligands. DLL1 was expressed (Figure 10F) in maternal cells adjacent to CTBs in the interstitial and endovascular compartments. DLL4 staining (Figure 10G) was not detected in CTB progenitors but increased as the cells entered the columns. However, DLL4 immunoreactivity was rapidly lost as CTBs invaded the uterine wall, although small fields of immunopositive cells were occasionally observed in the deeper regions. JAG1 expression (Figure 10H and 10I), which was absent in early stages of CTB

differentiation/invasion, was significantly upregulated in CTBs that associated with the maternal spiral arterioles. Together, these results show that CTBs dramatically altered their expression of Notch receptors and ligands as they differentiated/invaded.

As a first step in understanding Notch function during CTB differentiation/invasion, we used a RT-qPCR approach to assess Notch family mRNA expression patterns in an *in vitro* model of this process (Figure 11A) in which primary CTBs are cultured on a Matrigel substrate. We previously demonstrated that CTBs grown on Matrigel differentiate along the invasive pathway in a manner that recapitulates interstitial differentiation/invasion *in vivo* (Librach *et al.,* 1991; Zhou *et al.,* 1997a). As to results, *NOTCH2* mRNA levels peaked at 3 hours, *NOTCH3* mRNA levels remained constant and *NOTCH4* expression quickly declined with differentiation. *DLL4* mRNA levels increased with differentiation. In contrast, we repeatedly failed to detect *JAG1* expression at either mRNA or protein levels under a variety of culture conditions we used to simulate the uterine vascular environment, *e.g.*, EC, decidual cell, or explanted spiral arteriole co-culture as well as physiological hypoxia, shear stress, or high serum concentrations (data not shown). This observation is consistent with our repeated finding that this culture model does not replicate the terminal stages of CTB endovascular invasion, *e.g.* upregulation of NCAM1 expression (Blankenship and King, 1996). Thus, the results of these experiments show that this culture model is useful for studying Notch function during the interstitial phases of differentiation/invasion but not during the final stages of endovascular remodeling.

Notch Signaling Regulated CTB Invasion and Expression of EFRNB2, an Arterial Marker

In these experiments, isolated CTBs were plated with L-685,458, a chemical inhibitor of gamma secretase proteolytic activity, which is required for Notch protein activation. Control CTBs were cultured in 0.1% DMSO to account for the fact that the inhibitor was dissolved in this vehicle. First, we determined whether L-685,458, at concentrations that are typically used to inhibit Notch signaling (Williams *et al.,* 2006) had toxic effects on CTBs. Briefly, the cells were cultured in either 1, 10, or 50 μM L-685,458, or DMSO alone. After 36 hours, the percentage of CTBs undergoing programmed cell death was assessed by using the terminal deoxynucleotidyltransferase-mediated dUTP-biotin nick end labeling method (TUNEL). Virtually no apoptosis was detected at L-685,458 concentrations ≤10 μM (Figure 11B and 11C, and data not shown). Therefore, this inhibitor concentration was employed in the remaining experiments. Next, we assessed the effects of inhibiting Notch activation on CTB invasion. L-685,458 significantly decreased invasion (Fig. 11D), evidence that Notch family members play an important role in this process. Finally, we were interested in whether inhibiting Notch activation affected the cells' ability to upregulate the expression of markers of arterial ECs as they differentiate/invade in culture. These experiments exploited our observation that, during this process, CTBs downregulate *EPHB4* and upregulate *EFRNB2*, markers of venous and arterial ECs, respectively (Red-Horse *et al.,* 2005). As expected, very low levels of *EFRNB2* mRNA were detected before the cells were plated (Figure 11E). Under control conditions, we observed robust upregulation of this ligand after 36 hours. In the presence of L-685,458, *EFRNB2* mRNA expression was blunted by ~40% as measured by densitometry. In contrast L-685,458 had no effect on *EPHB4* (data not shown). Taken together, these results support a model in which Notch activity promotes CTB differentiation/invasion and acquisition of an arterial EC-like phenotype. Because our human CTB cell culture model failed to

replicate the terminal stages of CTB endovascular differentiation, we used a mouse model to study the role of Notch in this process.

Placental Notch Activity is Largely Confined to the Mouse Ectoplacental Cone and Endovascular Trophoblasts

Since the co-expression of Notch ligands and receptors does not necessarily correlate with function, independent methods are required to estimate Notch activity. However, few tools have been developed for use in human cells. Accordingly, we used the mouse *Transgenic Notch Reporter* (*Tnr*) line that expresses *Gfp* under the control of a Notch responsive promoter (Duncan *et al.,* 2005) to assess Notch activity during development of the chorioallantoic placenta. *Tnr* offspring and placentas were generated from timed matings between wild-type females and males harboring the *Tnr* transgene. By passing the *Tnr* allele through the father, this scheme ensured that *Gfp* expression was restricted to the fetal compartment of the placenta. Notch activity was first observed at E7.5 in only a few rare cells at the leading edge of the ectoplacental cone (EPC), the primary source of invasive trophoblasts (data not shown). By E8.5, Notch activity was detected in association with many more EPC cells, particularly in the outer layers that were in close contact with the uterus (Figure 12A). Between E8.5 and E10.5, a subset of parietal TGCs acquired Notch activity, which was also evident in a growing population of trophoblast cells within the junctional zone (Figure 13A-C), a region analogous to the maternal-fetal interface in humans. By E14.5 (Figure 12B and 12C), the highest Notch activity was restricted to trophoblasts that were associated with maternal spiral arterioles with lower levels observed in the spongiotrophoblast region and in association with other cells that were sparsely distributed throughout the labyrinth.

Placentas without the *Tnr* allele lacked *Gfp* signal (Figure 13D). In mice, spiral artery-associated TGCs (SpA-TGCs) and GlyTCs carry out endovascular invasion, suggesting that Notch activity was dramatically increased in these cells. To confirm this theory, we performed double RNA *in situ* hybridization for *Tnr* (Notch activity) and either the TGC marker, *Prl2c2* (Figure 12D) or the GlyTC marker, *Pcdh12* (Figure 12E). The results showed that a subset of *Prl2c2*-positive SpA-TGCs and *Pcdh12*-positive GlyTCs (both interstitial and endovascular) had Notch activity. Accordingly, we profiled mouse TB expression of Notch family members with the goal of studying their functions. Specifically, we compared RNA levels in trophoblast stem (TS) cells, known to express all components of the Notch pathway (Cormier *et al.,* 2004), to their differentiated progeny, grown under normoxic conditions that produce primarily TGCs (Figure 12F). Very similar to the patterns observed in human CTBs *in vivo*, only *Notch2*, *Jag1*, and *Dll4* expression increased with differentiation, while *Notch1*, *-3*, *-4*, *Jag2*, and *Dll1* expression declined. Taken together, these findings bolstered the conclusions of the *in vitro* human experiments that implicated Notch activity as a driver of CTB endovascular invasion.

Notch2 Deletion in Invasive Trophoblast Lineages Led to Litter-wide Lethality in Proportion to the Number of Mutant Offspring

To investigate Notch function with regard to trophoblast invasion of spiral arterioles, we designed a strategy for conditional deletion of *Notch2* in the invasive trophoblast lineages, which includes all SpA-TGCs and GlyTCs. Briefly, we bred mice harboring floxed alleles of *Notch2* (*Notch2*^{flox}) (McCright *et al.,* 2006) to *Tpbpa-Cre* mice (Simmons *et al.,* 2007) in which *Cre Recombinase* is specifically expressed by EPC cells

that later give rise to all GlyTCs, SpA-TGCs, and spongiotrophoblasts. Following their differentiation from EPC precursors, spongiotrophoblasts normally maintain *Tpbpa* expression, which GlyTCs and SpA-TGCs lose. To confirm the expected expression pattern, we performed serial RNA *in situ* hybridization for both *Tpbpa* and *Gfp*, which is also a component of the *Tpbpa-Cre* construct. *Gfp* expression by spongiotrophoblasts typically occurred in nearly all of the cells at E9.5 (Figure 14A-B) and the majority of cells at E12.5 (Figure 14 C-D), evidence that the construct was expressed in the desired location.

Accordingly, we generated *Notch2*$^{floxl+}$;*Tpbpa-Cre* (heterozygote) and *Notch2*^{floxlflox};*Tpbpa-Cre* (mutant) embryos and offspring by breeding *Notch2*^{floxlflox} and *Tpbpa-Cre* founders. In preliminary crosses, *Notch2*^{floxlflox};*Tpbpa-Cre* offspring were born that were used for breeding purposes. Given that complete embryonic loss of *Notch2* results in lethality by E11.5 (Hamada *et al.,* 1999), we focused our analysis on this developmental window. First, we surveyed resorption rates in litters generated from different combinations of *Notch2*$^{floxl+}$;*Tpbpa-Cre* or *Notch2*^{floxlflox};*Tpbpa-Cre* parents, designed to produce 25%, 50% or 100% *Notch2*^{floxlflox};*Tpbpa-Cre* progeny (Table 2). In litters bred from *Notch2*$^{floxl+}$;*Tpbpa-Cre* animals, only one resorption was observed among the 39 implantation sites (2.6%) examined between E10.5-E12.5. Breeding of *Notch2*$^{floxl+}$;*Tpbpa-Cre* and *Notch2*^{floxlflox};*Tpbpa-Cre* animals produced litters with many more resorptions. Loses, which were observed as early as E9.5, increased to a maximal frequency of 29% by E11.5. A similar temporal pattern was observed in *Notch2*^{floxlflox};*Tpbpa-Cre* matings, but the resorption rate increased to 54%. Maternal factors did not contribute to increases in embryonic lethality as crosses of *Notch2*$^{floxl+}$;*Tpbpa-Cre* females to *Notch2*^{floxlflox};*Tpbpa-Cre* males and reciprocal crosses of *Notch2*^{floxlflox};*Tpbpa-Cre* females to *Notch2*$^{floxl+}$;*Tpbpa-Cre* males exhibited similar rates

of resorption (Table 3). Next, we correlated embryonic genotype with resorption/survival (Table 4). Surprisingly, in *Notch2*$^{floxl+}$;*Tpbpa-Cre* x *Notch2*^{floxlflox};*Tpbpa-Cre* matings, resorptions involved equal numbers of *Notch2*$^{floxl+}$;*Tpbpa-Cre* and *Notch2*^{floxlflox};*Tpbpa-Cre* embryos. This conclusion was substantiated by the fact that the surviving offspring had the same genetic distribution. Consistent with this observation, we did not note any differences in embryonic or placental weight between *Notch2*$^{floxl+}$;*Tpbpa-Cre* and *Notch2*^{floxlflox};*Tpbpa-Cre* offspring (Table 5). Taken together, these results suggest that embryonic lethality correlated with the presence of *Notch2*^{floxlflox};*Tpbpa-Cre* embryos rather than genotype of individual fetuses.

In initial breeding experiments, we noted that *Notch2*^{floxlflox};*Tpbpa-Cre* mothers had significantly fewer implantation sites than *Notch2*$^{floxl+}$;*Tpbpa-Cre* mothers (5.7+/-2.8 vs. 7.5+/-2.8; p=0.03). This result was independent of embryonic genotype as the implantation rate was identical in *Notch2*^{floxlflox};*Tpbpa-Cre* females bred to *Notch2*$^{floxl+}$;*Tpbpa-Cre* or *Notch2*^{floxlflox};*Tpbpa-Cre* males. In searching for a possible explanation, we discovered that the *Notch2*^{floxlflox};*Tpbpa-Cre* females exhibited severe ovarian defects, including hemorrhagic and cystic follicles, which were not observed in *Notch2*$^{floxl+}$;*Tpbpa-Cre* females (Figure 15A). These observations suggested that the *Tpbpa-Cre* transgene might also have ovarian expression. To address this possibility, we bred *Tpbpa-Cre* females to males of the Cre reporter strain, *Gt(ROSA)26Sor*^{tm1Sor}, which has a *ROSA26-lox-stop-lox-lacZ* sequence, and examined *Gt(ROSA)26Sor*^{tm1Sor}; *Tpbpa-Cre* embryos and offspring for β-galactosidase activity, evidence of *Tpbpa-Cre* expression. In placentas, we observed β-galactosidase activity in spongiotrophoblasts, TGCs, and GlyTCs as previously reported (Simmons *et al.,* 2007). In the adult ovaries, we observed β-galactosidase activity in the granulosa cells (Figure 15B). We also noted infrequent *Rosa26-lacZ* recombination events in a small percentage of cells (~1-5%) in

other tissues or organs including the uterus (Figure 15C). We performed RNA *in situ* hybridization for *Tpbpa* to assess possible ovarian expression. In the absence of signal (Figure 15D), the ovarian phenotype was attributable to nonspecific promoter activity. Thus, to avoid possible confounding ovarian effects in *Notch2*^{floxlflox};*Tpbpa-Cre* mothers, all the data used to compare *Notch2*$^{floxl+}$;*Tpbpa-Cre* and *Notch2*^{floxlflox};*Tpbpa-Cre* offspring were generated from experiments utilizing *Notch2*$^{floxl+}$;*Tpbpa-Cre* mothers and comparisons were made between offspring of the same litter. Additionally, to ensure that *Notch2*$^{floxl+}$;*Tpbpa-Cre* mothers (n = 8) had normal reproductive function, we confirmed that they exhibited normal birth rates in comparison to *Notch2*^{floxlflox} mothers (wild-type; n = 7) (8.38 +/- 1.1 vs. 8.44 +/- 2.6; p = 0.95).

In the Absence of Notch2, TGCs and GlyTCs Failed to Invade Maternal Spiral Arterioles, which was Associated with Reduced Canal Size and Placental Perfusion

To assess whether trophoblast differentiation/invasion failed in *Notch2*^{floxlflox};*Tpbpa-Cre* placentas, we used RNA *in situ* hybridization to survey lineage-specific markers. No overt differences were observed at E9.5 and E12.5 between *Notch2*$^{floxl+}$, *Notch2*$^{floxl+}$;*Tpbpa-Cre* and *Notch2*^{floxlflox};*Tpbpa-Cre* placentas with regard to the presence/absence of markers of labyrinthian trophoblast cell types (*Gcm1*, *Hand1*), spongiotrophoblasts (*Tpbpa*), TGCs (*Prl3d1*, *Prl3b1*, and *Prl2c2*), or GlyTCs (*Pcdh12*) (Figure 16 and data not shown). However, while TGCs and GlyTCs of *Notch2*$^{floxl+}$;*Tpbpa-Cre* placentas robustly invaded maternal spiral arterioles at E12.5 (Figure 17A and 17C; enlarged in 17E and 17G, respectively), this process failed in the large majority of the *Notch2*^{floxlflox};*Tpbpa-Cre* placentas (Figure 17B and 17D; enlarged in 17F and 17H, respectively).

Accordingly, we explored the functional consequences of these observations. Specifically, we looked for abnormalities in the structure of the trophoblast-lined canals that transport maternal blood to the placenta. To obtain an integrated view of the anatomical basis of placental perfusion, we prepared vascular corrosion casts of the maternal circulation at E10.5 and E14.5 (Figure 18). Overall, the branching patterns in *Notch2*^{floxlflox};*Tpbpa-Cre* and *Notch2*$^{floxl+}$;*Tpbpa-Cre* placentas were similar; maternal blood entered the decidua through a tortuous network of ~8-12 interconnected spiral arterioles that converged into ~1-4 canals at the junctional zone boundary before spreading into a sinusoidal network at the base of the labyrinth. Given the complexity of the spiral artery network, we focused our analysis on the terminal portions of the canals. At E10.5, the canals in *Notch2*$^{floxl+}$;*Tpbpa-Cre* placentas (Figure 18A; magnified in Figure 18C) were larger than those in *Notch2*^{floxlflox};*Tpbpa-Cre* placentas (Figure 18B; magnified in 18D). We noted similar differences between *Notch2*$^{floxl+}$;*Tpbpa-Cre* (Figure 18E; magnified in 18G) and *Notch2*^{floxlflox};*Tpbpa-Cre* animals (Figure 18F; magnified in 18H) at E14.5. These results were quantified by translating the estimated vessel diameters into cross-sectional areas (Figure 18I). The results showed significant decreases in *Notch2*^{floxlflox};*Tpbpa-Cre* placentas at E10.5 (40%) and E14.5 (34%). No significant differences were observed between *Notch2*$^{floxl+}$;*Tpbpa-Cre* (n = 14) and *Notch2*^{floxlflox};*Tpbpa-Cre* (n = 11) animals in the average number of canals per placenta (3.2 +/- 1.2 vs. 2.9 +/- 1.0; p = 0.51).

The reduced canal size in *Notch2*^{floxlflox};*Tpbpa-Cre* placentas suggested that placental perfusion might be compromised in these animals. To test this theory, we performed experiments to estimate possible differences by injecting a 70 KDa fluorescein-conjugated dextran via the tail vein and measuring its short-term accumulation within the labyrinth at E12.5 (Plaks *et al.,* 2010). Analysis of placental

tissue sections revealed that, *Notch2*$^{floxl+}$;*Tpbpa-Cre* animals (Figure 19A and 19B), as compared to *Notch2*^{floxlflox};*Tpbpa-Cre* animals (Figure 19C and 19D) exhibited visibly increased fluorescence intensity. While we did not observe any differences in the relative size of the placental labyrinth or its vascular spaces between *Notch2*^{floxlflox};*Tpbpa-Cre* and *Notch2*$^{floxl+}$;*Tpbpa-Cre* placentas, quantification of the total labyrinthian-FITC signal showed that *Notch2*^{floxlflox};*Tpbpa-Cre* placentas accumulated 23% less of the fluorescein-conjugated dextran (Figure 19E). Together, the results of the marker analyses, vascular corrosion casting, and placental perfusion experiments support a possible causal relationship between *Notch2*-directed trophoblast invasion of spiral arteries and corresponding increases in placental perfusion.

Spiral Artery-Associated CTBs Failed to Express JAG1 in PE

Based on the mouse data, we tested the hypothesis that the faulty CTB differentiation/invasion observed in PE is associated with alterations in the expression of a subset of Notch molecules. As we previously described, preterm labor (PTL) cases, which we used as controls, were associated with normal levels of CTB interstitial, perivascular (near or around the vessels), and endovascular invasion (Zhou *et al.,* 2007) (Figure 20A-C). Also, CTB differentiation in PTL is normal as are gene expression patterns in the basal plate (Winn *et al.,* 2009). In contrast, CTB invasion was variably reduced in severe preeclampsia (SPE) and in the hemolysis, elevated liver enzymes, and low platelets syndrome (HELLP). In some instances, CTB invasion failed altogether. In others, CTBs were either confined to perivascular spaces (Figure 20D), exhibited limited endovascular invasion (Figure 20E), or transformed maternal arteries as in normal pregnancy (Figure 20F). To assess the expression of Notch family

members we used immunolocalization and RNA *in situ* hybridization approaches. We failed to detect any differences between cases and controls in CTB *NOTCH2-4* and *DLL4* expression patterns and staining intensities (data not shown). Similar to our observations in second trimester biopsies, the majority of perivascular and endovascular CTBs exhibited robust *JAG1* mRNA expression in PTL samples (Figure 20A-C). However, a CTB *JAG1* signal was absent in many vessels from PE cases (Figure 20D-F) regardless of the extent of vascular remodeling. We confirmed these findings at the protein level (Figure 20G and 20H). We calculated the percentage of *JAG1*-positive CTB-modified vessels in individual PTL and PE cases (Figure 20I and Table 6). 100% of modified vessels in each of 6 PTL control cases contained *JAG1*-positive CTBs. This fraction was reduced to 56% in 10 SPE cases and to 26% in 3 HELLP cases. Taken together, the correlation between reduced *JAG1* expression and failed vascular remodeling in PE suggests that Notch signaling plays a functional role in remodeling of human spiral arterioles.

Discussion

The success of human pregnancy critically depends on the unique actions of CTBs that, through their aggressive invasion/remodeling of vessels in the uterine wall, incorporate the placenta into the maternal circulation. Given that this phenomenon is consistently rudimentary in uterine veins, where CTB invasion progresses only as deep as is necessary to complete the utero-placental circulation, it is clear that CTBs have evolved the machinery to distinguish between vessel types and target arteries. Our work provides new insights into the mechanisms in terms of Notch signaling.

The first evidence that Notch might be an important regulator of CTB differentiation/invasion came from experiments in which we profiled Notch expression in tissue sections of the human placenta and in isolated CTBs that were differentiating *in vitro*. Notably, multiple Notch pathway components were similarly expressed by CTBs in both contexts and were precisely modulated during specific stages of the differentiation/invasion process. Functional inhibition in cultured CTBs confirmed that Notch signaling was required for interstitial CTB invasion and *EFRNB2* expression. To understand Notch function during endovascular invasion, we used a mouse model, first demonstrating that endovascular trophoblast populations possessed the highest levels of Notch activity and, further, that Notch expression patterns were similar in both species. Since *Notch2* was the only receptor upregulated during mouse trophoblast differentiation, we targeted this molecule for deletion in the invasive trophoblast lineages. Unexpectedly, *Notch2*$^{floxl+}$;*Tpbpa-Cre* and *Notch2*^{floxlflox};*Tpbpa-Cre* embryos were lost in proportion to the number of *Notch2*^{floxlflox};*Tpbpa-Cre* offspring, suggesting that failures of individual feto-placental units had litter-wide effects. *Notch2* proved to be a critical determinant of endovascular invasion; TGCs and GlyTCs from *Notch2*^{floxlflox};*Tpbpa-Cre* placentas failed to invade maternal spiral arterioles in its absence. We also found that failed endovascular invasion was associated with decreased canal size in *Notch2*^{floxlflox};*Tpbpa-Cre* animals, a likely cause of the observed decline in placental perfusion. Having shown that Notch signaling was required for trophoblast endovascular invasion in the mouse, we investigated the expression of family members in PE, which is associated with failures in this process. The results showed that artery-associated CTBs often lacked JAG1 expression. To our knowledge, JAG1 is the only marker that distinguishes between endovascular CTBs in normal pregnancies and those complicated by PE.

Notch functions in other cellular contexts offer unique insights into how these signaling pathways specify trophoblast identity and regulate endovascular invasion. *Notch2* is the only receptor that has not been associated with arterial identity (Villa *et al.,* 2001). In developing vascular beds, Notch signaling in EC progenitors promotes their assumption of arterial identity, which is characterized by *Efrnb2* expression in the absence *Ephb4*. The converse is observed in venous endothelium, helping to organize arterio-venous boundaries through repulsive interactions generated through bi-directional signaling between adjacent cells. We previously demonstrated that *EFRNB2/EPHB4* play similar roles in directing CTB invasion away from the placenta and toward uterine spiral arterioles (Red-Horse *et al.,* 2005). Here, we showed that Notch plays an upstream role in regulating CTB *EFRNB2* expression.

The striking upregulation of CTB JAG1 expression and Notch activity in the endovascular trophoblast populations suggests that these placental cells experience physiological cues that promote Notch signaling and subsequent *EFRNB2*-dependent endovascular invasion. Shear stress and cyclic strain, which are high in uterine spiral arterioles and low in uterine veins during pregnancy, offer possible explanations as to how Notch signaling is initiated in the arteries. In ECs, these forces rapidly enhance Notch receptor cleavage/activation, increase expression of Notch receptors and ligands, and promote Notch-dependent *EFRNB2* upregulation (Masumura *et al.,* 2009; Morrow *et al.,* 2007; Wang *et al.,* 2007). Interestingly, ligand endocytosis potentiates cleavage and activation of Notch receptors, leading several groups to propose that mechanical forces expose the S2 cleavage site within the Notch receptor (Kopan and Ilagan, 2009). Thus, it is possible that cyclic strain and shear stress experienced by CTBs near spiral arterioles may provide a mechanical force that potentiates Notch activation, JAG1 upregulation, and EFRNB2-dependent signaling. In this regard, our attempts to

modulate CTB expression of Notch family members with shear stress were not successful. Likewise, CTB co-culture with ECs or decidual cells, and in a low oxygen tension environment failed to upregulate JAG1 expression. Thus, it is likely that a complex interplay among cell types and physiologic factors is required. Although we are trying to develop this aspect of our model, as yet our human model does not enable analysis of the terminal steps in CTB endovascular invasion.

Notch2 function is required for mouse placental development (Hamada *et al.,* 2007). Tetraploid complementation, in which *Notch2*-deficient embryos were provided with wild-type placentas, revealed placental insufficiency as the primary cause of lethality. Interestingly, *Notch2*$^{-/-}$ animals exhibited dramatic reductions in maternal blood spaces within the placental labyrinth without obvious defects in the differentiation of labyrinthian trophoblasts, spongiotrophoblasts, or TGCs. However, the mechanism of placental insufficiency remained to be elucidated. Our observation that Notch activity was highest in the endovascular trophoblast populations suggested that this remodeling process played an important role in the phenotypic alterations that were originally observed in *Notch2*$^{-/-}$ placentas. We addressed this possibility by specifically eliminating *Notch2* in this population. Our experiments revealed similar phenotypes in terms of the timing of embryo loss and reduced accumulation of maternal blood in the labyrinth, but differed in that we did not observe changes in the size of the maternal sinusoidal spaces. Rather, our study uniquely identified deficits in endovascular trophoblast invasion and decreases in the cross-sectional area of the vascular canals that supply blood to the labyrinth. The disparate phenotypic outcomes of the two gene deletion strategies may highlight unique functions of endovascular and labyrinthian *Notch2* activity; labyrinthian cells appear to play a distinct role in organizing the sinusoidal blood spaces, while endovascular trophoblasts coordinate maternal increases in blood supply.

Interestingly, disrupting blood flow to individual placentas had litter-wide effects on pregnancy outcome. The frequency of fetal resorption correlated with the percentage of *Notch2*^{floxlflox};*Tpbpa-Cre* offspring in the litter. Unexpectedly, fetal loss was equally distributed among littermates regardless of genotype. As mice with *Notch2* haploinsufficiency are viable (Witt *et al.,* 2003), these results suggested that reducing blood flow to *Notch2*^{floxlflox};*Tpbpa-Cre* offspring had negative effects on the survival of both *Notch2*$^{floxl+}$;*Tpbpa-Cre* and *Notch2*^{floxlflox};*Tpbpa-Cre* animals. While we have not yet identified the mechanism of the observed litter-wide lethality, it is well established that endovascular trophoblast invasion produces local decreases in vascular resistance through the arteries that supply each fetus. Conversely, failed vascular transformation is associated with local increases in vascular tone that drive parallel systemic changes. As such, these effects could account for our finding. This theory is supported by observations made in the reduced utero-placental perfusion model (RUPP) in which the uterine blood flow of pregnant rats is surgically reduced. RUPP increases sensitivity to vasoactive factors at both local and systemic levels, which results in hypertension (Anderson *et al.,* 2005; Crews *et al.,* 2000). These findings were further substantiated by a recent study of placental gene expression in the Norway Brown rat (Goyal *et al.,* 2010), a strain that exhibits significantly decreased trophoblast vascular invasion. Compared to control strains, placentas of these animals secrete increased levels of vasoconstrictive factors and decreased amounts of vasodilators. Additionally, they have a much higher rate of fetal loss. Taken together, these studies may explain how local reductions in utero-placental blood flow can produce systemic changes in vascular contractility that could produce litter-wide effects.

Our findings that *Notch2*^{floxlflox};*Tpbpa-Cre* placentas failed to adequately remodel maternal blood vessels, which resulted in reduced placental perfusion, suggested that

aberrations in the expression of Notch family members might be associated with PE. One other investigator who has addressed this possibility reported expression patterns that were markedly different from those we observed at both protein and RNA levels (Cobellis *et al.,* 2007; De Falco *et al.,* 2007). Specifically, we found that the absence of *JAG1* expression was a common feature of perivascular and endovascular CTBs in PE. The distinctive expression pattern of *JAG1* combined with the failure of endovascular remodeling in PE, suggests that Notch signaling is a critical component of this unusual process. Although it is difficult to determine whether altered *JAG1* expression in PE is a prerequisite or byproduct of failed endovascular invasion, the phenotype of the *Notch2*$^{flox/flox}$;*Tpbpa-Cre* placenta supports a causal role.

In summary, we provide novel evidence that Notch signaling is a critical component of the process whereby fetal trophoblast cells invade and remodel maternal blood vessels during pregnancy. Furthermore, failure of this physiological transformation in the absence of *Notch2* is associated with reduced vessel diameter and placental perfusion, findings that support the conclusion that trophoblasts coordinate increases in maternal vascular supply through the progressive invasion and the resultant dilation of maternal vessels. The finding that peri- and endovascular CTBs often fail to express JAG1 in PE provides further evidence that defects in Notch signaling are an important part of the pathogenesis of this pregnancy complication.

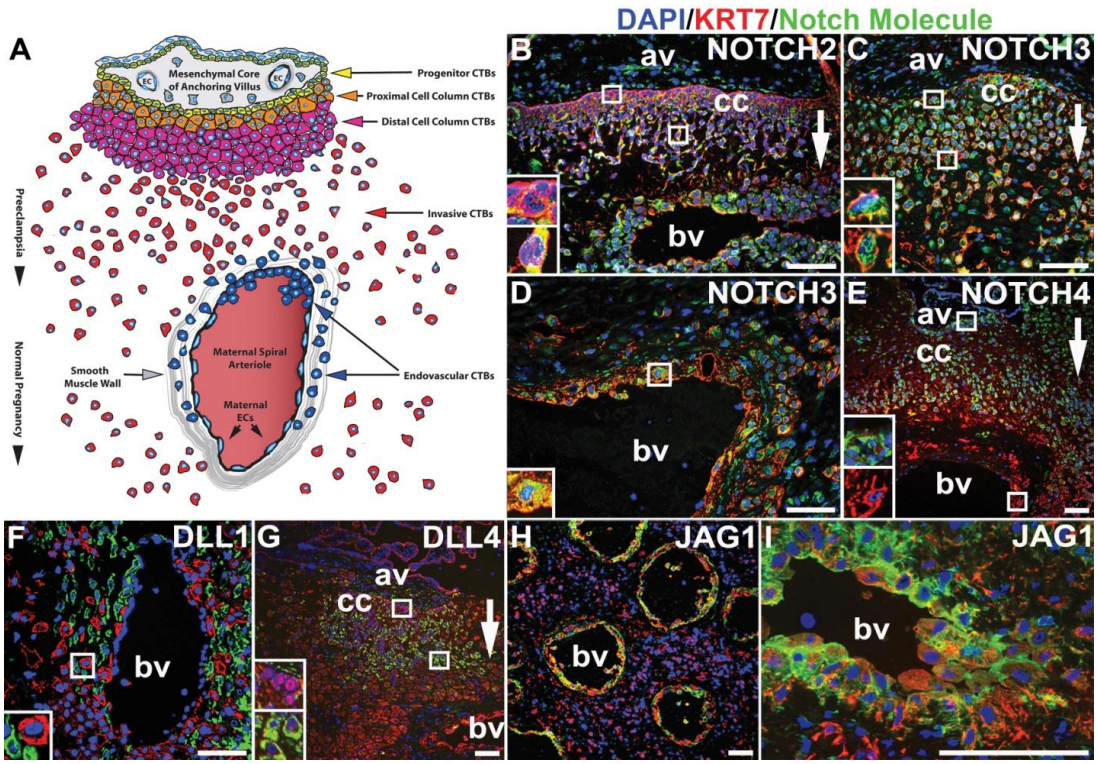

Figure 10. *CTBs Modulated Expression of Notch Receptors/Ligands as they Invaded the Uterine Wall and Vasculature.*

(A) CTBs of anchoring chorionic villi differentiate as they invade the maternal uterus. Undifferentiated CTB progenitors (yellow) surround the mesenchymal cores of anchoring villi (av). These progenitors differentiate as they move into the proximal and distal regions of the cell columns (cc; orange and purple). Invasive CTBs (red) leave the columns and migrate through the uterine interstitium. Endovascular CTBs (blue) disrupt the smooth muscle layer of maternal blood vessels (bv) where they also replace ECs. The depth of CTB invasion in normal pregnancy and in preeclampsia is indicated by arrowheads. (B-I) Double indirect immunofluorescence was performed on tissue sections of 2nd trimester basal plate biopsies using antibodies that specifically reacted with KRT7 (red), expressed exclusively by trophoblasts, and Notch family members (green). Nuclei were labeled with DAPI (blue). Scale bars: 100 µm. The direction of invasion is indicated by arrows. (B) CTB progenitors (upper inset) upregulated NOTCH2 expression (lower inset) as they invaded the uterine wall and blood vessels. (C-D) CTBs expressed NOTCH3 at all stages of differentiation/invasion (insets). (E) CTB progenitors and cell columns (upper inset) expressed NOTCH4, which was downregulated in proximity to maternal BVs (lower inset). (F) DLL1 was expressed by maternal cells in the uterine wall that associated with CTBs (inset). (G) DLL4 immunoreactivity, which was absent in progenitors (upper inset), increased as CTBs entered the cell columns (lower inset) and declined with deeper invasion. (H and I) CTBs expressed JAG1 only in proximity to maternal spiral arterioles.

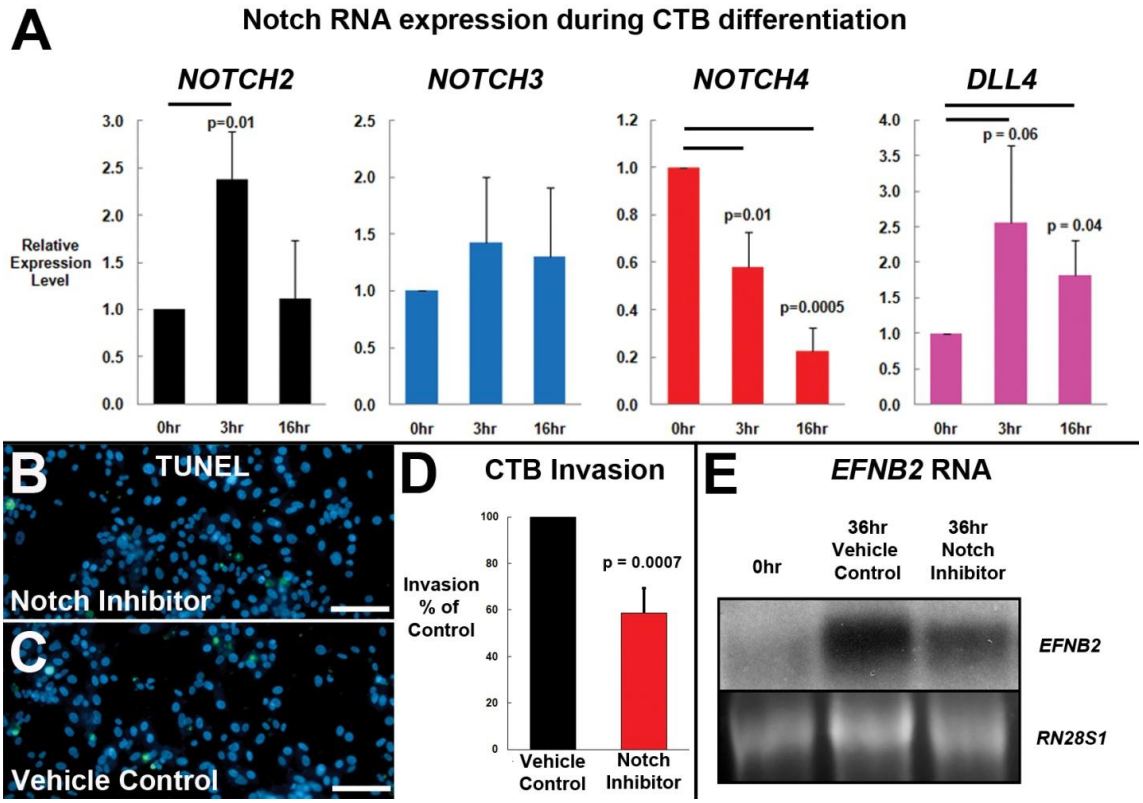

Figure 11. *Notch Inhibition Reduced CTB Invasion and EFRNB2 Expression In Vitro.*

(A) CTB expression of Notch family members at the RNA level was quantified as the cells differentiated in culture over a 16 hour (hr) period. *NOTCH2* and *DLL4* expression increased, *NOTCH3* expression levels remained constant, and *NOTCH4* expression decreased. (B and C) The level of CTB apoptosis, which was assessed by the TUNEL method, was negligible in experimental cultures that contained the Notch inhibitor (10 µM; B) and in control conditions (C). TUNEL-positive apoptotic cells were visualized with FITC (green) and cell nuclei were stained with DAPI (blue). Scale bars: 100 µm. (D) Notch inhibition reduced CTB invasion through Matrigel by 40% (n=10). (E) CTB *EFRNB2* RNA expression was measured by Northern blot hybridization at 0 hrs and after the cells had fully differentiated in culture (36 hrs) +/- the Notch inhibitor. As compared to controls, CTBs that were cultured in the presence of the inhibitor expressed lower levels. RN*28S1* RNA served as a loading control. Data are represented as mean +/- s.d.

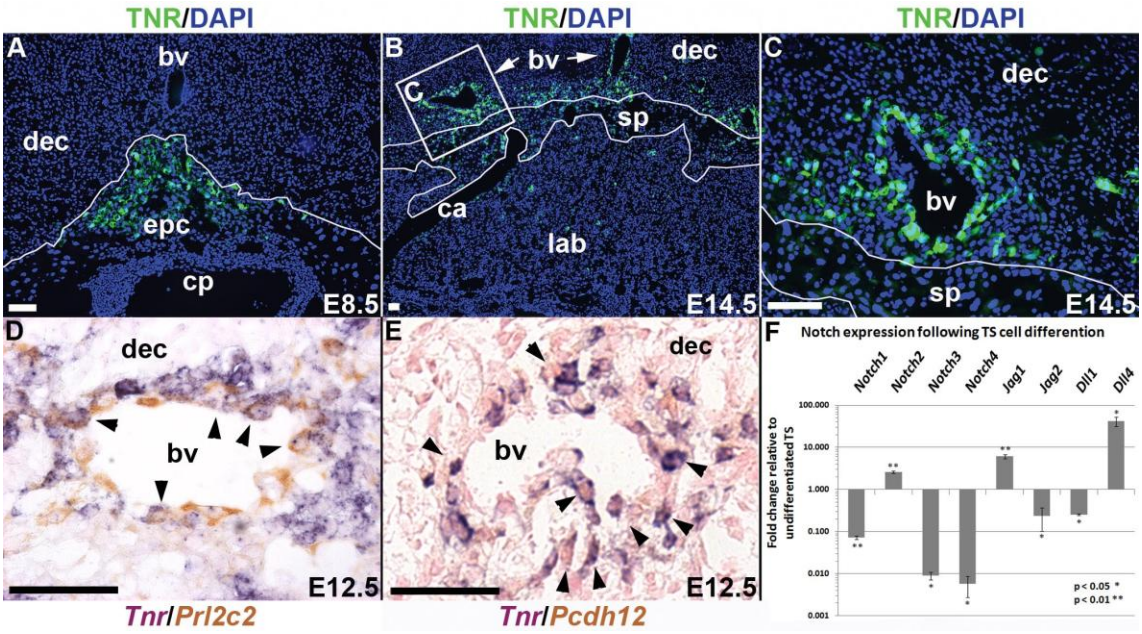

Figure 12. *Notch Activity was Highest in Invasive GlyTCs and TGCs that Associated with Uterine Spiral Arterioles.*

(A-C) Tissue sections from the placentas of *Tnr* mice enabled assessment of Notch activity (green) across gestation. Nuclei were stained with DAPI (blue). (A) At E8.5, Notch activity was observed in the ectoplacental cone (epc). (B and C) At E14.5, Notch activity was highest in invasive trophoblast cells surrounding maternal blood vessels (bv). (D and E) Double *in situ* hybridization was performed on serial sections of E12.5 *Tnr* placentas to detect Notch activity (purple) and expression of the mouse trophoblast lineage-specific markers *Prl2c2* (TGCs) or *Pcdh12* (GlyTCs; brown). Nuclei were stained with nuclear fast red. Arrowheads indicate double positive cells. A subset of spiral artery-associated TGCs (D) and GlyTCs (E) had Notch activity. (F) Mouse trophoblast stem cells regulated the expression of Notch family members as they differentiated *in vitro*. Notch RNA expression levels were normalized to *Rn18s*. *Notch2*, *Jag1*, and *Dll4* were upregulated with trophoblast differentiation; levels of all other family members declined. Data are represented as mean +/- s.d. Scale bars: 100 µm. ca; canal. cp; chorionic plate. dec; decidua. lab; labyrinth sp; spongiotrophoblast.

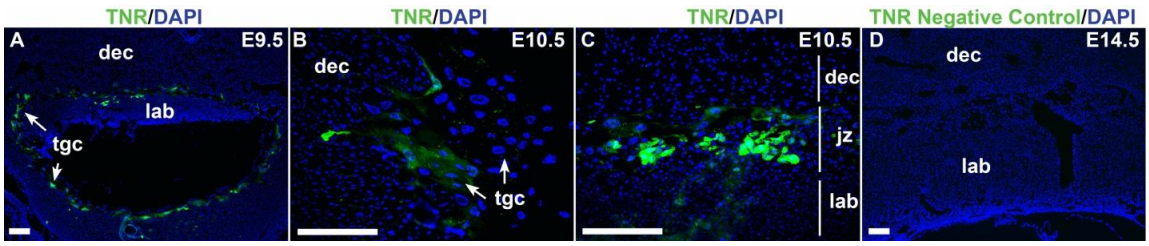

Figure 13. *Expanded Analysis of Transgenic Notch Reporter Placentas.*

(A-D) Tissue sections from the placentas of *Tnr* mice enabled assessment of Notch activity (green) across gestation. Nuclei were stained with DAPI (blue). Scale bars: 200 µm. (A) At E9.5, Notch activity was observed in parietal TGCs and in cells at the junctional zone (jz), which lies between the decidua (dec) and labyrinth (lab). At E10.5, Notch activity was observed in parietal TGCs (B) and in a growing population of trophoblast cells at the junctional zone (C). (D) No *Gfp* expression was observed in placentas that lacked the *Tnr* allele.

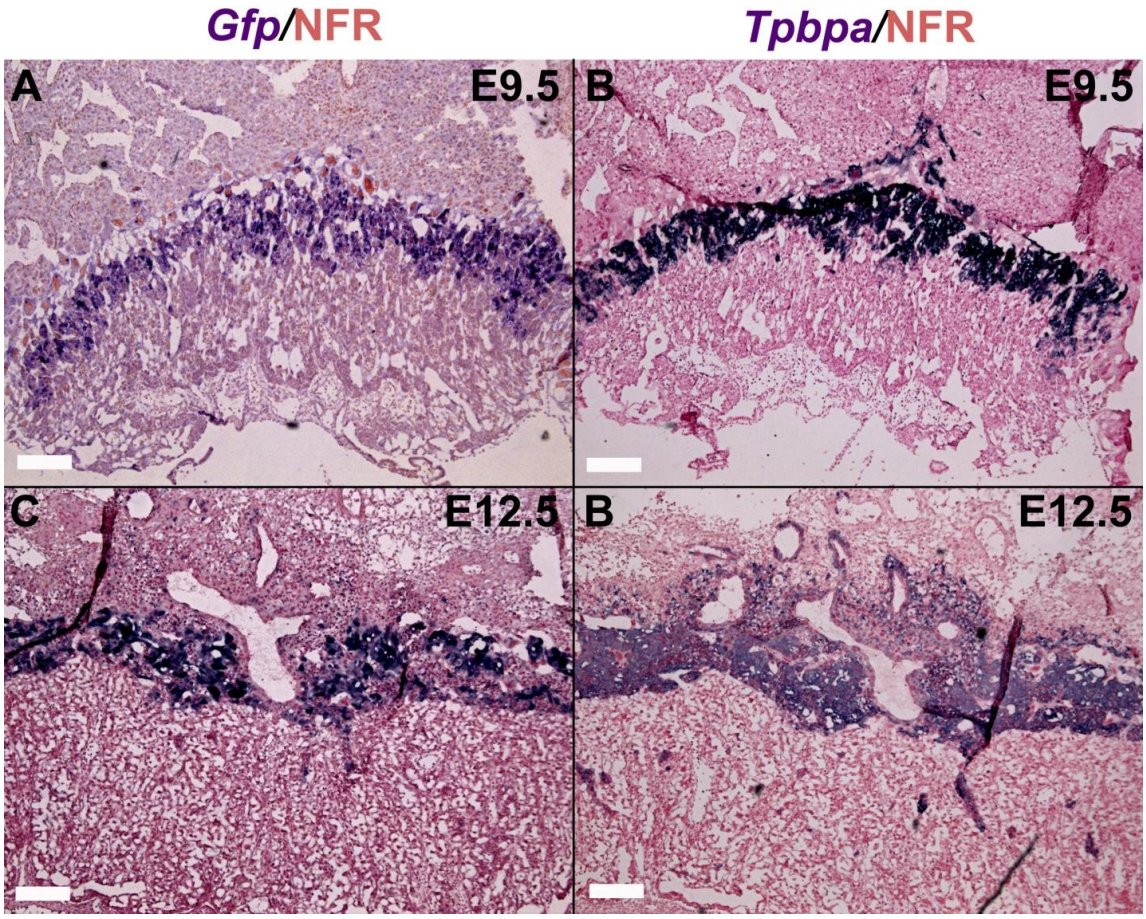

Figure 14. *In the Placenta, Tpbpa-Cre was Expressed in the Expected Pattern.*

(A-D) To assess *Tpbpa-Cre* expression, we performed serial RNA *in situ* hybridization for both *Tpbpa* and *Gfp*, which is also a component of the *Tpbpa-Cre* construct. Hybridization was visualized by NBT/BCIP staining (purple). Nuclei were stained with nuclear fast red (NFR). Scale bars: 200 µm. (A-B) At E9.5, *Gfp* (A) was expressed by nearly all spongiotrophoblast cells (B). (C-D) At E12.5, *Gfp* (C) was expressed by the majority of spongiotrophoblasts (D), although the signal was weaker or absent in a subset of these cells.

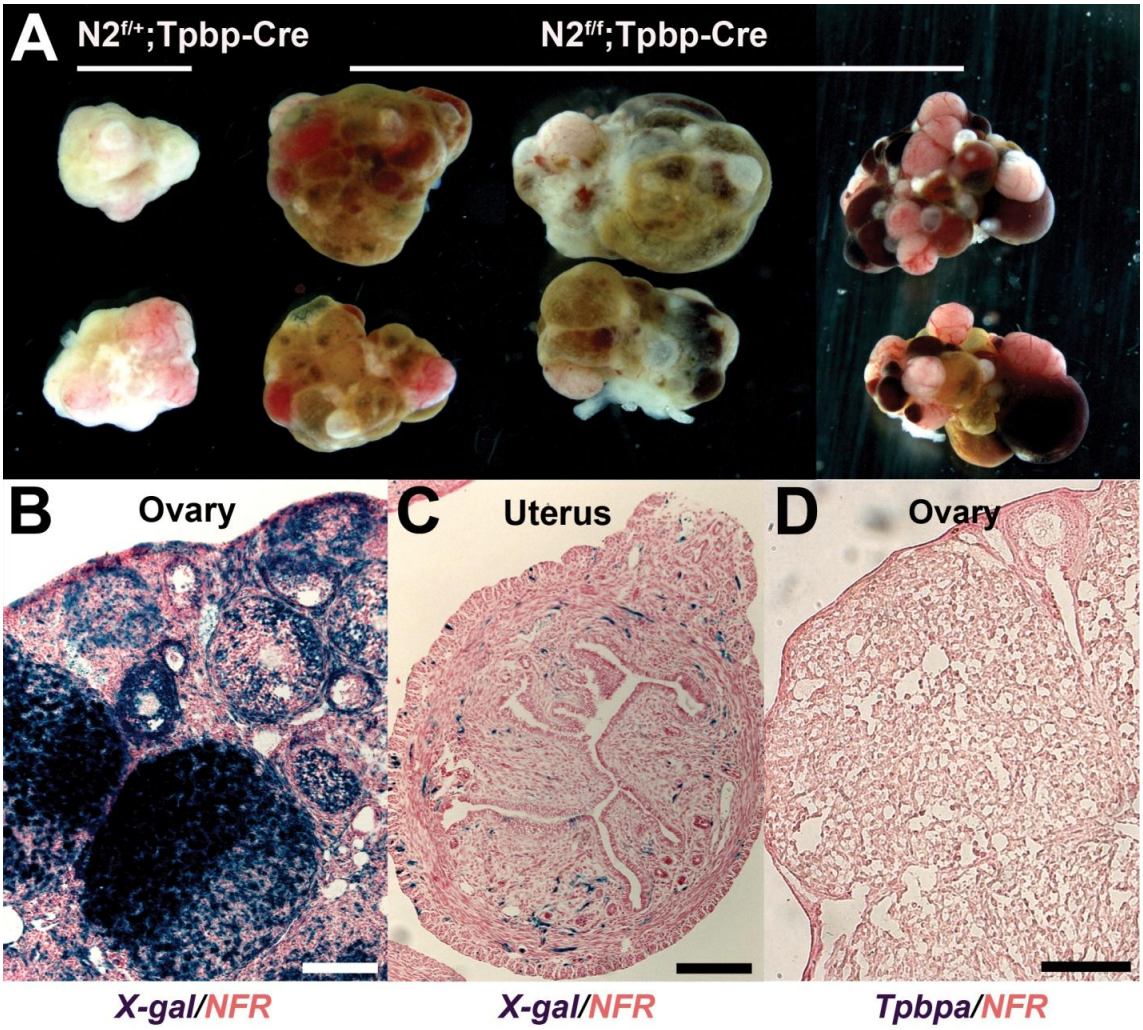

Figure 15. *Notch2^{floxlflox};Tpbpa-Cre Mice had Severe Ovarian Defects Resulting from Non-specific Tpbpa-Cre Promoter Activity.*

(A) *Notch2^{floxlflox}*;*Tpbpa-Cre* but not *Notch2^{floxl+}*;*Tpbpa-Cre* females exhibited severe ovarian defects, which included hemorrhagic and cystic follicles. (B and C) To detect whether ovarian (B) and uterine (C) tissues expressed *Tpbpa-Cre*, we bred offspring from *Tpbpa-Cre* females and *Gt(ROSA)26Sor^{tm1Sor}* males. X-gal staining of tissue sections from their adult female progeny revealed widespread *Tpbpa-Cre/Rosa26* recombination in the ovarian granulosa cells and much lower levels in the uterus. (D) *In situ* hybridization on sections of adult ovaries failed to detect *Tpbpa* RNA. Scale bars: 200 µm

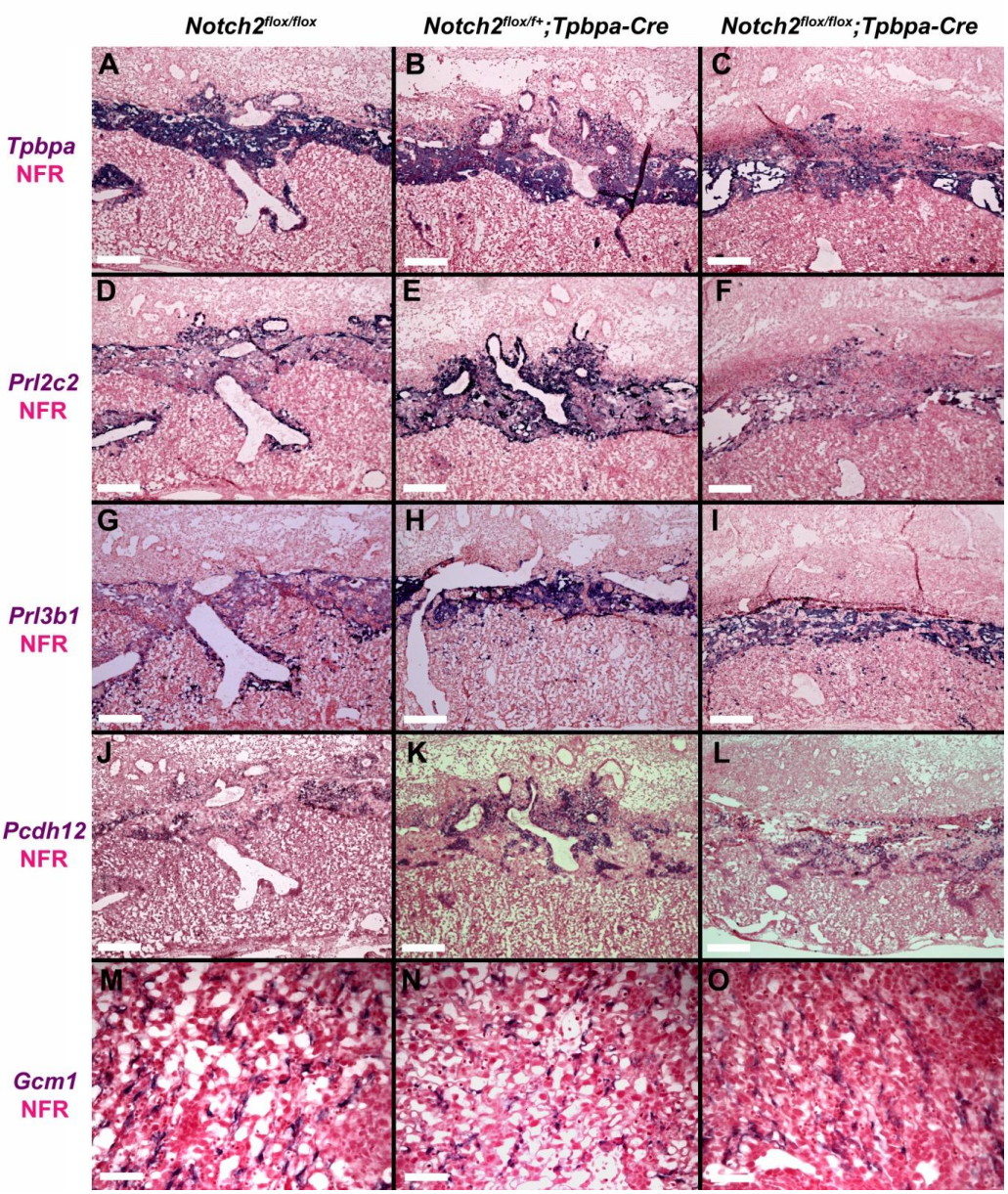

Figure 16. *Trophoblast Lineage Marker Analysis in Notch2^{floxlflox}, Notch2^{floxl+};Tpbpa-Cre, and Notch2^{floxlflox};Tpbpa-Cre placentas .*

(A-O) RNA *in situ* hybridization for trophoblast lineage-specific markers was performed on tissue sections of E12.5 *Notch2^{floxlflox}, Notch2^{floxl+};Tpbpa-Cre,* and *Notch2^{floxlflox};Tpbpa-Cre* placentas. Hybridization was visualized by NBT/BCIP staining (purple). Nuclei were visualized with nuclear fast red (NFR). Scale bars: 400 µm, (A-L); 80 µm, (M-O). No differences were observed between *Notch2^{floxlflox}, Notch2^{floxl+};Tpbpa-Cre,* and *Notch2^{floxlflox};Tpbpa-Cre* placentas with regard to the presence or absence of cells expressing *Tpbpa* (A-C), *Prl2c2* (D-F), *Prl3b1* (G-I), *Pcdh12* (J-L), or *Gcm1* (M-O). TGCs that expressed *Prl2c2* (F) and GlyTCs that expressed *Pcdh12* (L) in *Notch2^{floxlflox};Tpbpa-Cre* placentas failed to invade maternal spiral arterioles.

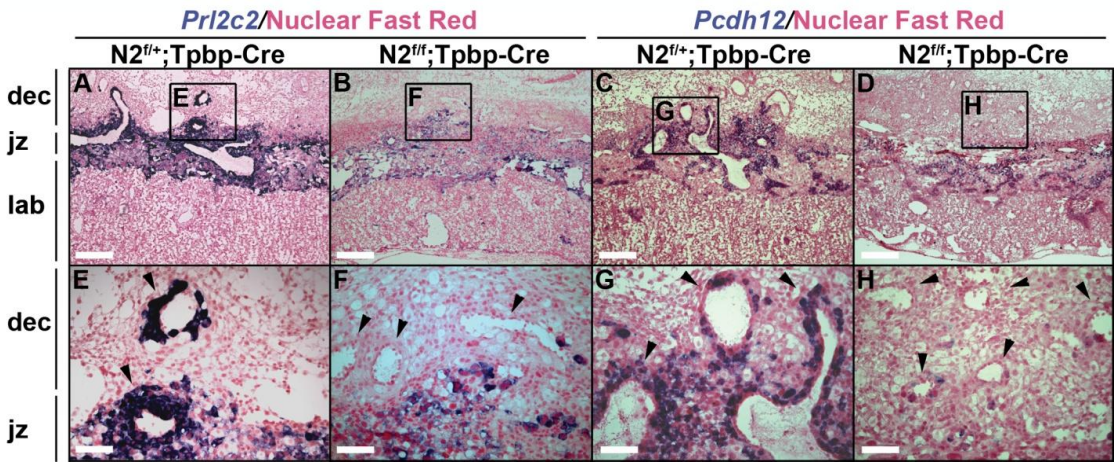

Figure 17. *Conditional Deletion of Notch2 in Invasive Trophoblasts Reduced TGC and GlyTC Invasion of Spiral Arterioles.*

(A-H) *In situ* hybridization was performed on tissue sections of E12.5 *Notch2*$^{floxl+}$;*Tpbpa-Cre* and *Notch2*^{floxlflox};*Tpbpa-Cre* placentas for the TGC marker, *Prl2c2* (A and B, magnified in E and F, respectively), and the GlyTC marker, *Pcdh12* (C and D, magnified in G and H, respectively). Hybridization was visualized by NBT/BCIP staining (purple). Nuclei were stained with nuclear fast red. The decidua (dec), junctional zone (jz), and labyrinth (lab) are shown. In *Notch2*^{floxlflox};*Tpbpa-Cre* mice, TGCs and GlyTCs failed to invade spiral arterioles (arrowheads). Scale bars: 400 µm, (A-D); 100 µm, (E-H).

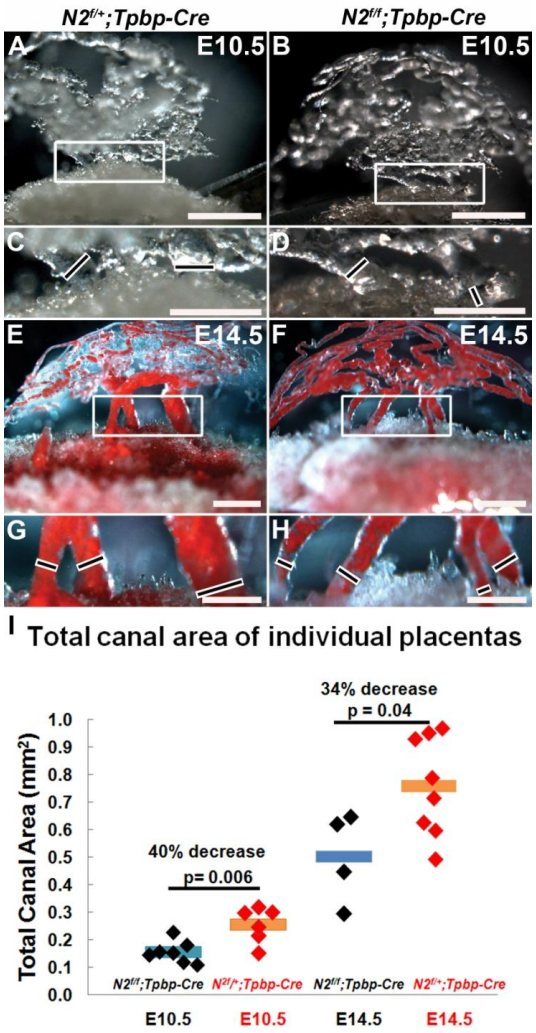

Figure 18. *The Trophoblast-Lined Vascular Canals that Supply Blood to the Placenta were Smaller in Notch2^{floxlflox};Tpbpa-Cre Mice.*

(A-H) Vascular corrosion casts of the maternal blood spaces of the placenta were prepared at E10.5 and E14.5. In the placentas of both *Notch2*$^{floxl+}$;*Tpbpa-Cre* and *Notch2*^{floxlflox};*Tpbpa-Cre* offspring, a complex array of maternal spiral arterioles converged into several large canals before branching into the labyrinthian sinusoids. At E10.5 the canals in *Notch2*$^{floxl+}$;*Tpbpa-Cre* placentas (A; enlarged in C) were larger than those in *Notch2*^{floxlflox};*Tpbpa-Cre* placentas (B; enlarged in D). We noted similar differences between *Notch2*$^{floxl+}$;*Tpbpa-Cre* (E; enlarged in G) and *Notch2*^{floxlflox};*Tpbpa-Cre* animals (F; enlarged in H) at E14.5. Scale bars: 1 mm, (A, B, E, and F); 500 µm, (C, D, G, and H). (I) The vessel diameter was used to calculate the cross-sectional areas of the canals. At E10.5 and E14.5, vessels in *Notch2*^{floxlflox};*Tpbpa-Cre* placentas were 40% and 32% smaller, respectively, as compared to *Notch2*$^{floxl+}$;*Tpbpa-Cre* animals. Group means are represented as solid bars.

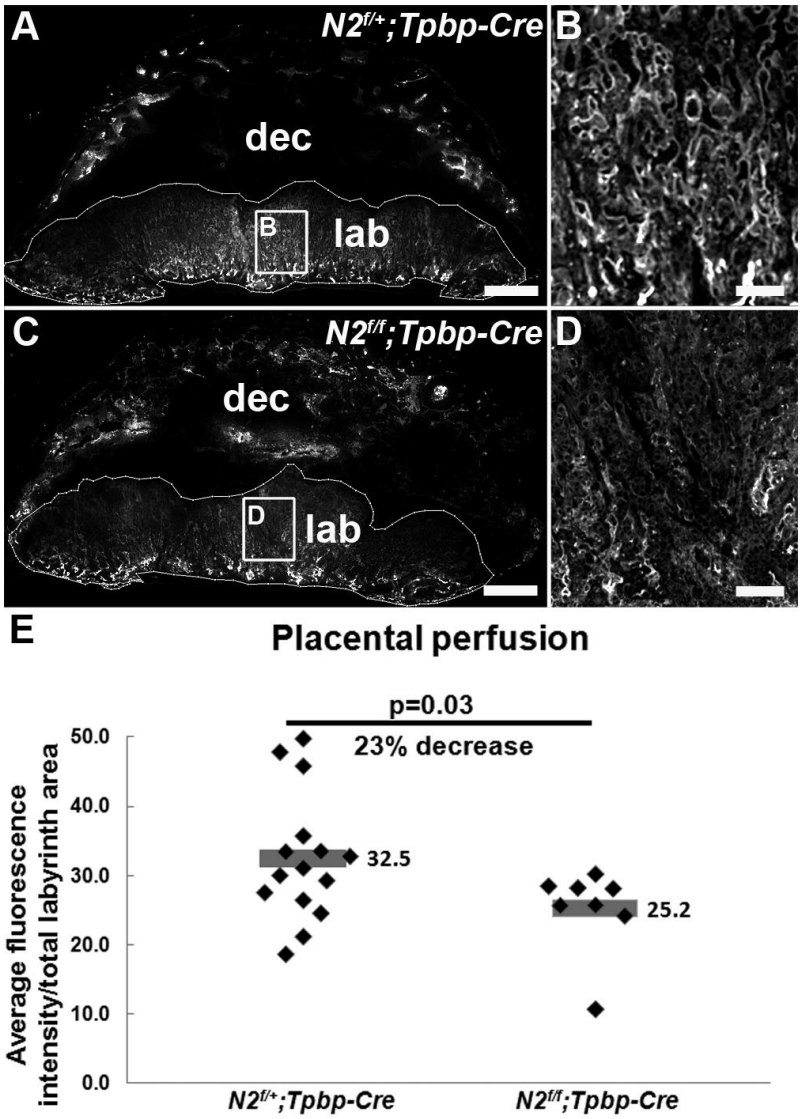

Figure 19. *Placental Perfusion was Compromised in Notch2^{floxlflox};Tpbpa-Cre Animals.*

(A-D) To approximate placental perfusion, animals were injected i.v. with fluorescein-conjugated dextran and tissue sections of the labyrinth were analyzed for the short-term (3 minute) accumulation of this tracer. The FITC signal, which appeared to be stronger in the labyrinth (outlined) of *Notch2^{floxl+}*;*Tpbpa-Cre* placentas(A; enlarged in B) as compared to *Notch2^{floxlflox}*;*Tpbpa-Cre* littermates (C; enlarged in D), was quantified by using ImageJ (E). Placental perfusion was reduced ~23% in *Notch2^{floxlflox}*;*Tpbpa-Cre* placentas. Group means are represented as solid bars. Scale bars: 1 mm, (A and C); 200 µm, (B and D).

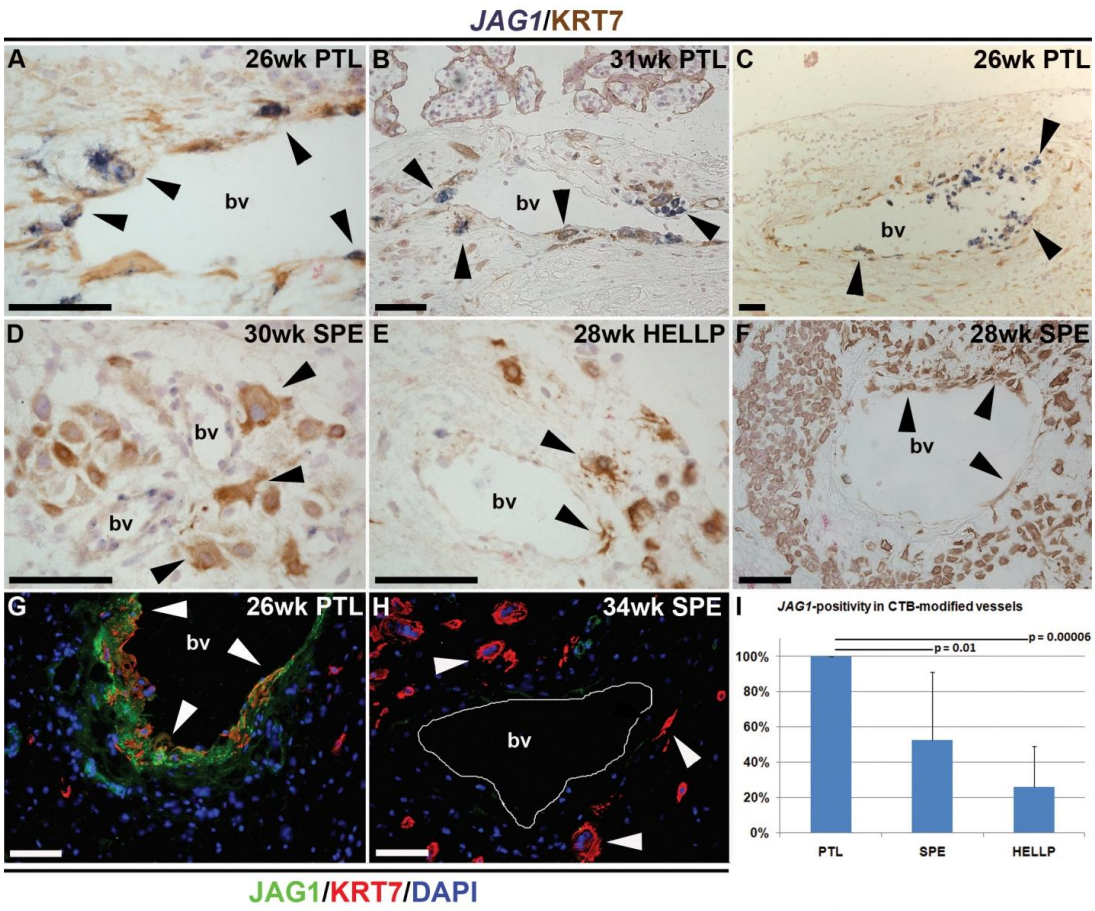

Figure 20. *In PE, Endovascular and Perivascular CTBs Failed to Express JAG1.*

(A-F) Dual *JAG1 in situ* hybridization (purple) and KRT7 immunolocalization (brown) were performed on tissue sections of basal plate biopsies from PTL and PE cases (SPE and HELLP). (A-C) In PTL, endovascular and perivascular CTBs (arrowheads) expressed *JAG1.* (D-F) In PE, fewer vessels were modified and many of the associated CTBs lacked *JAG1* expression. (G and H) Double indirect immunolocalization of JAG1 and KRT7 confirmed these results at the protein level. Nuclei were stained with DAPI. (I) Tissue sections from 6 PTL, 10 SPE, and 3 HELLP cases were scored for the percent of modified maternal vessels that contained JAG1-positive CTBs. The mean decreased to 56% in SPE and to 26% in HELLP. Individual results are reported in Table 6. Data are represented as mean +/- s.d. Scale bars: 100 µm.

Parental Cross	Gestational Age	Resorptions	Implantation Sites	Litters Surveyed	Resorption Rate
Notch2^{floxl+};*Tpbpa-Cre* ♂	E9.5	0	2	1	0%
x	E10.5	1	26	3	4%
Notch2^{floxl+};*Tpbpa-Cre* ♀	E11.5	0	6	1	0%
	E12.5	0	7	1	0%
	E11.5-E12.5	**0**	**13**	**2**	**0%**
Notch2^{floxl+};*Tpbpa-Cre* ♀/♂	E9.5	1	11	2	9%
x	E10.5	8	59	9	14%
Notch2^{floxlflox};*Tpbpa-Cre* ♀/♂	E11.5	3	12	3	25%
	E12.5	20	68	7	29%
	E13.5	5	16	3	31%
	E14.5	12	39	5	31%
	E15.5	3	12	2	25%
	E11.5-E15.5	**43**	**147**	**20**	**29%**
Notch2^{floxlflox};*Tpbpa-Cre* ♂	E9.5	1	6	1	17%
x	E10.5	1	9	2	11%
Notch2^{floxlflox};*Tpbpa-Cre* ♀	E11.5	9	16	3	56%
	E12.5	12	19	2	63%
	E13.5	8	20	3	40%
	E14.5	1	1	1	100%
	E11.5-E14.5	**30**	**56**	**9**	**54%**

Table 2. *Characterization of the Timing of Embryonic Lethality in Notch2*$^{floxl+}$*; Tpbpa-Cre and Notch2*^{floxlflox}*;Tpbpa-Cre Embryos.*

Resorption rates were surveyed throughout mid-late gestation in litters that contained 25%, 50% or 100% *Notch2*^{floxlflox};*Tpbpa-Cre* progeny. Resorptions increased to maximal levels by E11.5 and occurred at the highest frequency in *Notch2*^{floxlflox};*Tpbpa-Cre* crosses.

Parental Cross	Resorptions	Implantation Sites	Litters Surveyed	Resorption Rate
Notch2^{floxl+};*Tpbpa-Cre* ♀ x *Notch2*^{floxlflox};*Tpbpa-Cre* ♂ (E11.5 on)	36	121	16	30% p = 0.59
Notch2^{floxlflox};*Tpbpa-Cre* ♀ x *Notch2*$^{floxl+}$;*Tpbpa-Cre* ♂ (E11.5 on)	7	26	4	27%

Table 3. *The Maternal Genotype Did Not Contribute to Embryonic Lethality Observed After E11.5 in Crosses that Produced 50% Notch2*^{floxlflox}*;Tpbpa-Cre Progeny.*

Outcome of *Notch2*$^{floxl+}$;*Tpbpa-Cre* x *Notch2*^{floxlflox};*Tpbpa-Cre* Litters	*Notch2*$^{floxl+}$;*Tpbpa-Cre* Offspring	*Notch2*^{floxlflox};*Tpbpa-Cre* Offspring	Total Offspring	Litters Surveyed
Live Births	67	66	133	18
	p = 0.94			
Resorptions (E10.5-15.5)	20	18	142	18
	p = 0.74			

Table 4. *Resorptions/Live Births were Evenly Distributed Between the Notch2*$^{floxl+}$*;Tpbpa-Cre and Notch2*^{floxlflox}*;Tpbpa-Cre Offspring of Notch2*$^{floxl+}$*;Tpbpa-Cre x Notch2*^{floxlflox}*;Tpbpa-Cre Litters.*

Embryo Weight (mg)		Placenta Weight (mg)	
Notch2^{floxl+};*Tpbpa-Cre*	*Notch2*^{floxlflox};*Tpbpa-Cre*	*Notch2*$^{floxl+}$;*Tpbpa-Cre*	*Notch2*^{floxlflox};*Tpbpa-Cre*
76+/-6	74+/-11	64+/-9	57+/-10
n=11	n=8	n=11	n=8
p = 0.62		p = 0.12	

Table 5. *Embryonic and Placental Weights Did Not Significantly Differ Between Notch2*$^{floxl+}$*;Tpbpa-Cre and Notch2*^{floxlflox}*;Tpbpa-Cre Animals at E12.5.*

The group mean weight is expressed in milligrams +/- s.d.

Diagnosis	Gestational Age (weeks)	CTB-Modified Vessels	JAG1+ CTB-Modified Vessels	% JAG1+ vessels
PTL	26	7	7	100%
PTL	26	12	12	100%
PTL	28	4	4	100%
PTL	31	3	3	100%
PTL	33	1	1	100%
PTL	34	3	3	100%
SPE	28	4	1	25%
SPE	28	4	3	75%
SPE	29	3	3	100%
SPE	29	7	6	86%
SPE	30	5	0	0%
SPE	31	4	4	100%
SPE	31	2	1	50%
SPE	31	6	4	67%
SPE	33	2	0	0%
SPE	33	4	1	25%
HELLP	24	31	0	0%
HELLP	28	3	1	33%
HELLP	34	9	4	44%

Table 6. *The Percentage of JAG1-Positive CTB-Modified Vessels is Decreased in PE, as Shown by the Data Collected for Individual Cases.*

Tissue sections from 6 PTL, 10 SPE, and 3 HELLP cases were scored for the percent of modified maternal vessels that contained JAG1-positive CTBs.

RT-qPCR primers used in human and mouse experiments

Target Gene	Forward Primer 5'-3'	Reverse Primer 5'-3'	Product Size
NOTCH1	CTCACCTGGTGCAGACCCAG	GCACCTGTAGCTGGTGGCTG	383
NOTCH2	CAGTGTGCCACAGGTTTCACTG	GCATATACAGCGGAAACCATTCAC	456
NOTCH3	CGCCTGAGAATGATCACTGCTTC	TCACCCTTGGCCATGTTCTTC	352
NOTCH4	ATGACCTGCTCAACGGCTTC	GAAGATCAAGGCAGCTGGCTC	237
JAG1	GCTTGGATCTGTTGCTTGGTGAC	ACTTTCCAAGTCTCTGTTGTCCTG	386
JAG2	GCTATTTCGAGCTGCAGCTGAG	GCGGCAGGTAGAAGGAGTTG	236
DLL1	CTACACGGGCAGGAACTGCAG	CGCCTTCTTGTTGGTGTTCTTG	441
DLL4	CGGGTCATCTGCAGTGACAAC	AGTTGAGATCTTGGTCACAAAACAG	348
RN18S1	CGCCGCTAGAGGTGAAATTCT	CGAACCTCCGACTTTCGTTCT	101

Genotyping primers

Target Allele	Forward Primer 5'-3'	Reverse Primer 5'-3'	Product Size
Tnr and *Tpbpa-Cre*	CACATGAAGCAGCACGACTT	ACTGGGTGCTCAGGTAGTGG	385
Notch2$^{flox/+}$	TAGGAAGCAGCTCAGCTCACAG	ATAACGCTAAACGTGCACTGGAG	200/161
Gt(ROSA)26Sor^{tm1Sor}	CGCCCGTTGCACCACAGATG	CCAGCTGGCGTAATAGCGAAG	370

Table 7. *Primer Sequences*

Methods

Human Tissue Collection

All portions of this study were approved by the UCSF Institutional Review Board. Written informed consent was obtained from all tissue donors. Biopsies of normal placentas were either fresh-frozen for immunolocalization, paraformaldehyde-fixed for *in situ* hybridization or immediately processed for CTB isolation. Equivalent specimens were obtained from women who experienced either PTL, SPE, or HELLP using the clinical criteria and methods we published (Zhou *et al.,* 2007).

Immunofluorescence

Fresh-frozen basal plate biopsies were embedded and sectioned as described (Zhou *et al.,* 2007). Following fixation in cold methanol:acetone (1:6) for 5 minutes, sections were washed in PBS and nonspecific reactivity was blocked by incubation in 0.3% bovine serum albumin/PBS. They were incubated (overnight at 4°C) with anti-KRT7 (diluted 1:50; produced by the Fisher group) that reacts with all trophoblast populations and one of the following anti-Notch family antibodies diluted 1:200: NOTCH2 (R&D Systems, AF3735), NOTCH3 (Santa Cruz Biotechnology, sc-5593), NOTCH4 (Santa Cruz Biotechnology, sc-8643), JAG1 (Santa Cruz Biotechnology, sc-8303), DLL1 (Santa Cruz Biotechnologies, sc-9102), and DLL4 (Santa Cruz Biotechnology, sc-18640). Subsequently, the sections were rinsed in PBS, incubated with the appropriate species-specific secondary antibody conjugated to either fluorescein (Notch family members) or rhodamine (KRT7), washed in PBS, and mounted under Vectashield

containing DAPI. Controls were incubated with the primary or secondary antibody alone. Sections were photographed using a Leica DM5000B microscope.

Cell Isolation and Culture

Primary human CTBs were isolated and cultured up to 36 hours as described (Hunkapiller and Fisher, 2008). Mouse TS cells were cultured and differentiated using published methods (Maltepe *et al.,* 2005).

RT-qPCR

CTB and TS RNA samples were isolated using an RNeasy Plus kit (Qiagen). RNA concentration/quality was assessed using a Nanodrop spectrophotometer (Thermo-Scientific). cDNA libraries were prepared with 1 µg of RNA using the iScript kit (Biorad) and diluted 20-fold in water. SYBR green RT-qPCR reactions were carried out in triplicate. Reaction specificity was confirmed by determining the melting curve of the products or by gel electrophoresis. Differences among target expression levels were estimated by the ΔΔCT method with normalization to *RN18S1*. The primer sequences are described in Table 7.

TUNEL Assays

CTBs were cultured in either 1, 10, or 50 µM L-685,458 (Bachem), or DMSO alone. After 36 hours, the percentage of cells undergoing programmed cell death was

estimated using an *In situ* Cell Death Detection kit according to the manufacturer's instructions (Roche).

Invasion Assays

CTB invasion was assessed as described (Librach *et al.,* 1991). Cells were plated in either 10 µM L-685,458/0.1% DMSO or 0.1% DMSO and cultured for 36 hours.

Northern Blotting

RNA samples were prepared immediately before the CTBs were plated and after 36 hours in culture in medium containing either 10 µM L-685,458/0.1% DMSO or 0.1% DMSO. *EphrinB2* and *EphB4* mRNA levels were estimated by Northern blot hybridization using the methods and probes that we published (Red-Horse *et al.,* 2005). *RN28S1* levels served as controls.

Mice

All protocols were approved by the UCSF Institutional Animal Care and Use Committee. For timed pregnancies, the day of vaginal plug detection was considered as E0.5. For assessment of placental *Tnr* activity, *Tnr* males (Jackson Laboratories; *Tg(Cp-EGFP)25Gaia/J*) were bred to wild-type FVB/NJ females (Jackson Laboratories). For *Notch2* deletion experiments, *Tpbpa-Cre* mice (Simmons *et al.,* 2007) and *Notch2*$^{flox/flox}$ mice (McCright *et al.,* 2006) were crossed. The sequences of primers that

were used for genotyping are described in Table 7. Paraformaldehyde-fixed, frozen placentas (E7.5-E15.5) were prepared and the embryos were genotyped.

Evaluation of Tpbpa-Cre Expression

Tpbpa-Cre females were bred with *Gt(ROSA)26Sor*^{tm1Sor} males (Jackson Laboratories). Adult female F1 offspring were euthanized and ovarian and uterine tissues were embedded in OCT medium. Sections (5 µM) were fixed for 15 minutes in 0.1 M phosphate buffer (pH 7.3) supplemented with 5 mM EGTA, 2 mM $MgCl_2$, and 0.2% glutaraldehyde. Sections were washed (2x, 5 minutes) in 0.1 M phosphate buffer (pH 7.3) supplemented with 2 mM $MgCl_2$. Staining was performed overnight at 37°C in 0.1 M phosphate buffer (pH 7.3) with 2 mM $MgCl_2$, 5 mM $K_3[Fe(CN)_6]$, 5 mM $K_4[Fe(CN)_6]\bullet 3H_2O$, and 5-Br-4-Cl-3-indolyl-β-D-galactoside (1 mg/ml) (Invitrogen). Sections were counterstained with nuclear fast red, dehydrated, and mounted under Cytoseal 60 (Thermo-Scientific).

Generation of cDNAs and Probes for In situ Hybridization

Notch family cDNAs were amplified from CTB RNA by using the RT-qPCR primers described in Table 7, which included either a 5' T7 promoter sequence (forward primers; TAATACGACTCACTATAGGG) or a 5' T3 promoter sequence (reverse primers; AATTAACCCTCACTAAAGGG). Mouse cDNAs for *Prl2c2, Pcdh12* (Simmons *et al.,* 2008), *Gcm1* (Basyuk *et al.,* 1999), *Hand1* (Cross *et al.,* 1995), and *Tpbpa* (Lescisin *et al.,* 1988) were described. The cDNA for *Prl3b1* was a gift from J. Rossant and the

cDNA for *Prl3d1* was kindly provided by D. Linzer. cDNAs were used for *in vitro* digoxigenin probe synthesis according to the manufacturer's protocol (Roche).

RNA In Situ Hybridization and KRT7 Immunohistochemistry

Single probe RNA *in situ* hybridization was performed as previously described (Simmons *et al.,* 2007). cDNAs used for probe generation are described above. *JAG1* hybridizations were followed by KRT7 immunolocalization as described (Winn *et al.,* 2009). For double *in situ* hybridization, binding of the *Tnr* probe was detected by incubation with alkaline phosphatase-conjugated, anti-digoxigenin followed by NBT/BCIP staining. Bound antibody was heat-inactivated (65°C; 30 minutes) in maleic acid buffer/0.1% tween-20. Then the slides were incubated in 0.1 M glycine pH 2.2 for 30 minutes. Non-specific reactivity was blocked (Simmons *et al.,* 2008) and fluorescein-labeled *Prl2c2*/*Pcdh12* probes were detected following incubation with alkaline phosphatase-conjugated, anti-fluorescein (Roche, 1:2500) and INT/BCIP staining. Sections were counterstained with nuclear fast red and mounted under 50% glycerol in PBS.

Vascular Corrosion Casting

Notch2^{floxl+};*Tpbpa-Cre* females bred to *Notch2*^{floxlflox};*Tpbpa-Cre* males were euthanized on day 10.5 or 14.5 of pregnancy and vascular corrosion casts were made as described previously (Adamson *et al.,* 2002). Maternal canals were visualized by dissecting away venous and sinusoidal structures. The casts were photographed with a Leica MZ16 microscope, the diameter of individual canals was measured at the

narrowest point, and the cross-sectional area was calculated and summed for each placenta.

Placental Perfusion

Placental perfusion was estimated as described with the exceptions noted (Plaks *et al.,* 2010). At E12.5, *Notch2*$^{flox/+}$;*Tpbpa-Cre* females bred to *Notch2*$^{flox/flox}$;*Tpbpa-Cre* males were given a tail vein injection of 200 µl (2mg/ml) fluorescein-conjugated 70 KDa dextran (Invitrogen; D-1822). After 3 minutes, animals were euthanized. Placentas were dissected in cold PBS, fixed in Carnoy's solution, and embedded in paraffin. Sections (5 µM) were deparaffinized, rehydrated, and mounted in Vectashield medium containing DAPI. Multiple sections from different areas of the placentas were imaged with a Leica DMI6000B microscope at 20x magnification and a photomontage of the entire sample was created. Average fluorescence intensity within the labyrinth was calculated using ImageJ software.

Statistics

Differences between means were assessed using either a paired two-tailed student's t-test (alpha=0.05) for RT-qPCR and CTB invasion experiments or assuming equal variance for the perfusion and casting experiments.

Chapter 4: CTB Gene Expression Profiling Reveals Unique Changes in Preeclampsia

Introduction

Knowledge of the mechanisms that regulate CTB differentiation in normal pregnancy has enabled studies of the analogous processes in PE. Several reviews summarize the current state of knowledge regarding PE and the pressing importance of understanding the causes of this syndrome, which continues to be a primary driver of obstetric care in the developed world (Redman and Sargent, 2005; Ilekis *et al.,* 2007; Cetin *et al.,* 2011). This is due, in large part, to the sometimes rapid onset of PE—hence, the name preeclampsia (derived from the Greek *eklampsis*, sudden flash or development). Another important factor is the prevalence of this syndrome, which affects 5-8% of all pregnancies (Sibai *et al.,* 1997; American College of Obstetrics and Gynecology [ACOG], 2002). Accordingly, as pregnancy progresses, women are checked with increasing frequency for the signs and symptoms of PE. These include the new onset of hypertension and proteinuria. Additional signs and symptoms are observed in other forms of this pregnancy complication, *e.g.*, severe PE (SPE), which is diagnosed in women having at least one of the following additional criteria: elevated systolic blood pressure and/or diastolic pressure, proteinuria, neurological disturbances, elevated liver enzymes, evidence of hemolysis, renal impairment, thrombocytopenia, or pulmonary edema. The HELLP syndrome is associated with hemolysis, elevated liver enzymes and low platelet count. Finally, in addition to the maternal signs, there can be devastating effects on the fetus. For example, 15% of all preterm deliveries (<34 wks of

gestation) in the U.S. occur as the treatment of last resort for PE, because removal of the placenta is the only known cure (Goldenberg and Rouse, 1998).

Alterations in the expression patterns of numerous stage-specific antigens that play important roles in the mature human TB populations—STBs and/or invasive CTBs—have been described and we recently reviewed these data (Maltepe *et al.,* 2010). With regard to STBs, PE is associated with fundamental disturbance in basic processes such as the turnover of this population (Mayhew, 2009; reviewed in Gauster *et al.,* 2009). At a molecular level, cathepsin expression, which could play a role in this process, is perturbed (Varanou *et al.,* 2006). Other proposed mechanisms include reduced GCM expression (Chen *et al.,* 2004), which leads to parallels reductions in syncytin-mediated TB fusion (Langbein *et al.,* 2008). In PE, STBs exhibit increased staining for endoglin, a TGF-β co-receptor, and forced expression of this molecule produced a PE-like syndrome in rats (Venkatesha *et al.,* 2006). In contrast, human STB expression of adrenomedullin, a peptide vasodilator, goes down in PE (reviewed by Wilson *et al.,* 2004) and mice with reduced maternal ± fetal expression of this molecule also develop signs of PE including growth restriction (Li *et al.,* 2006). Lower STB expression of VEGF and VEGFR2 has also been described (Groten *et al.,* 2010). These findings led to the concept that PE is associated with an imbalance in angiogenic factors (Maynard *et al.,* 2008).

With regard to invasive CTBs, PE is associated with defects in the epithelial-to-endothelial transition; the cells fail to express a subset of the adhesion molecules that also play roles in invasion and vascular mimicry (Zhou *et al.,* 1997a, Zhou *et al.,* 1997b). In PE, their production of vasculogenic/angiogenic molecules also changes. Invasive CTBs express lower levels of VEGF-A and VEGFR-1 and their secretion of sFlt-1 *in vitro* increases (Zhou *et al.,* 2002). Interestingly, excess sFlt-1 produces a PE-like syndrome in rats (Maynard *et al.,* 2003). At a transcriptional level, invasive CTBs express much

higher levels of Id2, a negative regulator of basic helix-loop-helix transcription factors that promote differentiation of the invasive CTB population (Janatpour *et al.,* 1999). Together, findings in STB and CTBs have led to the hypothesis that PE is associated with fundamental defects in TB differentiation.

In previous work, we used a variety of genetic and molecular techniques to ask whether PE-associated defects in the cytotrophoblast (CTB) subpopulation that invades the uterine wall are specific to this syndrome or observed in other pregnancy complications. The results of these studies showed that PE and preterm labor (with no signs of inflammation; nPTL) are distinct entities with regard to their effects on invasive CTBs, our impetus for using the latter cases as gestation-matched controls for our PE experiments. In parallel, our group has completed two microarray analyses of the maternal-fetal interface. In the first, we characterized gene expression as a function of gestational age (Winn *et al.,* 2007). In the second, we compared the effects of PE and nPTL at the tissue level during 24-36 wks of pregnancy (Winn *et al.,* 2009).

Accordingly, we analyzed the effects of PE on the CTB subpopulation that invades the uterus. Specifically, we isolated CTB progenitors from affected and control placentas and compared, at a global level, their patterns of gene expression as they differentiated along the invasive pathway in culture. These experiments uncovered fundamental differences in the CTB progenitor population in PE and in PTL. We subsequently determined the functional significance *SEMA3B*, one of the molecules most highly upregulated in CTBs of PE-complicated pregnancies. We found that SEMA3B antagonized VEGF signaling through the PI3K/AKT pathways and negatively influenced aspects of CTB and endothelial cell invasion, migration, and survival, *i.e*., replicated the phenotypic alterations observed in these cell types that are associated with PE.

Results

Microarray Profiling Revealed Abberations in CTB Differentiation in PE

We identified 33 genes that were differentially expressed in CTBs that were isolated from PE placentas as compared to those obtained from pregnancies that were complicated by nPTL (Figure 21). A subset of the results was confirmed by qRT-PCR (Figure 22) and, in some cases, at the protein level (data not shown). The upregulated molecules included factors that have previously been described as misregulated in PE, for example, corticotropin releasing hormone (*CRH*) and leptin (*LEP*) (Winn *et al.,* 2009). We were most interested in the novel candidate regulators, which included the HOP homeobox gene (*HOPX*) and semaphorin 3B (*SEMA3B*). We also found up regulation of the gene, *OLAH*, which is involved in fatty acid release. Downregulated were molecules that are involved in arachidonate acid metabolism (*ALOX5*), prevention of maternal immune rejection (*S100A8*) (Passey *et al.,* 1999), and cell adhesion (*PECAM1*). We previously described abnormally low expression of the latter molecule in PE (Zhou *et al.,* 1997b).

Most remarkably we found that by 48 hours the expression patterns of most of the affected molecules were either up- or downregulated such that they were very similar to those observed in CTBs that were isolated from placentas of women who had preterm births. These results suggested the novel concept that PE-associated CTB defects, which self-correct when the cells are isolated, are caused by an unfavorable placental or uterine milieu.

The following section describes additional work that was primarily completed by by Dr. Yan Zhou. These results are included as confirmation that the differentially regulated targets play important roles in the placental component of the PE syndrome.

Expression of SEMA3B and its Receptor, NRP-2, in the Placentas of Women with PTL or PE

To confirm the expected localization of *SEMA3B* expression, which was based on the results of our gene array experiments, we performed RNA *in situ* hybridization on tissue sections of basal plate biopsies collected from 1st, 2nd, 3rd trimester, and PE-complicated placentas. *SEMA3B* mRNA was confined to STB and villous CTB progenitors (Figure 23A-E). While strong *SEMA3B* hybridization was detected in association with syncytial sprouts, none was detected with invasive CTBs (data not shown). Compared to normal term controls (Figure 23D), stronger signals were detected from PE STBs and CTBs (Figure 23E). Northern blot hybridization analyses also revealed a similar transcriptional pattern in vitro, in which *SEMA3B* hybridization was detected with increasing intensity in 1st, 2nd, and 3rd trimester, and PE chorionic villi (Figure 23F). To confirm these results at the protein level, we performed indirect immunofluorescence staining on tissue sections of basal plate biopsies from nPTL- and PE-complicated pregnancies. As compared to the villous trophoblasts in the placentas of women who experienced PTL (Figure 23H and 23J), SEMA3B protein levels were increased in PE villous trophoblasts (Figure 23I and 23J).

Decreased utero-placental perfusion and placental hypoxia are commonly associated with PE (Granger *et al.,* 2002). To address whether hypoxia regulated *SEMA3B* expression in PE placentas, we cultured *SEMA3B*-transfected COS-1 cells

(tagged with V5) for 36 hours in normoxia (20% O_2) and hypoxia (2% O_2) and assessed SEMA3B expression levels by anti-V5 antibody immunoblotting analyses. The data showed that SEMA3B was significantly upregulated at 2% O_2 (Figure 23G), suggesting that SEMA3B could serve as a marker to monitor the development of placental hypoxia in PE.

To understand the function of SEMA3B, we studied the expression pattern of its primary receptor, NRP-2 (Takahashi *et al.,* 1998). RNA *In situ* hybridization and immunolocalization for NRP-2 on 1st, 2nd and 3rd trimester placental sections showed that NRP-2 was expressed by villous and invasive CTBs, uterine endothelial cells (ECs), but not STBs (data not shown). These results suggested that SEMA3B regulated the function of invasive CTBs and uterine ECs, hypotheses that were tested in the following sections.

SEMA3B Antagonized VEGF Signaling Through the NRP-2 Receptor Pathway

Neuropilins are VEGFR-2 co-receptors that potentiate signaling induced by VEGF ligands (Shraga-Heled *et al.,* 2007). Both SEMA3B and $VEGF_{165}$ can bind to Neuropilin receptors but mediate unique phenotypic effects, evidence that these ligands antagonize each other (Castro-Rivera *et al.,* 2004). In response to VEGF signaling, VEGFR-2 is phosphorylated and becomes a docking site for the p85 subunit of PI3K (Dayanir *et al.,* 2001). To determine the molecular mechanism by which SEMA3B antagonized the actions of VEGF, we asked whether SEMA3B opposed VEGF signaling by inhibiting the activity of PI3K, as measured by the production of phosphatidylinositol 3,4,5-triphosphate (PIP_3) (Figure 24). Addition of recombinant SEMA3B to cultured CTBs reduced PIP_3 production by 41%. In contrast, when CTBs were cultured in the

presence of VEGF, PIP_3 production increased two-fold over control levels. As expected, treatment with the PI3K inhibitor, wortmannin, reduced PIP_3 production by 32% compared to CD6-Fc-treated controls.

Next, we determined the molecular mechanism by which SEMA3B inhibited PI3K signaling. We theorized that NRP-2, a dual receptor for both SEMA3B and VEGF, played an important role in mediating PI3K activity. To test this possibility, COS-1 cells, which endogenously expressed VEGFR-2, were transiently transfected with a *SEMA3B* expression vector. Ectopic *SEMA3B* expression led to *de novo* expression of NRP-2. Transfection with SEMA3B or control vectors generated COS-1 cells expressing the following molecular combinations: SEMA3B/NRP-2/VEGFR-2 or VEGFR-2, respectively. These patterns were confirmed by PCR and immunoblot analyses (data not shown). We assessed whether SEMA3B and $VEGF_{165}$ exerted opposing effects on PI3K signaling by detecting association between the p85 and p110 PI3K subunits, which is required for PI3K activation. The lysates from *SEMA3B*- and empty vector-transfected COS-1 cell lines were immunoprecipitated with an antibody specific for the p85 subunit. The products were immunoblotted with antibodies specific for NRP-2, VEGFR-2, and p110 (Figure 24B). In COS-1 cells transfected with an empty vector, high levels of p110 were detected in the p85 immunoprecipitates. In cells transfected with SEMA3B, p110 did not co-immunoprecipitate with p85. This was consistent with the observed reduction of PI3K activity associated with SEMA3B treatment (Figure 24A). In contrast, incubation of SEMA3B-transfected COS-1 cells with $VEGF_{165}$ restored the ability of p85 to bind p110, suggesting PI3K was re-activated in this condition. Taken together, these results indicated that SEMA3B inhibited PI3K activation by preventing the association of p85 and p110.

In response to PI3K signals, Akt is activated by phosphorylation at threonine 308 and serine 437 (Datta *et al.*, 1997; Kandel and Hay, 1999). To ask whether PI3K/Akt signaling was reciprocally regulated by SEMA3B and VEGF, p-Akt (Ser473) levels were analyzed in the lysates of *SEMA3B*- or insert-free vector-transfected COS-1 cells (Figure 24C, top left). In controls, p-Akt (Ser473) was detected in abundance, while in cells transfected with SEMA3B, p-Akt (Ser473) was not detected. Next, we asked whether PI3K signal transduction was associated with CTB differentiation. p-Akt (Ser473) was examined in undifferentiated (0 hour) and differentiated (12 hour) 1^{st} and 2^{nd} trimester CTBs (Figure 24C, top middle). p-Akt (Ser473) was not detected in undifferentiated CTBs but was upregulated after the cells were differentiated for 12-hours in culture. Addition of wortmannin to the cultures abrogated this signal. As controls, when the same blots were stripped and re-probed with anti-total Akt antibody, the levels of Akt protein were comparable in all samples. To further assess possible reciprocal regulation by SEMA3B and VEGF, the levels of p-Akt were measured in CTBs cultured for 30 min in the presence of exogenously added proteins (Figure 24C). These data supported the results seen in the PIP_3 production assays. p-Akt levels were lower in cells treated with wortmannin or SEMA3B and higher in cells treated with VEGF as compared to controls.

SEMA3B Antagonized VEGF-induced CTB and EC Invasion and Survival by Negatively Regulating PI3K Activity

Given that SEMA3B inhibited the activity of PI3K, we asked whether this inhibition was associated with functional changes in CTB and EC behavior. We assessed the effect of PI3K inhibition on CTB and EC invasion and migration, respectively, and survival. Chen *et al.* (1997) have previously shown that SEMA3

ligands have similar binding affinities to NRP-1 or NRP-2. To determine how SEMA3B might interact with VEGF to regulate CTB invasion and apoptosis, we took advantage of the fact that isolated CTBs spontaneously invade when plated on Matrigel (Librach et al., 1991) and that SEMA3B ligand-receptor interactions can be blocked by the addition of NRP-1-Fc or NRP-2-Fc fusion proteins to the culture. In the following experiments, we tested the effects of NRP-1-Fc, NRP-2-Fc, recombinant SEMA3B, and a function-blocking anti-VEGF antibody on CTB invasion and apoptosis. CD6-Fc, which we previously demonstrated as having no effect on CTB invasion or apoptosis (Zhou *et al.,* 2002), was used to control for the addition of Fc proteins to the cultures.

With regard to CTB invasion (Figure 25A), culture of CTBs with an anti-VEGF antibody for 36 hours reduced invasion to 43-44% of control cultures, a result we previously published (Zhou *et al.,* 2002); inclusion of NRP-1-Fc or NRP-2-Fc fusion proteins with the anti-VEGF antibodies restored CTB invasion to 84-86% of controls. Addition of recombinant SEMA3B proteins to CTB cultures decreased invasion by 57%. With regard to apoptosis (Figure 25B), addition of anti-VEGF antibody increased the level of apoptosis to more than twice that of the control cultures. In contrast, addition of NRP-1-Fc or NRP-2-Fc along with the anti-VEGF antibody reduced the apoptosis to 52% and 70% of control levels, respectively. Inclusion of recombinant SEMA3B protein in CTB cultures enhanced apoptosis by ~100%. Taken together, these results suggested that PI3K activity played important roles downstream of SEMA3B signaling during CTB invasion and apoptosis.

Endothelial dysfunction is a common pathophysiological outcome of PE. To further investigate the pathogenic actions of SEMA3B during PE-pregnancies, we investigated its function in ECs. First, we assessed the effects of SEMA3B on UtVEC migration by time-lapse video microscopy, which we used to track the motility of

individual ECs. UtVECs were grown to confluence and a scratch was made in the middle of the monolayer to promote directional cell migration. Recombinant $VEGF_{165}$ accelerated the migration of UtVECs toward the scratch, while recombinant SEMA3B decelerated this movement (Figure 25C). Quantitative analysis was used to determine the distances traveled by UtVEC in the following conditions. The cells moved 245 pixels on average when treated with $VEGF_{165}$, 43 pixels in SEMA3B conditions, 96 pixels when cultured with $VEGF_{165}$ plus SEMA3B, and 108 pixels in negative controls (Figure 25D)

VEGF is necessary for EC survival. We theorized that increased expression of SEMA3B in PE could influence VEGF-dependent survival in ECs. To test this theory, we performed chromium-51 (^{51}Cr) release assays (Figure 25E), which measure apoptosis as a function of membrane integrity. After labeling with ^{51}Cr, UtVECs were cultured in the presence of recombinant $VEGF_{165}$, SEMA3B, or the VEGF antagonists, Flt-1-Fc and NRP-2-Fc. SEMA3B treatment triggered significant increases (3.3 fold) in UtVEC apoptosis when compared to negative controls. As expected, VEGF treatment exerted a protective effect on ECs. Apoptosis induced by SEMA3B was attenuated in the presence of NRP-2-Fc or $VEGF_{165}$. Taken together, these results suggested that SEMA3B inhibits migration and increases apoptosis of ECs by antagonizing the VEGF/PI3K pathway.

Discussion

Our long-term goal has been to elucidate the molecular bases of the placental defects that occur in preeclampsia (PE) and to explain their relationship to the clinical signs of this syndrome. We theorized that defects in CTB differentiation were central to the pathology of this syndrome and carried out microarray gene expression profiling

experiments to identify molecular differences in CTBs from nPTL and PE placentas undergoing differentiation in culture. Our study confirmed previously reported molecular alterations associated with PE and identified unique aspects of CTB gene expression in this pregnancy complication. An in depth functional study of *SEMA3B,* which was highly upregulated in the CTBs of preeclamptic placentas, allowed us to associate enhanced *SEMA3B* expression with some of the classical phenotypic consequences of PE. Specifically, at a mechanistic level, we demonstrated that SEMA3B antagonizes VEGF signaling through interactions induced by the Neuropilin2 receptor, which resulted in inhibition of the PI3K-AKT signaling pathway. At a functional level, CTBs cultured in the presence of recombinant SEMA3B displayed decreased invasion and increased apoptosis. Similarly, ECs grown with exogenous SEMA3B exhibited reduced migration and increased programmed cell death. Taken together, these results support the conclusion that defects in the differentiation of CTBs in PE underlie both fetal and maternal pathogenesis that are the hallmark of this syndrome.

A surprising finding of the array portion of this study was that the initial differences in gene expression that were observed between freshly isolated CTBs from pregnancies complicated by PE or nPTL normalized over the culture period such that the gene expression patterns were much more similar at the 48 hour time point. This suggested that maternal or fetal factors not intrinsic to the CTB population were responsible for the observed changes in gene expression, a novel finding. These conclusions were bolstered by our observation that hypoxia, which can occur during preeclamptic pregnancies as result of placental insufficiency or altered maternal vascular physiology, upregulated SEMA3B expression, suggesting that placental hypoxia contributed to at least a portion of the differences seen in PE.

Whether the changes in CTB gene expression in this study were the result of maternal or fetal factors is difficult to determine. More broadly, the maternal vs. fetal causes of PE are a subject of debate (reviewed in Gilbert *et al.,* 2008). For instance, there is evidence that abnormalities originating from either fetal trophoblast invasion or maternal hypertension can lead to hypoxia. Failures in trophoblast invasion and vascular remodeling are widely believed to be initiating events in PE (Gilbert *et al.,* 2008). Our work on Notch in this dissertion and additional work by others shows that decreased trophoblast invasion limits utero-placental perfusion (Verlohen et al., 2010), which is known to result in placental hypoxia. Subsequently, factors released by the placenta under hypoxic stress, such as sFLT and endoglin, contribute to maternal hypertension through alterations in endothelial function (Maynard *et al.,* 2003; Venkatesha *et al.,* 2006). Conversely, it is interesting to note that women with a history of hypertension are far more likely to have pregnancies complicated by PE (Odegard et al., 2000), suggesting that hypertension may also be directly involved in the pathology of PE. As to possible mechanism, hypertension increases systemic vascular resistance, which lowers rates of systemic perfusion and presumably would lower oxygen concentrations in the placenta, although this has not been directly shown. Furthermore, CTBs grown in physiological hypoxia fail to differentiate and produce fewer invasion progeny (Genbacev *et al.,* 1997), suggesting that maternal hypoxia could produce the defects in CTB vascular remodeling observed in PE. Altogether, the aforementioned findings indicate that the symptoms of PE likely result from complex and variable origins, although data presented here presents at least one line of evidence that placental hypoxia plays and upstream role.

Class III Semaphorins were first described as tumor suppressors (Zhiang *et al.,* 1996; Tomizawa *et al.,* 2001). In the case of SEMA3B, function was primarily attributed

to its ability to antagonize the effects of VEGF on EC phenotypes (Miao *et al.,* 1999 PMID). Subsequently, mechanistic studies revealed this antagonistic relationship to be the result of two properties of these molecules. Both SEMA3B and VEGF can bind the VEGF co-receptors, NRP-1 and NRP-2, but they elicit unique signaling responses through the VEGF receptor (Soker *et al.,* 1998; Favier *et al.,* 2006). As such, SEMA3B and VEGF promote opposing effects on angiogenesis, in which SEMA3B is anti-angiogenic and VEGF is proangiogenic. We have confirmed that this regulatory model also exists in the human placenta. Given the fact that SEMA3B, a secreted molecule, was upregulated in PE and in hypoxic conditions, we speculated that increased SEMA3B serum levels might create an overwhelming antiangiogenic state that triggers endothelial crisis in PE. In support of this theory, we performed a series of functional assays that were designed to test the function of SEMA3B in uterine vascular endothelial cells (UtVECs). We demonstrated that SEMA3B inhibited VEGF-induced network formation, motility and survival. These results strongly support the current opinion that antiangiogenic factors contribute to the pathogenesis of PE (Maynard *et al.,* 2003; Venkatesha *et al.,* 2006). It may be possible to remove SEMA3B from the circulation using sNRP-1 or sNRP-2 and to shift the angiogenic balance in the favor of VEGF. As such, our studies support the development of new therapeutic strategies for PE management.

Semaphorins play important roles as regulators of neuronal guidance and, specifically, act as potent axon repellents for specific populations of neurons (reviewed in Huber *et al.,* 2003). These chemorepulsive effects occur downstream of Nueropilin receptors (Gu *et al.,* 2003). We know from previous studies that CTBs use similar pathways involved in neuronal guidance, such as the Eph/Ephrin family members, to direct their migration away from CTB progenitors and toward uterine blood vessels (Red-

Horse *et al.,* 2005). We theorized that SEMA3B plays a similar role during trophoblast invasion. In our experiments, CTB invasion and EC migration depended on carefully balanced SEMA3 and VEGF signals. Specifically, titration of SEMA3B ligands with NRP1-Fc or NRP2-Fc (removal of SEMA3B) fusion proteins significantly reversed the inhibition of invasive and migratory effects that occurred when the cells were deprived of VEGF signals. Together these findings suggested that the changes we observed in CTB VEGF and SEMA3 expression in PE may explain, in part, why this pregnancy complication is associated with shallow CTB invasion and poor endovascular invasion.

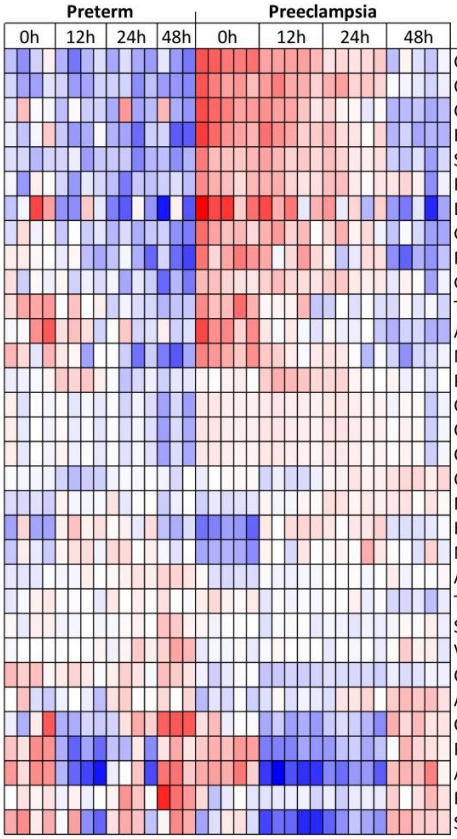

Symbol	Title	Fold Δ
CRH	corticotropin releasing hormone	10
OLAH	oleoyl-ACP hydrolase	7
CYP19A1	cytochrome P450, 19A1	5
HOPX	HOP homeobox	5
SEMA3B	semaphorin 3B (secreted Ig domain)	4
PSG5	pregnancy specific beta-1-glycoprotein 5	3
LEP	leptin	3
GPC3	glypican 3	3
FRZB	frizzled-related protein	3
GH1	growth hormone 1	3
TIMD4	T-cell immunoglobulin and mucin domain containing 4	3
ANXA1	annexin A1	2
NID2	nidogen 2 (osteonidogen)	2
PDGFB	platelet-derived growth factor β (simian sarcoma viral (v-sis) oncogene homolog)	2
CSHL1	chorionic somatomammotropin hormone-like 1	2
CSH1	chorionic somatomammotropin hormone 1 (placental lactogen)	2
CSH2	chorionic somatomammotropin hormone 2	2
CRIPT	cysteine-rich PDZ-binding protein	2
MTRR	5-methyltetrahydrofolate-homocysteine methyltransferase reductase	2
HMGA1	high mobility group AT-hook 1	-2
NETO2	neuropilin (NRP) and tolloid (TLL)-like 2	-2
AP3D1	adaptor-related protein complex 3, delta 1 subunit	-2
TUG1	taurine upregulated 1 (non-protein coding)	-2
SIGLEC7	sialic acid binding Ig-like lectin 7	-2
VILL	villin-like	-2
CHURC1	churchill domain containing 1	-2
ALG10	asparagine-linked glycosylation 10, α-1,2-glucosyltransferase homolog	-2
CCR2	chemokine (C-C motif) receptor 2	-2
PECAM1	platelet/endothelial cell adhesion molecule	-2
ALOX5	arachidonate 5-lipoxygenase	-2
RETN	resistin	-4
S100A8	S100 calcium binding protein A8	-4

Figure 21. *Differentially Expressed mRNAs in the CTBs of PE- vs. nPTL-complicated Pregnancies*

Global gene expression profiling (Affymetrix) was performed using cDNA samples prepared from the CTBs of preterm and preeclamptic placentas that were differentiated for 0, 12, 24, or 48 hours (h) in culture. The relative gene expression levels are presented in heat map view for the listed transcripts with values ranging from low (blue) to high (red). Fold change (Δ) values (PE-PTL) are displayed on the right side of the diagram.

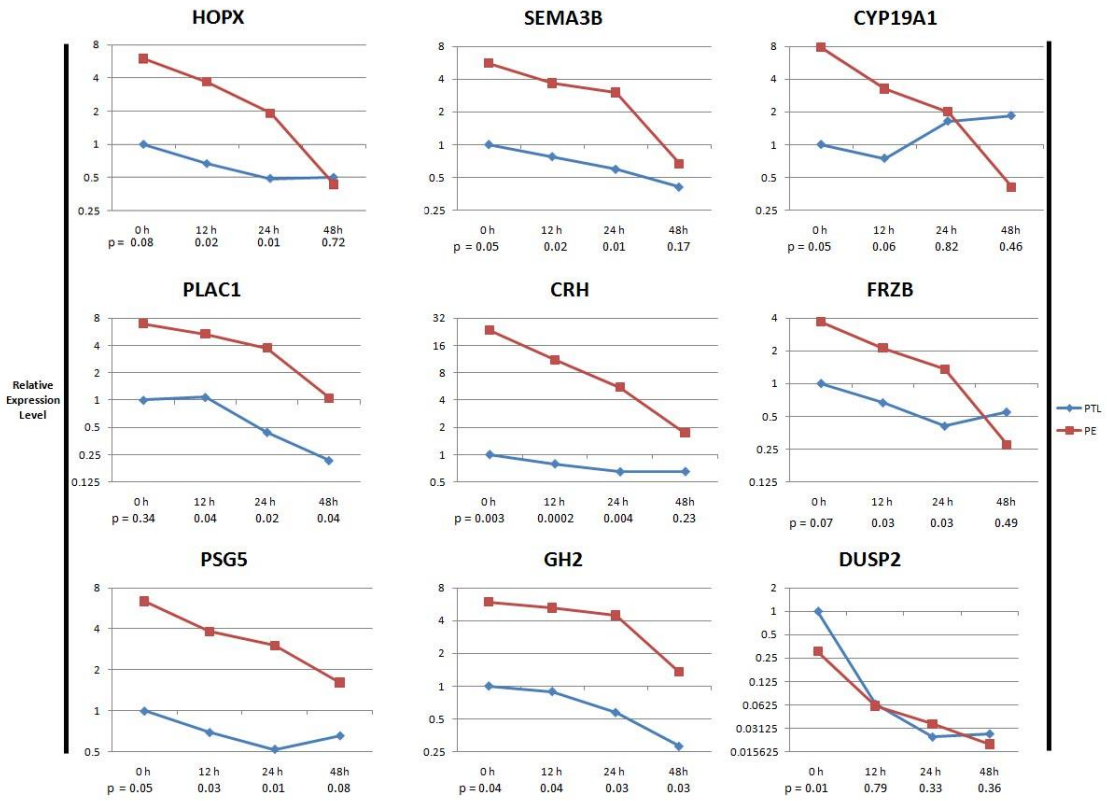

Figure 22. *Quantitative PCR Validation of Selected Array Targets*

Taqman RT-qPCR was performed using cDNA samples prepared from the CTBs of preterm (PTL) and preeclamptic (PE) placentas that were differentiated for 0, 12, 24, or 48 hours (h) in culture. The relative gene expression levels were plotted for each transcript on the y-axis. Differences in fold change between the PE and nPTL CTBs at each time point were assessed with a Students' T-Test. P-Values are displayed at the bottom of each chart.

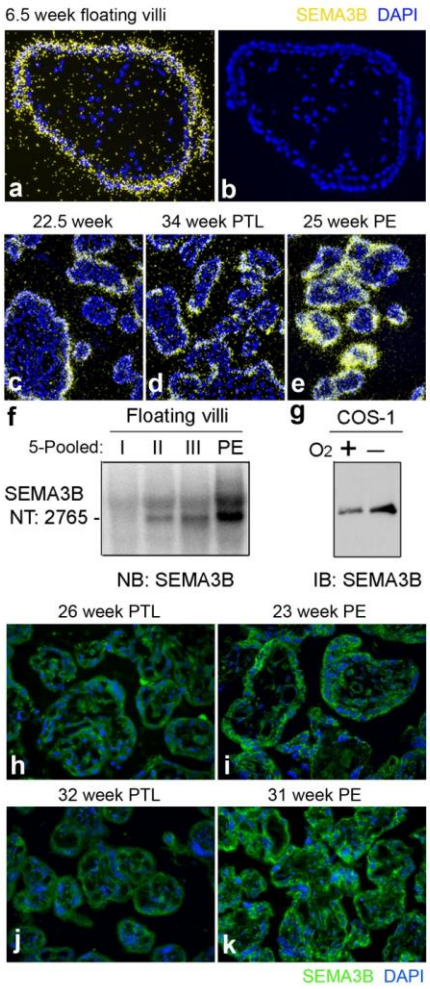

Figure 23. *SEMA3B Expression was Upregulated in the Trophoblasts of Women with PE.*

(A-E) RNA *in situ* hybridization was performed on tissue sections of 2nd and 3rd trimester basal plate biopsies to detect *SEMA3B* expression (yellow). Nuclei were stained with DAPI (blue). (A) SEMA3B was expressed by trophoblast cells on the surfaces of floating villi. (B) DAPI staining demonstrated that SEMA3B was expressed by the CTB and STB layers. (C) As compared to the villi of 2nd trimester and (D) 3rd trimester control samples, (E) *SEMA3B* expression was increased in the villi of PE samples. (F) Northern blot hybridization was performed using villous lysates of 1st, 2nd, and 3rd trimester and PE placentas to detect SEMA3B expression, which was increased in PE. (G) Immunoblotting was performed using lysates of COS-1 cells, which were grown under either normoxic or hypoxic conditions, to detect SEMA3B expression. In these cells, physiological hypoxia upregulated SEMA3B expression. (H-K) Indirect immunofluorescence staining was performed on tissue sections from the basal plate biopsies of women who experienced pregnancies complicated by (H and J) nPTL or (I and K) PE to detect SEMA3B (green). Nuclei were stained with DAPI (blue). SEMA3B immunoreactivity was increased in PE.

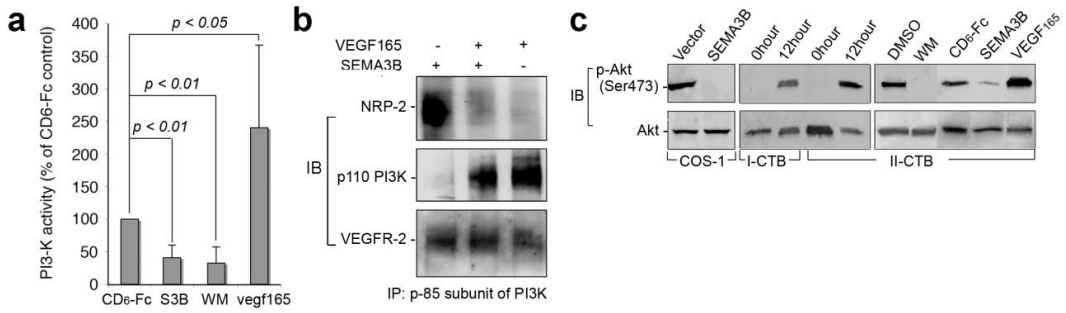

Figure 24. *SEMA3B Signals Through the PI3K/AKT Pathways.*

(A) PI3-Kinase activity decreased in CTBs that were treated with SEMA3B or wortmannin (a control PI3K inhibitor) and increased in CTBs that were treated with $VEGF_{165}$ as compared to CTBs that were treated with CD6-Fc (a negative control). (B) Immunoprecipitation of the p85 subunit of PI3K followed by immunoblotting for NRP-2, VEGFR-2, and the p110 subunit of PI3-K was performed on the lysates of COS-1 cells that were treated with SEMA3B, $VEGF_{165}$, or both SEMA3B and $VEGF_{165}$. p85 coimmunoprecipitated with NRP-2, but not p110 when the cells were treated with SEMA3B. The converse was observed when COS-1 cells were treated with $VEGF_{165}$, or both SEMA3B and $VEGF_{165}$. p85 coimmunoprecipitated with VEGFR-2 under in all conditions. (C) Immunoblotting was performed using the lysates COS-1 cells and CTBs to detect activated phosho-AKT (p-AKT). Immunoblotting analysis of non-phosphorylated AKT was performed to control for loading variability. In COS-1 cells, transfection of a SEMA3B expression vector reduced levels of p-AKT as compared to controls. In 1st and 2nd trimester CTBs that were differentiated for 12 hours in culture, levels of p-AKT increased relative to undifferentiated cells. In 2nd trimester CTBs that were differentiated in the presence of wortmannin, levels of p-AKT declined as compared to DMSO and CD6-FC treatments, which served as controls. SEMA3B treatment decreased levels of p-AKT while $VEGF_{165}$ treatment had the opposite effect.

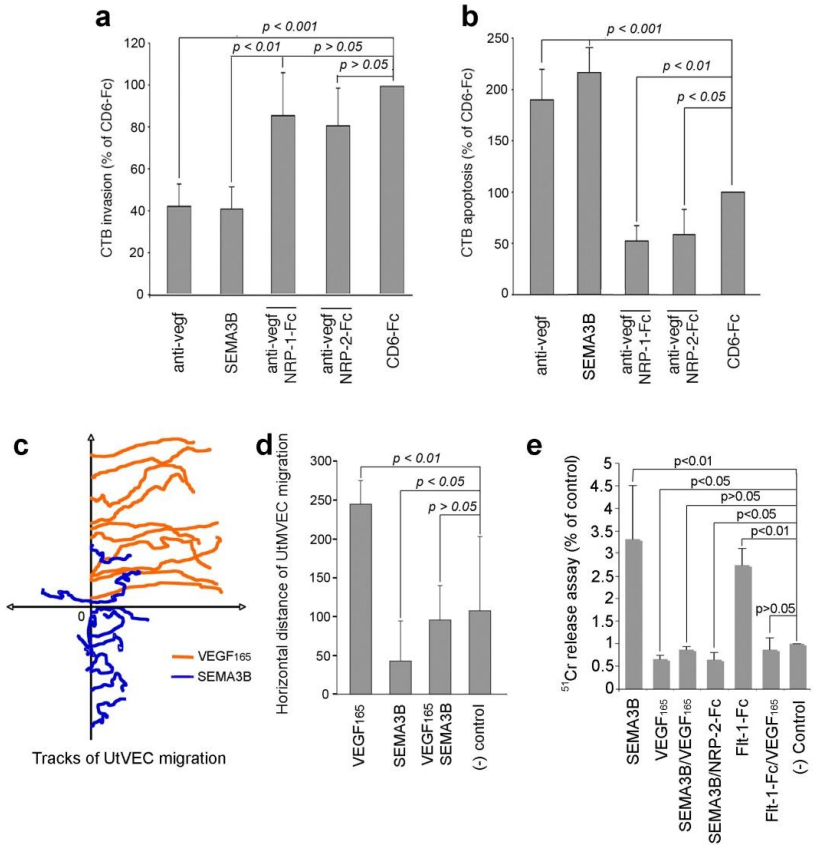

Figure 25. *SEMA3B Exposure Decreased CTB Invasion, EC Migration, and CTB/EC Survival.*

(A) CTB invasion through Matrigel decreased in the presence of recombinant SEMA3B and anti-VEGF antibody as compared to the level observed following treatment with control anti-CD6-FC, which was set at 100%. NRP-1-Fc and NRP-2-Fc treatment partially rescued the effects of anti-vegf antibody treatment on CTB invasion. (B) CTB apoptosis increased in the presence of recombinant SEMA3B or anti- VEGF antibody as compared to the level observed following treatment with anti-CD6-FC, which was set at 100%. NRP-1-Fc or NRP-2-Fc treatment reduced CTB apoptosis to levels lower than those observed in controls. (C and D) Uterine vascular endothelial cell (UtVEC) migration was assessed following treatment with $VEGF_{165}$, SEMA3B, or $VEGF_{165}$/SEMA3B and in control conditions. (C) Time lapse video microscopy was used to record tracks of UtVEC migration, which decreased when the cells were treated with SEMA3B as compared to $VEGF_{165}$. (D) UtVEC migration was quantitated. As compared to $VEGF_{165}$/SEMA3B and control conditions, which were set to 100%, migration was increased and decreased with $VEGF_{165}$ and SEMA3B treatment, respectively. (E) UtVEC death was measured by chromium release and increased when the cells were cultured with either SEMA3B or Flt-1-Fc as compared to control culture conditions.

Methods

Human Tissue Collection

All portions of this study were approved by the UCSF Institutional Review Board. Informed consent was obtained from all tissue donors. Biopsies of normal placentas were either fresh-frozen for immunolocalization, paraformaldehyde-fixed for *in situ* hybridization or immediately processed for CTB isolation. Equivalent specimens were obtained from women who experienced either PTL, SPE, or HELLP using the clinical criteria and methods we published (Zhou *et al.,* 2007).

Cell Isolation, Culture, and RNA Isolation

Primary human CTBs were isolated and cultured up to 48 hours as described (Hunkapiller and Fisher, 2008). CTB RNA samples were isolated using an RNeasy Plus kit (Qiagen). RNA concentration/quality was first assessed using a Nanodrop spectrophotometer (Thermo-Scientific). Aliquots were further evaluated by using the Agilent RNA 6000 Nano LabChip kit (Agilent Technologies) on an Agilent Bioanalyzer 2100 system and only samples with a RIN number >9 were used in subsequent microarray experiments.

Microarray-based Gene Expression Profiling and Data Analysis

The microarray platform was the high-density HG-U133A and HG-U133B GeneChips (Affymetrix, Santa Clara, CA). Sample processing and hybridization was

accomplished by using the protocols devised by the UCSF Gladstone (NHLBI) Genomics Core Facility as previously described (Winn *et al.,* 2009). For data analysis, the raw images were analyzed by using GeneChip Expression Analysis software (Affymetrix) to produce perfect match and mismatch values. Subsequently, quality control, preprocessing, and linear modeling were performed using Bioconductor (Gentleman *et al.,* 2004), an open-source and open-development software project based on the R statistical package. Estimated log ratios (M value) between PE and PTL samples were determined by using the limma software package in R. Then differentially expressed genes were selected by statistical analysis of log odds-ratios and B > 0 was set as significance.

Taqman-qPCR

cDNA libraries were prepared with 500 ng of RNA using the iScript kit (Biorad) and diluted 20-fold in water. Taqman qPCR reactions were carried out in triplicate. Differences among target expression levels were estimated by the ΔΔCT method with normalization to *GAPDH*. Differences between means were assessed using a two-tailed student's t-test (alpha=0.05) assuming equal variance.

Chapter 5: The Design and Optimization of a Microfluidic Taqman Approach to Study miRNA Expression in Preeclampsia

Introduction

The placenta is a transient organ with remarkable functions whose formation is intimately linked to differentiation of the placenta's specialized progenitors, termed cytotrophoblasts (CTBs). Proper CTB differentiation and invasion into the uterine wall is essential to normal pregnancy as this process anchors the placenta to the uterus and diverts uterine blood flow towards the fetus. Given this organ's complexity, the explosive nature by which it develops and its many critical functions it is not surprising that many pregnancy complications are associated with placental anomalies. Preeclampsia (PE), a syndrome that adversely affects the mother (by altering vascular function) and the fetus (by restricting intrauterine growth; IUGR), is a prime example. Highlighting the importance of this condition is its high prevalence (affecting 5-8% of first pregnancies), rapid onset, and often severe symptoms including hypertension, proteinuria, neurological disturbances, hemolysis, renal impairment, and pulmonary edema. In addition to the maternal signs, there can be devastating effects on the fetus. For example, 15% of all preterm deliveries (<34 wks of gestation) in the U.S. occur as the treatment of last resort for PE, because removal of the placenta is the only known cure (Goldenberg and Rouse, 1998).

Our long-term goals with regard to PE have been to elucidate the molecular bases of the placental defects that occur in PE and to explain their relationship to the clinical signs of this syndrome. We hypothesized that PE-specific alterations would help us understand the etiology of this pregnancy complication. In previous chapters, we

described a variety of genetic approaches, including microarray gene expression profiling, that addressed whether PE-associated defects in the CTB subpopulation that invades the uterine wall are specific to this syndrome or observed in other pregnancy complications. As described in this chapter, we have expanded our approaches to understand these changes within the context of microRNA (miRNA) regulation. miRNAs are small RNA molecules approximately 18-25 nucleotides in length that regulate mRNA degradation and stability (Bartel, 2004). Additionally, within the last year, miRNAs in human serum emerged as exciting and novel biomarker candidates. Given the placenta's intimate communication with the maternal circulatory system, we also hypothesized that miRNAs are a part of the vast array of molecules secreted by the placenta and may serve as early markers of placental abnormalities in maternal serum. The broad involvement of miRNAs in development, tissue homoeostasis and disease makes them candidates of great interest. To utilize the high potential of miRNA to explain the biology of PE and to serve as biomarkers of this syndrome, the accuracy and integrity of the profiled microRNA expression levels are essential prerequisites. However, the current methods utilized for the comprehensive study of miRNA expression have major drawbacks, including requiring significant biological input and outputting results with limited quantitative accuracy. Together, these challenges significantly limit the types of studies that can be designed to deliver useful results. Accordingly, we designed and optimized a new approach to comprehensively and quantitatively profile the expression of hundreds of miRNAs using limited RNA with a microfluidic Taqman-based approach.

Approach

For these experiments, we partnered with Fluidigm to develop a novel high-throughput miRNA detection technology utilizing Taqman chemistry. miRNA detection by Taqman differs from standard Taqman gene expression assays in that each target miRNA must be reverse transcribed with a unique stem-loop primer (Figure 26). Therefore, multi-plexing of the reverse transcription reaction is required for compatibility with the Fluidigm Dynamic Arrays, within which individual samples are spread across an array of 48 or 96 unique Taqman assays. Additionally, the nanoliter scale of the Dynamic Array reaction chambers necessitates preamplification of the target miRNA template prior to the Taqman detection step. In our experiments, we chose to study a group of 677 human miRNAs, composed of both validated and predicted sequences from the miR BASE miRNA database. We modeled our approach based on publications demonstrating multi-plexing success with more than 200 assays (Tang, *et al.,* 2006) and subdivided our 677 assays into 4 groups of a similar scale (Figure 27).

Methods

A diagrammatic representation of the experimental workflow is shown in Figure 26. CTBs from normal and PE-complicated pregnancies were isolated from placentas following patient consent and cultured on Matrigel. RNA was isolated from CTBs both immediately after the cell isolation and following 48 hours of differentiation in culture using the Qiagen RNeasy Plus Mini Kit. Additional RNA samples were isolated from maternal serum samples, the Ambion FirstChoice Human Total RNA Survey Panel (composed of 20 human tissues), and, as controls, wild-type and DGCR8 knockout MEFs and mESCs. 100ng of total RNA from each cell or tissue sample was reverse transcribed in each of the four multi-plex groups containing either 192 or 102 stem loop

primers. As serum samples produced very low quantities of RNA, we used 50% of the total RNA sample as input for the reverse transcription reaction. Afterwards, each sample was preamplified between 0 and 18 PCR cycles with target specific primers. To reduce primer carryover into the final single-plex Taqman detection step, multi-plexed preamplification products were diluted between 10 and 10,000 fold before loading into the 96.96 Dynamic Array. Proprietary software provided by Fluidigm was used for data analysis.

Results

To maximize detection sensitivity of low abundance miRNAs while reducing PCR bias that can hinder quantitative sensitivity of high abundance miRNAs, we first conducted optimization experiments to determine the ideal number of preamplification cycles as well as the optimal preamplification product dilution. The high density of the Fluidigm Dynamic Array allows for testing a great number of experimental variables in a single experiment. Several CTB samples from each experimental time point were reverse transcribed, subjected to either 0, 8, 10, 12, 14 or 18 cycles of pre-amplification, and then run across a group of 96 assays. While none of the 96 assays gave a detectable product without preamplification, an increasing number of assays gave a detectable product as cycles were increased from 8 to 14. Surprisingly, additional cycles beyond 14 markedly decreased assay success. Quantitative sensitivity, evaluated by comparison of the actual delta Ct to the expected delta Ct of a given sample, decreased rapidly above 12 cycles. To balance product detection (for lower abundance miRNAs) with quantitative sensitivity (for higher abundance miRNAs) we chose to use 12 preamplification cycles. Given that excess primer from the preamplification step is

necessarily carried into the Taqman reaction, potentially inhibiting the reaction, we conducted similar experiments to determine the optimal dilution of preamplification product. Using 12 preamplification cycles, we compared dilutions of preamplification product ranging from 10 fold to 10,000 fold. Similar to the analysis above, a 100 fold dilution best balanced detection of lower abundance miRNAs with quantitative sensitivity of higher abundance miRNAs.

To determine whether our methods produced a Taqman product specific to the mature miRNAs and not to pri-miRNAs or other cellular RNAs, we compared miRNA signal in wild-type MEFs and ESCs to cells in which the miRNA processing enzyme, DGCR8, had been removed. Knock-out of DGCR8 eliminated signal in all but one of 29 assays that produced a product in wild-type cells (Figure 28). Product signal for this assay in the absence of DGCR8 was shifted 12 cycles, accounting for only 0.1% of the measured product in the wild-type state.

Given that only 30-40% of the Taqman assays from our DGCR8 experiments produced a signal, we conducted a preliminary screen of all 677 human assays across a subset of our CTB samples as well as 20 tissues from the Ambion FirstChoice Human Total RNA Survey Panel. The purpose of these experiments was twofold. First, we planned to compare results of our multi-plexing method with another quantitative miRNA study in which the same tissue RNA panel was used in 48-plex Taqman experiments (Lee *et al.,* 2008). Second, we wanted to eliminate assays that failed to produce a product in any of the tissue samples (so as not to pursue them further) as well as focus the CTB study on those miRNAs present in these cells.

Our miRNA screen of the Ambion tissue bank revealed that approximately 64% (430/677) of the assays gave a detectable product in at least 2 of the 20 tissues. Given that a large number of our miRNA targets from miR BASE were not validated miRNAs

and that we expected many miRNAs to be below our detection threshold, it was not surprising that 36% of the assays failed to produce a product. We compared results of these experiments to Ct values obtained from a similar study in which 205 ABI miRNA assays were tested across the Ambion tissue panel in 48-plex. In this comparison, 7% of our assays gave a signal in the absence of measured product in the study by Lee *et al.,* potentially representing false positive reads. Additionally, 10% of our assays failed to give a product even though they were detected in the study by Lee, *et al*. For all data points, the correlation coefficient reached 0.42, yet increased to 0.71 when potential false positives and false negatives were removed (Figure 29).

Our screen of miRNA expression changes during CTB differentiation to an invasive phenotype in culture identified a subset of miRNAs that were dramatically regulated in both normal and PE-complicated pregnancies. While these data were the result of only 2 replicates and not statistically significant or validated by other methods, there was a consistent overlap in the two data sets (Table 8); 6 of the 7 most highly upregulated miRNAs in CTB differentiation were common in normal and disease states. Downregulated miRNAs showed a lesser degree of overlap, perhaps illustrating key miRNA processing differences in these unique biological states.

As a next step, we also conducted a screen to identify PE-associated miRNA expression changes in the serum of pregnant women, with the goal of identifying PE biomarkers. We collected patient serum samples prospectively at 20 weeks of gestation from 48 women whose pregnancies were later complicated by PE and also from 48 women whose pregnancies were normal. Using our Fluidigm workflow, we identified 41 miRNAs with statistically significant differences ($p < 0.05$) in expression level between PE and control serum samples (Table 9). Of particular interest, we performed an Ingenuity pathway analysis using the differentially expressed miRNAs and discovered

that a number of our miRNAs were predicted to target Semaphorin3F and VEGF-A, molecules known to be dysregulated in PE. However, our attempts to validate these miRNA changes using conventional Taqman approaches did not succeed and we conclude that further study with alternative approaches will be necessary to validate the results.

Discussion

The methods we have devised and tested for high throughput miRNA detection offer considerable advantages over conventional methods of miRNA expression analysis. Coupling of our methods with the reaction scale of the Dynamic Array reduces reagent and RNA sample needs to nanoliter levels, allowing for cost-effective miRNA screening, particularly when the RNA sample is limited. We chose to multi-plex at very high density to reduce the scale of our experiments, yet the Fluidigm 96.96 Dynamic Arrays are compatible with as low as 32-plex reactions. While high level multi-plexing is a valuable tool for reagent conservation, we recognize it adds considerable complexity to the RT and preamplification reactions. We are aware that this may decrease the specificity as well as the detection sensitivity of our assays, as indicated in the tissue miRNA screen by the numbers of false positives and negatives relative to the study by Lee *et al*. However, because we are screening for changes in miRNA expression, we are less interested in absolute miRNA quantitation and more in relative quantitation comparisons. Additionally, we have optimized our experimental conditions to bias for quantitative sensitivity of the most highly abundant miRNAs, which are most likely to be biologically relevant. Regardless, targets identified by this screening method will be

validated by other means. Together, we believe this approach provides the best balance between throughput, cost, and quantitative sensitivity.

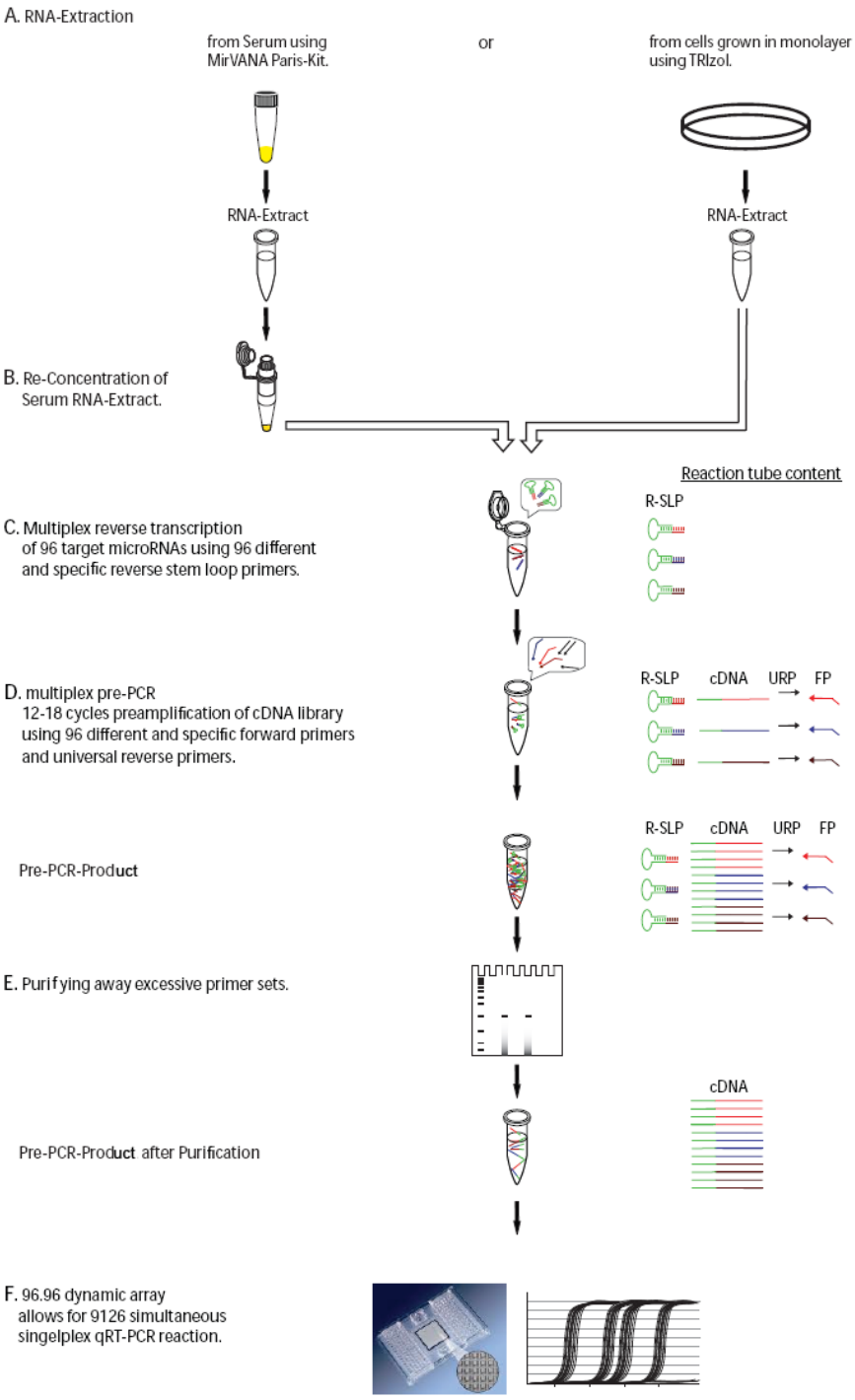

Figure 26. *Fluidigm Workflow for miRNA Detection by Taqman.*

miRNA were isolated from maternal serum or CTBs, reversed transcribed with a specific stem-loop primer, and detected during PCR amplification with a Taqman probe.

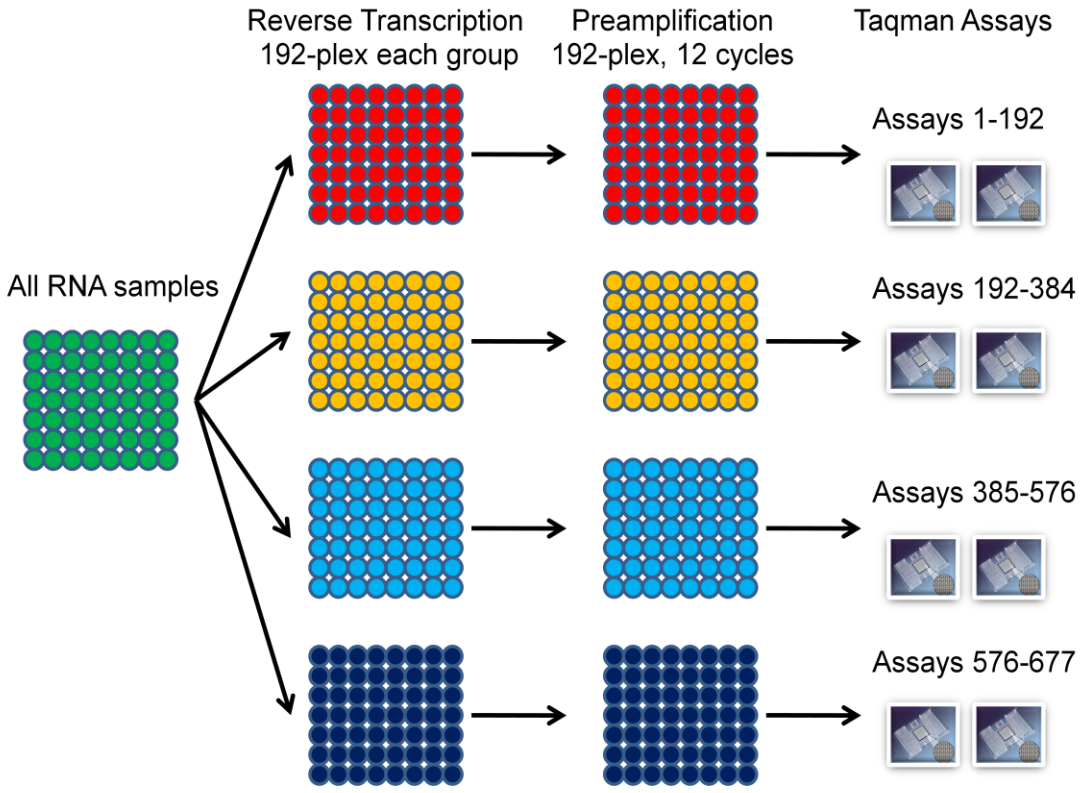

Figure 27. *Multi-plexing Approach.*

Each RNA sample is subdivided into 4 multi-plex groups of either 192 or 102 assays, reverse transcribed in multi-plex with all stem loop primers of the group, pre-amplified for 12 cycles, and used for single-plex Taqman on the Fluidigm 96.96 Dynamic Array.

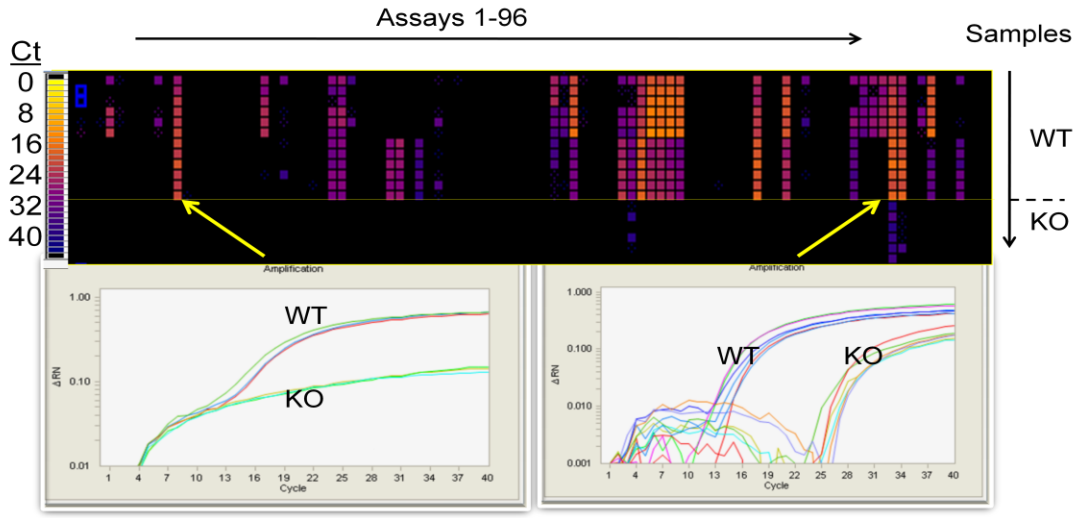

Figure 28. *DGCR8 Knock-out Eliminates miRNA Signal.*

Heat map view (top) of Ct values produced for 96 assays (columns 1-96) run with samples from wild-type (WT) MEFs (rows 1-6) and mES cells (rows 7-12) andDGCR8 knock-out MEFs (rows 13-15) and mES cells (rows 16-18). Data for individual assays clearly distinguishes WT and KO samples (bottom left and right).

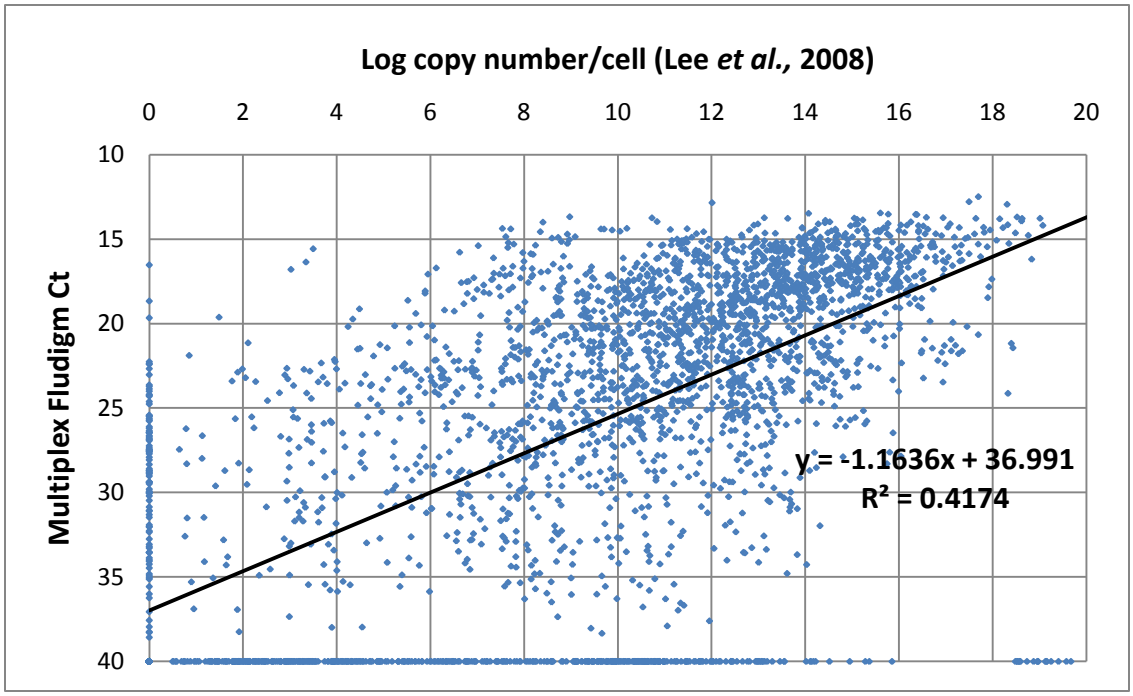

Figure 29. *Correlation of Quantitation Between Fluidigm 192-plex and ABI 48-plex.*

CTBs from Normal Pregnancies		CTBs from PE-Complicated Pregnancies	
Upregulated miRNAs	**delta CT**	**Upregulated miRNAs**	**delta CT**
***Homo miR-146a**	-7.5	**Homo miR-1290**	-8.99
Homo miR-1290	-4.43	***Homo miR-146a**	-6.61
Homo miR-636	-4.27	**Homo miR-1291**	-5.37
Homo miR-1291	-3.42	**Homo miR-1246**	-4.86
Homo miR-1268	-3.24	**Homo miR-636**	-4.22
Homo miR-1207-5p	-2.6	**Homo miR-1207-5p**	-4.21
Homo miR-1246	-2.33	*Homo let-7ilet-7i	-4.2
Downregulated miRNAs	**delta CT**	**Downregulated miRNAs**	**delta CT**
*Homo miR-590-5p	4.86	*Homo miR-23b	3.72
Homo miR-769-5p	5	Homo miR-1226	4.02
*Homo miR-127-3p	5.22	Homo miR-1249	4.35
*Homo miR-671-3p	5.42	Homo miR-555	4.38
*Homo miR-433	5.68	*Homo miR-744	5.83
Homo miR-1224-5p	6.97	**Homo miR-769-5p**	6.13

Table 8. *miRNA Changes During CTB Differentiation in Normal and PE-Complicated Pregnancies.*

The listed miRNAs were regulated during CTB differentiation with the indicated delta Ct values. miRNAs that were common to both normal and PE states are highlighted in blue and red.

miRNA	Ct Control	Ct PE	St. Dev	Delta Ct	Fold Change	P-value
let-7e	22.08	23.54	2.09	1.45	-2.74	0.00190
miR-101	24.16	25.61	2.44	1.45	-2.73	0.00956
miR-543	26.26	27.12	1.35	0.86	-1.81	0.01566
miR-652	22.98	23.82	0.80	0.84	-1.79	0.00004
miR-191	21.37	22.12	0.77	0.75	-1.68	0.00004
miR-1307	22.71	23.34	1.33	0.63	-1.55	0.03141
miR-636	18.34	18.96	1.08	0.62	-1.54	0.01201
miR-182	25.14	25.73	0.97	0.60	-1.51	0.00639
miR-200c	23.29	23.88	0.99	0.59	-1.50	0.00734
miR-34b	17.89	18.42	0.83	0.53	-1.45	0.00673
miR-223	27.47	27.99	0.75	0.52	-1.43	0.00366
miR-142-5p	26.25	26.75	0.84	0.50	-1.41	0.00768
miR-149	26.54	26.90	0.51	0.37	-1.29	0.00194
miR-649	18.79	19.16	0.57	0.37	-1.29	0.00522
miR-106a	21.56	21.87	0.31	0.31	-1.24	0.00001
miR-362-3p	22.19	21.94	0.42	-0.25	1.19	0.00773
miR-29a	24.73	24.45	0.42	-0.28	1.21	0.00297
miR-301a	25.33	25.02	0.46	-0.31	1.24	0.00333
miR-515-3p	24.66	24.28	0.42	-0.38	1.30	0.00013
miR-768-5p	24.93	24.49	0.50	-0.43	1.35	0.00034
miR-1246	24.43	23.98	0.74	-0.45	1.37	0.00588
miR-363	24.54	24.08	0.71	-0.46	1.38	0.00356
miR-1283	23.42	22.94	0.53	-0.48	1.39	0.00009
miR-532-5p	26.58	26.07	0.89	-0.50	1.41	0.01204
miR-378	26.22	25.71	1.01	-0.51	1.42	0.02478
miR-140-3p	25.78	25.26	0.71	-0.52	1.43	0.00170
miR-342-3p	24.57	24.03	1.08	-0.54	1.45	0.02519
miR-494	21.42	20.86	0.48	-0.56	1.47	0.00000
miR-519a	26.08	25.51	0.68	-0.57	1.48	0.00043
miR-30e	23.34	22.75	0.89	-0.59	1.51	0.00285
miR-487a	22.01	21.41	0.59	-0.60	1.52	0.00001
miR-197	21.26	20.66	0.77	-0.60	1.52	0.00051
miR-766	18.14	17.52	1.06	-0.62	1.54	0.01813
miR-324-3p	17.98	17.36	1.01	-0.62	1.54	0.00924
miR-28-3p	28.17	27.51	1.03	-0.67	1.59	0.00400
miR-421	15.19	14.47	0.92	-0.71	1.64	0.00052
let-7a	27.70	26.95	1.13	-0.75	1.68	0.00286
miR-15b	18.36	17.56	0.69	-0.80	1.74	0.00000
miR-455-3p	19.38	18.53	0.86	-0.85	1.80	0.00003
miR-19a	28.06	27.09	0.94	-0.97	1.96	0.00001

Table 9. *Differential Serum miRNA Expression in Normal and PE-Complicated Pregnancies*

The listed miRNAs were differentially expressed in maternal serum between normal and PE-complicated pregnancies with the indicated delta Ct values and fold changes. Cells highlighted in blue and red indicate miRNAs that were upregulated and downregulated in PE, respectively.

Chapter 6: Conclusions and Future Directions

The work described in this dissertation significantly advances our understanding of maternal-fetal vascular interactions during pregnancy. Because human endovascular trophoblast invasion is challenging to model, the factors that regulate this process are enigmatic. Here, we used a combination of human and mouse models to answer fundamental questions about trophoblast biology during endovascular remodeling. Additionally, we explored the molecular changes that underlie pregnancies complicated by PE. Our findings open up new avenues of exploration that may help illuminate the causes of PE given that future studies on the molecules we identified may be able to address how and why trophoblast differentiation and endovascular invasion go awry in this syndrome.

A Role for Notch Signaling in Trophoblast Endovascular Invasion and in the Pathogenesis of Preeclampsia

In order to understand the arterial specificity of CTB endovascular invasion, we studied the expression and function of Notch family signaling molecules, known to play a role in arterial differentiation and function, during human placentation. Notch receptors and ligands were dramatically regulated during both human and mouse trophoblast differentiation/invasion, and Notch activity was observed during endovascular invasion, suggesting that Notch signaling played an important role during this process. Functional inhibition studies in human and mouse models revealed that Notch is required for trophoblast endovascular invasion likely through mechanisms that involve arterial mimicry. This study also identified disruptions in Jag1 expression during CTB

endovascular invasion in PE, further functional evidence that Notch signaling is a critical component of this process.

While this body of work highlights new developments in both the placental biology and Notch fields, this study raises many more questions that beg future investigation. One of the disadvantages of working with human model systems is that they have limited potential to address molecular function. In this regard, our exploration of Notch function during human endovascular CTB invasion was largely phenotypic and descriptive, rather than mechanistic. A major question that remains is how Notch influences trophoblast behavior at the molecular and cellular levels during this process. Our attempts to recreate the uterine vascular environment *in vitro* failed to model the conditions that enhance Notch activity *in vivo*. More specifically, we were unable to define culture conditions that produced CTB JAG1 expression and high levels of Notch activity as seen in endovascular CTBs. Consistent with this theory, experiments we undertook to inhibit Notch signaling during CTB cell culture produced few, if any, changes at the global gene expression level, suggesting that Notch was largely inactive in culture (data not shown). Chapter 2 reviewed several models that have been used successfully to recapitulate certain aspects of endovascular invasion. However, none of these were appropriate as models of Notch function, as many of them failed to replicate the terminal stages of trophoblast endovascular invasion with regard to Notch signaling.

Further exploration in the mouse system may be the best strategy to probe the molecular and cellular outcomes of Notch signaling during endovascular invasion. As to future experiments, approaches utilizing trophoblast stem (TS) cells derived from *Notch2*-deficient embryos may help identify the mechanisms by which *Notch2* loss resulted in spiral artery remodeling insufficiency. Based on the results presented in Chapter 3, several mechanisms are likely causes: failures in TGC and GlyTC

differentiation, proliferation, invasion, and/or artery-directed migration. All these possibilities can be addressed with TS cell culture assays and are obvious next steps. For instance, a quantitative lineage marker analysis could address whether TGCs and GlyTCs differentiate with lower frequency from *Notch2*-deficient TS cells as compared to wild-type TS cells. BrdU incorporation studies could answer whether *Notch2*-deficient TS cells proliferate at lower rates. Matrigel invasion assays could test the ability of trophoblasts derived from *Notch2*-deficient TS cells to invade through the extracellular matrix. Lastly, substrate choice assays (Red-Horse *et al.,* 2005) could help determine whether *Notch2*-deficient cells preferentially migrate away from EPHB4, which is expressed by CTB progenitors and venous endothelium, and toward EFRNB2, which is expressed in arteries. The outcomes of these experiments would focus future investigations at the molecular level.

In our studies of Notch activity and expression, we noted that Notch activity did not correlate with receptor/ligand co-localization. Specifically, despite observing co-expression of various Notch receptors and ligands in all regions of the placenta, Notch activity was limited to the endovascular compartment. Taken together, these results suggested that the presence or absence of specific factors in the arterial environment promoted Notch activity in that context. While we were unable to address this theory during the span of this work, future investigations would be particularly interesting. We have unpublished data that suggest that Notch signaling is actively inhibited in CTB progenitors. *Numb*, which promotes Notch receptor inactivation following productive receptor/ligand binding (McGill *et al.,* 2009), was highly expressed by CTB progenitors but not invasive cells (Figure 30). Similarly, *Mindbomb1*, which is indispensible for Notch signaling because it promotes the generation of functional ligands (Bray, 2006), was downregulated in villous CTB progenitors as compared to the chorion progenitors

from which they arise (Genbacev et al,. submitted). What role these molecules play during CTB differentiation/invasion remains to be determined, but given the enormous complexity of Notch regulation (Kopan and Ilagan, 2009), future investigation is merited.

As to the factors that upregulated JAG1 expression and Notch activity in endovascular CTBs, we theorized that physiological cues specific to the arterial environment were involved. Shear stress and cyclic strain, which are high in uterine spiral arterioles and low in uterine veins during pregnancy, are top candidates. In ECs, these forces rapidly enhance Notch receptor cleavage/activation, increase expression of Notch receptors and ligands (including *JAG1*), and promote Notch-dependent *EFRNB2* upregulation (Masumura *et al.,* 2009; Morrow *et al.,* 2007; Wang *et al.,* 2007). Interestingly, ligand endocytosis potentiates cleavage and activation of Notch receptors, leading several groups to propose that mechanical forces expose the S2 cleavage site within the Notch receptor (Kopan and Ilagan, 2009). Thus, it is possible that cyclic strain and shear stress experienced by CTBs near spiral arterioles may provide a mechanical force that potentiates Notch activation, JAG1 upregulation, and EFRNB2-dependent signaling. In this regard, our attempts to modulate CTB expression of Notch family members with shear stress were not successful. Likewise, we used a variety of other culture conditions to simulate the arterial environment, including EC, decidual cell, or explanted spiral arteriole co-culture as well as culture in different levels of oxygen tension or high serum concentrations. Thus, it is likely that a complex interplay among cell types and physiologic factors is required to initiate JAG1 upregulation and Notch activation. The development of more appropriate models to enable analysis of the terminal steps in CTB endovascular invasion would have particular relevance to understanding Notch regulation.

A surprising finding in our study of murine placental *Notch2* function was that disrupting blood flow to individual *Notch2*-deficient placentas had litter-wide effects on pregnancy outcome. In litters with equal numbers of mutant and heterozygote offspring, the frequency of fetal resorption correlated with the percentage of mutant animals in the litter and fetal loss was equally distributed among littermates regardless of genotype. As mice with *Notch2* haploinsufficiency are viable (Witt *et al.,* 2003), these results suggested that reducing blood flow to mutant offspring had negative effects on the survival of both heterozygote and mutant animals, although other factors may also have been responsible for the observed outcome. To our knowledge, similar phenotypes have not yet been reported. Therefore, this result presents an exciting opportunity to understand the vascular relationship between littermates of the same pregnancy, experiments that are discussed next.

One likely cause of the observed heterozygote lethality was disruption of systemic maternal vascular physiology by inadequate endovascular remodeling in mutant littermates. We established that *Notch2*-mutant placentas had decreased canal size and placental perfusion. Surgical reduction of placental perfusion in the rat as has been demonstrated in the reduced utero-placental perfusion (RUPP) model results in maternal hypertension and primes the vasculature to respond to vasoconstrictive factors (Anderson *et al.,* 2005; Crews *et al.,* 2000). Additionally, failed trophoblast invasion is associated with increased placental secretion of vasoconstrictive factors and decreased amounts of vasodilators (Goyal *et al.,* 2010). Taken together, these results could explain how local reductions in utero-placental blood flow, which are caused by failed trophoblast invasion, can produce systemic changes in vascular contractility that could produce litter-wide effects. To test this theory, it would be important to demonstrate that pregnancies with *Notch2*-deficient offspring were associated with maternal hypertension.

Direct blood pressure monitoring in mice is challenging to perform, but could offer the most direct evidence of this theory. Similarly, proteinurea, a common manifestation of PE, may also occur in these animals and be worth investigation. Secondarily, an assessment of classical vasoactive regulators in mice that are pregnant with different percentages of *Notch2*-mutant offspring would also be informative. Candidate vasoactive molecules would include renin-angiotensin family members, prostaglandin synthase, vasopressin, endothelin, and bradykinin among others. A survey of soluble factors associated with the pathogenesis of PE, such as sFLT, endoglin, and PLGF could also prove useful.

More broadly, investigators in fields outside of placental biology have noted several examples of vascular mimicry similar to what we have described here and in other studies we performed on endovascular CTB invasion (Zhou et al., 1997a, b). The first investigators to pioneer this concept outside of the placenta made the observation that melanoma cells frequently express molecules that are classically associated with endothelium and form vascular-like networks when cultured *ex vivo* in conditions that stimulate endothelial network formation (Maniotis *et al.,* 1999). Subsequently, vascular mimicry phenomena were reported in a variety of other tumor types (reviewed in Hess *et al.,* 2007) and, without direct evidence, were commonly attributed to the plasticity of tumor cells to acquire embryonic properties. Most recently, this theory was confirmed by a group who discovered that glioblastoma growth is supported by a population of glioblastoma stem-like cells that, in addition to maintaining the tumor cell population, transdifferentiates into functional ECs that contribute to the tumor vasculature (Ricci-Vittiani *et al.,* 2010). Our finding that Notch was a driver of endovascular invasion and arterial mimicry in trophoblast cells suggested that Notch may have analogous functions in other cases of vascular mimicry. While it may be outside the interests of our lab to

pursue this theory, it would be particularly interesting to study the possible roles of Notch signaling during tumor cell vascular mimicry.

CTB Gene Expression Profiling Reveals Unique Changes in Preeclampsia

In this work, we tested the theory that defects in trophoblast differentiation are fundamental properties of CTBs in PE and that such differences might account for the pathological outcomes of this syndrome. As to approach, we compared gene expression in differentiating CTBs derived from normal and PE placentas. The results identified differentially expressed genes that were previously known to be dysregulated in PE as well as newly associated factors. One of the most highly upregulated PE-associated genes was *SEMA3B*. The results of *in vitro* experiments performed by Dr. Yan Zhou demonstrated that SEMA3B treatment can account for the same alterations in CTB and EC phenotypes (increased apoptosis and decreased invasion/migration) that are commonly observed in PE. While these data are important in that they may explain how SEMA3B contributes to the pathology of PE, knowledge of the upstream regulatory mechanisms will provide additional insights.

Because we are most interested in upstream regulatory molecules that can account for the failures in trophoblast differentiation, our highest priority is to study HOP homeobox functions. In the mouse, *HOPX* deletion enhances the differentiation of invasive TGCs at the expense of the spongiotrophoblast population (Asanoma *et al.,* 2007). This finding adds great relevance to our discovery that *HOPX* is upregulated in preeclamptic CTB progenitors, which spawn fewer invasive progeny. Other studies that have identified *HOPX* as a tumor suppressor gene in choriocarcinoma, endometrial cancer, and lung cancer (Asanoma *et al.,* 2003; Yamaguchi *et al.,* 2009; Chen *et al.,*

2003) suggest that *HOPX* may contribute to the reduced invasive capacity of differentiated trophoblasts in PE or that *HOPX* may directly influence trophoblast differentiation.

In future experiments, we will use the following experimental design to test these theories. First, we want to confirm that this molecule is differentially expressed by CTBs in placentas from women who experience PE as compared to nPTL. If this is the case, we will overexpress HOPX and determine the consequences in terms of several phenotypes that are particularly relevant to PE. These include cell adhesion, invasion and production of vasculogenic/angiogenic substances. Because *HOPX* has important transcriptional regulation functions, we are also interested in determining the impact of increased expression on cell differentiation/behavior with the ultimate goal of understanding the root cause of PE. Finally, our data suggest that the subset of dysregulated genes, which encode secreted molecules, could be very interesting PE biomarkers. Further studies with a larger patient population will address the utility of measuring the concentration of these molecules in maternal blood.

The Design and Optimization of a Microfluidic Taqman Approach to Study miRNA Expression in Preeclampsia

The high-throughput PCR-based miRNA screening approach we developed will have great utility for groups who desire to profile sets of a several hundred miRNAs with the quantitative accuracy of Taqman. While current alternative methods are expensive and have large sample requirements, the methods we devised for the Biomark microfluidic platform are cost effective and require only nanograms of input cDNA. Having demonstrated the advantages of this protocol, our collaborators have

successfully used this approach to profile miRNA changes in the sera of prostate cancer patients, experiments that identified a disease-associated signature with clinical relevance (Moltzahn *et al.,* 2010).

We undertook a similar study to profile miRNA changes associated with pregnancies complicated by PE but did not uncover any significant changes in miRNA expression. Our goal was to identify clinically diagnostic biomarkers present in our patient population prior to the onset of PE at 20 weeks of gestation. It is possible that few miRNAs are differentially expressed at this early stage. However, given the important roles played by miRNAs in gene regulation and cellular function, a study of miRNA changes associated with the onset of PE would still be particularly relevant toward understanding the biology that underlies this syndrome. Because the placenta lies in direct contact with the maternal circulatory system, has a large surface area, and actively functions as a secretory organ, it is exciting to consider the possible roles that miRNAs might play in fetal-maternal communication. A variety of the maternal symptoms observed in PE are the result of systemic maternal endothelial dysfunction and molecules that are secreted by the placenta, including sFLT, Endoglin, and PEDF (Maynard *et al.,* 2003; Venkatesha *et al.,* 2006; Zhou *et al.,* 2011 submitted), are thought to play a role in this process. Recent studies have demonstrated that miRNAs can mediate paracrine cell-cell communication following their intercellular transport within membrane-bound microvesicles/exosomes (Thery *et al.,2009*). The placenta is an abundant source of exosomes (Mincheva-Nillson and Baranov *et al.,* 2010), but few studies have addressed the role of placental exosomal miRNA in PE. A basic characterization of miRNAs found in placenta-derived exosomes from women who experienced PE-complicated or normal pregnancies would be fascinating and our Taqman-based microfluidic platform is ideally suited for this experiment. Additional

experiments designed to test the effects of PE-derived placental exosomes on endothelial function would also be interesting. Toward that goal, we have most recently generated small RNA sequencing data for CTBs that were differentiated in culture, experiments that were run in parallel to those described in Chapter 4. These data may illuminate the molecular changes in CTB differentiation that occur as a result of PE as well as implicate candidate regulators of endothelial dysfunction in this pregnancy complication.

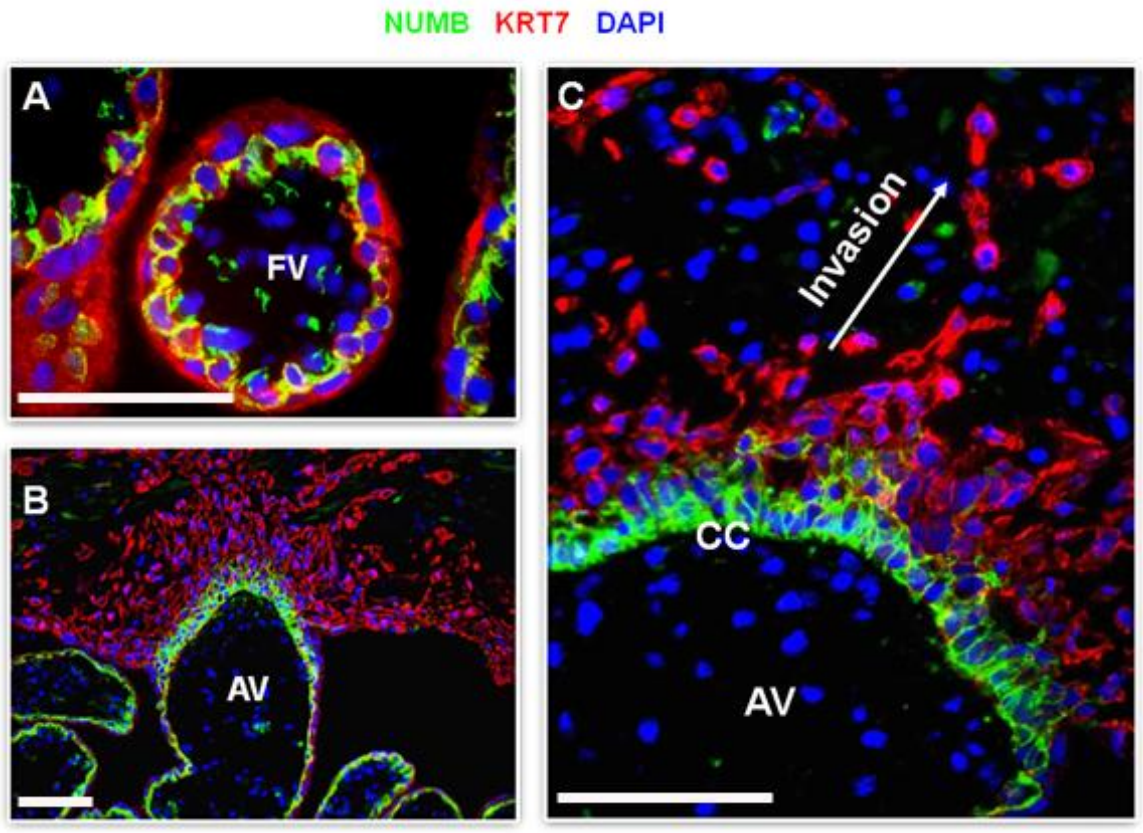

Figure 30. CTB *Progenitors Express Numb, which they Downregulated During Invasion.*

Double indirect immunofluorescence was performed on tissue sections of 2nd trimester basal plate biopsies using antibodies that specifically reacted with KRT7 (red), expressed exclusively by trophoblasts, and NUMB (green). Nuclei were visualized by staining with DAPI (blue). CTB progenitors in floating villi (FV) (A) and in anchoring villi (AV) (B-C) expressed NUMB. CTBs that had invaded the uterine wall (C) did not express NUMB. Scale bars: 100 microns.

Bibliography

Adamson, S.L., Lu, Y., Whiteley, K.J., Holmyard, D., Hemberger, M., Pfarrer, C., and Cross, J.C. (2002). Interactions between trophoblast cells and the maternal and fetal circulation in the mouse placenta. Dev Biol *250*, 358-373.

Aldo, P.B., Krikun, G., Visintin, I., Lockwood, C., Romero, R., and Mor, G. (2007). A novel three-dimensional in vitro system to study trophoblast-endothelium cell interactions. Am J Reprod Immunol *58*, 98-110.

Alva, J.A., and Iruela-Arispe, M.L. (2004). Notch signaling in vascular morphogenesis. Curr Opin Hematol *11*, 278-283.

Anderson, C.M., Lopez, F., Zhang, H.Y., Pavlish, K., and Benoit, J.N. (2005). Reduced uteroplacental perfusion alters uterine arcuate artery function in the pregnant Sprague-Dawley rat. Biol Reprod *72*, 762-766.

Asanoma, K., Kato, H., Yamaguchi, S., Shin, C.H., Liu, Z.P., Kato, K., Inoue, T., Miyanari, Y., Yoshikawa, K., Sonoda, K.*, et al.* (2007). HOP/NECC1, a novel regulator of mouse trophoblast differentiation. J Biol Chem *282*, 24065-24074.

Asanoma, K., Matsuda, T., Kondo, H., Kato, K., Kishino, T., Niikawa, N., Wake, N., and Kato, H. (2003). NECC1, a candidate choriocarcinoma suppressor gene that encodes a homeodomain consensus motif. Genomics *81*, 15-25.

Ashton, S.V., Whitley, G.S., Dash, P.R., Wareing, M., Crocker, I.P., Baker, P.N., and Cartwright, J.E. (2005). Uterine spiral artery remodeling involves endothelial apoptosis induced by extravillous trophoblasts through Fas/FasL interactions. Arterioscler Thromb Vasc Biol *25*, 102-108.

Avilion, A.A., Nicolis, S.K., Pevny, L.H., Perez, L., Vivian, N., and Lovell-Badge, R. (2003). Multipotent cell lineages in early mouse development depend on SOX2 function. Genes Dev *17*, 126-140.

Bartel, D.P. (2004). MicroRNAs: genomics, biogenesis, mechanism, and function. Cell *116*, 281-297.

Basyuk, E., Cross, J.C., Corbin, J., Nakayama, H., Hunter, P., Nait-Oumesmar, B., and Lazzarini, R.A. (1999). Murine Gcm1 gene is expressed in a subset of placental trophoblast cells. Dev Dyn *214*, 303-311.

Bazer, F.W., Wu, G., Spencer, T.E., Johnson, G.A., Burghardt, R.C., and Bayless, K. (2010). Novel pathways for implantation and establishment and maintenance of pregnancy in mammals. Mol Hum Reprod *16*, 135-152.

Benirschke, K., and Kaufmann, P. (1995). Pathology of the human placenta, 3rd edn (New York, Springer-Verlag).

Benson, G.V., Lim, H., Paria, B.C., Satokata, I., Dey, S.K., and Maas, R.L. (1996). Mechanisms of reduced fertility in Hoxa-10 mutant mice: uterine homeosis and loss of maternal Hoxa-10 expression. Development *122*, 2687-2696.

Berkowitz, R.S., and Goldstein, D.P. (1996). Chorionic tumors. N Engl J Med *335*, 1740-1748.

Bianchi, S., Dotti, M.T., and Federico, A. (2006). Physiology and pathology of notch signalling system. J Cell Physiol *207*, 300-308.

Blankenship, T.N., and Enders, A.C. (1997). Expression of platelet-endothelial cell adhesion molecule-1 (PECAM) by macaque trophoblast cells during invasion of the spiral arteries. Anat Rec *247*, 413-419.

Blankenship, T.N., and King, B.F. (1996). Macaque intra-arterial trophoblast and extravillous trophoblast of the cell columns and cytotrophoblastic shell express neural cell adhesion molecule (NCAM). Anat Rec *245*, 525-531.

Boyd, J.D., and Hamilton, W.J. (1970). The Human Placenta (Cambridge, Heffer).

Bray, S.J. (2006). Notch signalling: a simple pathway becomes complex. Nat Rev Mol Cell Biol *7*, 678-689.

Brosens, I.A., Robertson, W.B., and Dixon, H.G. (1972). The role of the spiral arteries in the pathogenesis of preeclampsia. Obstet Gynecol Annu *1*, 177-191.

Burton, G.J., Jauniaux, E., and Watson, A.L. (1999). Maternal arterial connections to the placental intervillous space during the first trimester of human pregnancy: the Boyd collection revisited. Am J Obstet Gynecol *181*, 718-724.

Carson, D.D., Julian, J., Lessey, B.A., Prakobphol, A., and Fisher, S.J. (2006). MUC1 is a scaffold for selectin ligands in the human uterus. Front Biosci *11*, 2903-2908.

Cartwright, J.E., Kenny, L.C., Dash, P.R., Crocker, I.P., Aplin, J.D., Baker, P.N., and Whitley, G.S. (2002). Trophoblast invasion of spiral arteries: a novel in vitro model. Placenta *23*, 232-235.

Castro-Rivera, E., Ran, S., Thorpe, P., and Minna, J.D. (2004). Semaphorin 3B (SEMA3B) induces apoptosis in lung and breast cancer, whereas VEGF165 antagonizes this effect. Proc Natl Acad Sci U S A *101*, 11432-11437.

Cetin, I., Huppertz, B., Burton, G., Cuckle, H., Gonen, R., Lapaire, O., Mandia, L., Nicolaides, K., Redman, C., Soothill, P.*, et al.* (2011). Pregenesys pre-eclampsia markers consensus meeting: What do we require from markers, risk assessment and model systems to tailor preventive strategies? Placenta *32 Suppl*, S4-16.

Chen, C.P., Chen, C.Y., Yang, Y.C., Su, T.H., and Chen, H. (2004). Decreased placental GCM1 (glial cells missing) gene expression in pre-eclampsia. Placenta *25*, 413-421.

Chen, H., Chedotal, A., He, Z., Goodman, C.S., and Tessier-Lavigne, M. (1997). Neuropilin-2, a novel member of the neuropilin family, is a high affinity receptor for the semaphorins Sema E and Sema IV but not Sema III. Neuron *19*, 547-559.

Chen, Q., Stone, P.R., McCowan, L.M., and Chamley, L.W. (2005). Interaction of Jar choriocarcinoma cells with endothelial cell monolayers. Placenta *26*, 617-625.

Chen, Q., Stone, P.R., McCowan, L.M., and Chamley, L.W. (2007). Activated endothelial cells resist displacement by trophoblast in vitro. Placenta *28*, 743-747.

Chen, Y., De Marco, M.A., Graziani, I., Gazdar, A.F., Strack, P.R., Miele, L., and Bocchetta, M. (2007). Oxygen concentration determines the biological effects of NOTCH-1 signaling in adenocarcinoma of the lung. Cancer Res *67*, 7954-7959.

Chen, Y., Petersen, S., Pacyna-Gengelbach, M., Pietas, A., and Petersen, I. (2003). Identification of a novel homeobox-containing gene, LAGY, which is downregulated in lung cancer. Oncology *64*, 450-458.

Cobellis, L., Mastrogiacomo, A., Federico, E., Schettino, M.T., De Falco, M., Manente, L., Coppola, G., Torella, M., Colacurci, N., and De Luca, A. (2007). Distribution of Notch protein members in normal and preeclampsia-complicated placentas. Cell Tissue Res *330*, 527-534.

Cooke, I.D. (1988). Failure of implantation and its relevance to subfertility. J Reprod Fertil Suppl *36*, 155-159.

Cormier, S., Vandormael-Pournin, S., Babinet, C., and Cohen-Tannoudji, M. (2004). Developmental expression of the Notch signaling pathway genes during mouse preimplantation development. Gene Expr Patterns *4*, 713-717.

Crews, J.K., Herrington, J.N., Granger, J.P., and Khalil, R.A. (2000). Decreased endothelium-dependent vascular relaxation during reduction of uterine perfusion pressure in pregnant rat. Hypertension *35*, 367-372.

Crocker, I.P., Wareing, M., Ferris, G.R., Jones, C.J., Cartwright, J.E., Baker, P.N., and Aplin, J.D. (2005). The effect of vascular origin, oxygen, and tumour necrosis factor alpha on trophoblast invasion of maternal arteries in vitro. J Pathol *206*, 476-485.

Cross, J.C., Flannery, M.L., Blanar, M.A., Steingrimsson, E., Jenkins, N.A., Copeland, N.G., Rutter, W.J., and Werb, Z. (1995). Hxt encodes a basic helix-loop-helix transcription factor that regulates trophoblast cell development. Development *121*, 2513-2523.

Cross, J.C., Werb, Z., and Fisher, S.J. (1994). Implantation and the placenta: key pieces of the development puzzle. Science *266*, 1508-1518.

Damsky, C.H., and Fisher, S.J. (1998). Trophoblast pseudo-vasculogenesis: faking it with endothelial adhesion receptors. Curr Opin Cell Biol *10*, 660-666.

Damsky, C.H., Fitzgerald, M.L., and Fisher, S.J. (1992). Distribution patterns of extracellular matrix components and adhesion receptors are intricately modulated during first trimester cytotrophoblast differentiation along the invasive pathway, in vivo. J Clin Invest *89*, 210-222.

Datta, S.R., Dudek, H., Tao, X., Masters, S., Fu, H., Gotoh, Y., and Greenberg, M.E. (1997). Akt phosphorylation of BAD couples survival signals to the cell-intrinsic death machinery. Cell *91*, 231-241.

Dayanir, V., Meyer, R.D., Lashkari, K., and Rahimi, N. (2001). Identification of tyrosine residues in vascular endothelial growth factor receptor-2/FLK-1 involved in activation of phosphatidylinositol 3-kinase and cell proliferation. J Biol Chem *276*, 17686-17692.

De Falco, M., Cobellis, L., Giraldi, D., Mastrogiacomo, A., Perna, A., Colacurci, N., Miele, L., and De Luca, A. (2007). Expression and distribution of notch protein members in human placenta throughout pregnancy. Placenta *28*, 118-126.

Domenga, V., Fardoux, P., Lacombe, P., Monet, M., Maciazek, J., Krebs, L.T., Klonjkowski, B., Berrou, E., Mericskay, M., Li, Z.*, et al.* (2004). Notch3 is required for arterial identity and maturation of vascular smooth muscle cells. Genes Dev *18*, 2730-2735.

Dotto, G.P. (2009). Crosstalk of Notch with p53 and p63 in cancer growth control. Nat Rev Cancer *9*, 587-595.

Duarte, A., Hirashima, M., Benedito, R., Trindade, A., Diniz, P., Bekman, E., Costa, L., Henrique, D., and Rossant, J. (2004). Dosage-sensitive requirement for mouse Dll4 in artery development. Genes Dev *18*, 2474-2478.

Ducibella, T., Ukena, T., Karnovsky, M., and Anderson, E. (1977). Changes in cell surface and cortical cytoplasmic organization during early embryogenesis in the preimplantation mouse embryo. J Cell Biol *74*, 153-167.

Duncan, A.W., Rattis, F.M., DiMascio, L.N., Congdon, K.L., Pazianos, G., Zhao, C., Yoon, K., Cook, J.M., Willert, K., Gaiano, N.*, et al.* (2005). Integration of Notch and Wnt signaling in hematopoietic stem cell maintenance. Nat Immunol *6*, 314-322.

Dunk, C., Petkovic, L., Baczyk, D., Rossant, J., Winterhager, E., and Lye, S. (2003). A novel in vitro model of trophoblast-mediated decidual blood vessel remodeling. Lab Invest *83*, 1821-1828.

Ellis, S.A., Palmer, M.S., and McMichael, A.J. (1990). Human trophoblast and the choriocarcinoma cell line BeWo express a truncated HLA Class I molecule. J Immunol *144*, 731-735.

Enders, A.C. (2000). Trophoblast-uterine interactions in the first days of implantation: models for the study of implantation events in the human. Semin Reprod Med *18*, 255-263.

Enders, A.C., and Blankenship, T.N. (1997). Modification of endometrial arteries during invasion by cytotrophoblast cells in the pregnant macaque. Acta Anat (Basel) *159*, 169-193.

Even-Ram, S., Uziely, B., Cohen, P., Grisaru-Granovsky, S., Maoz, M., Ginzburg, Y., Reich, R., Vlodavsky, I., and Bar-Shavit, R. (1998). Thrombin receptor overexpression in malignant and physiological invasion processes. Nat Med *4*, 909-914.

Favier, B., Alam, A., Barron, P., Bonnin, J., Laboudie, P., Fons, P., Mandron, M., Herault, J.P., Neufeld, G., Savi, P.*, et al.* (2006). Neuropilin-2 interacts with VEGFR-2 and VEGFR-3 and promotes human endothelial cell survival and migration. Blood *108*, 1243-1250.

Feinberg, R.F., Kao, L.C., Haimowitz, J.E., Queenan, J.T., Jr., Wun, T.C., Strauss, J.F., 3rd, and Kliman, H.J. (1989). Plasminogen activator inhibitor types 1 and 2 in human trophoblasts. PAI-1 is an immunocytochemical marker of invading trophoblasts. Laboratory investigation; a journal of technical methods and pathology *61*, 20-26.

Fisher, S.J., Cui, T.Y., Zhang, L., Hartman, L., Grahl, K., Zhang, G.Y., Tarpey, J., and Damsky, C.H. (1989). Adhesive and degradative properties of human placental cytotrophoblast cells in vitro. J Cell Biol *109*, 891-902.

Foltz, D.R., Santiago, M.C., Berechid, B.E., and Nye, J.S. (2002). Glycogen synthase kinase-3beta modulates notch signaling and stability. Curr Biol *12*, 1006-1011.

Fryer, C.J., White, J.B., and Jones, K.A. (2004). Mastermind recruits CycC:CDK8 to phosphorylate the Notch ICD and coordinate activation with turnover. Molecular cell *16*, 509-520.

Gallahan, D., and Callahan, R. (1987). Mammary tumorigenesis in feral mice: identification of a new int locus in mouse mammary tumor virus (Czech II)-induced mammary tumors. J Virol *61*, 66-74.

Gauster, M., Siwetz, M., and Huppertz, B. (2009). Fusion of Villous Trophoblast can be Visualized by Localizing Active Caspase 8. Placenta.

Genbacev, O., Zhou, Y., Ludlow, J.W., and Fisher, S.J. (1997). Regulation of human placental development by oxygen tension. Science *277*, 1669-1672.

Genbacev, O.D., Prakobphol, A., Foulk, R.A., Krtolica, A.R., Ilic, D., Singer, M.S., Yang, Z.Q., Kiessling, L.L., Rosen, S.D., and Fisher, S.J. (2003). Trophoblast L-selectin-mediated adhesion at the maternal-fetal interface. Science *299*, 405-408.

Gentleman, R.C., Carey, V.J., Bates, D.M., Bolstad, B., Dettling, M., Dudoit, S., Ellis, B., Gautier, L., Ge, Y., Gentry, J.*, et al.* (2004). Bioconductor: open software development for computational biology and bioinformatics. Genome Biol *5*, R80.

Gilbert, J.S., Ryan, M.J., LaMarca, B.B., Sedeek, M., Murphy, S.R., and Granger, J.P. (2008). Pathophysiology of hypertension during preeclampsia: linking placental ischemia with endothelial dysfunction. Am J Physiol Heart Circ Physiol *294*, H541-550.

Goldenberg, R.L., and Rouse, D.J. (1998). Prevention of premature birth. N Engl J Med *339*, 313-320.

Goyal, R., Yellon, S.M., Longo, L.D., and Mata-Greenwood, E. (2010). Placental gene expression in a rat 'model' of placental insufficiency. Placenta *31*, 568-575.

Granger, J.P., Alexander, B.T., Llinas, M.T., Bennett, W.A., and Khalil, R.A. (2002). Pathophysiology of preeclampsia: linking placental ischemia/hypoxia with microvascular dysfunction. Microcirculation *9*, 147-160.

Groten, T., Gebhard, N., Kreienberg, R., Schleussner, E., Reister, F., and Huppertz, B. (2010). Differential expression of VE-cadherin and VEGFR2 in placental syncytiotrophoblast during preeclampsia - New perspectives to explain the pathophysiology. Placenta.

Grummer, R., Donner, A., and Winterhager, E. (1999). Characteristic growth of human choriocarcinoma xenografts in nude mice. Placenta *20*, 547-553.

Gu, C., Rodriguez, E.R., Reimert, D.V., Shu, T., Fritzsch, B., Richards, L.J., Kolodkin, A.L., and Ginty, D.D. (2003). Neuropilin-1 conveys semaphorin and VEGF signaling during neural and cardiovascular development. Developmental cell *5*, 45-57.

Hamada, Y., Hiroe, T., Suzuki, Y., Oda, M., Tsujimoto, Y., Coleman, J.R., and Tanaka, S. (2007). Notch2 is required for formation of the placental circulatory system, but not for cell-type specification in the developing mouse placenta. Differentiation *75*, 268-278.

Hamada, Y., Kadokawa, Y., Okabe, M., Ikawa, M., Coleman, J.R., and Tsujimoto, Y. (1999). Mutation in ankyrin repeats of the mouse Notch2 gene induces early embryonic lethality. Development *126*, 3415-3424.

Harris, L.K., Keogh, R.J., Wareing, M., Baker, P.N., Cartwright, J.E., Aplin, J.D., and Whitley, G.S. (2006). Invasive trophoblasts stimulate vascular smooth muscle cell apoptosis by a fas ligand-dependent mechanism. Am J Pathol *169*, 1863-1874.

Hertig, A.T., and Rock, J. (1945). Two human ova of the pre-villous stage, having a developmental age of about seven and nine days respectively. Contrib Embryol *31*, 65-84.

Hertig, A.T., Rock, J., and Adams, E.C. (1956). A description of 34 human ova within the first 17 days of development. Am J Anat *98*, 435-493.

Hess, A.R., Margaryan, N.V., Seftor, E.A., and Hendrix, M.J. (2007). Deciphering the signaling events that promote melanoma tumor cell vasculogenic mimicry and their link to embryonic vasculogenesis: role of the Eph receptors. Dev Dyn *236*, 3283-3296.

Hrabe de Angelis, M., McIntyre, J., 2nd, and Gossler, A. (1997). Maintenance of somite borders in mice requires the Delta homologue DII1. Nature *386*, 717-721.

Hu, Q.D., Ang, B.T., Karsak, M., Hu, W.P., Cui, X.Y., Duka, T., Takeda, Y., Chia, W., Sankar, N., Ng, Y.K.*, et al.* (2003). F3/contactin acts as a functional ligand for Notch during oligodendrocyte maturation. Cell *115*, 163-175.

Huber, A.B., Kolodkin, A.L., Ginty, D.D., and Cloutier, J.F. (2003). Signaling at the growth cone: ligand-receptor complexes and the control of axon growth and guidance. Annu Rev Neurosci *26*, 509-563.

Hunkapiller, N.M., and Fisher, S.J. (2008). Chapter 12. Placental remodeling of the uterine vasculature. Methods Enzymol *445*, 281-302.

Ilekis, J.V., Reddy, U.M., and Roberts, J.M. (2007). Preeclampsia--a pressing problem: an executive summary of a National Institute of Child Health and Human Development workshop. Reprod Sci *14*, 508-523.

Iso, T., Maeno, T., Oike, Y., Yamazaki, M., Doi, H., Arai, M., and Kurabayashi, M. (2006). Dll4-selective Notch signaling induces ephrinB2 gene expression in endothelial cells. Biochemical and biophysical research communications *341*, 708-714.

Janatpour, M.J., Utset, M.F., Cross, J.C., Rossant, J., Dong, J., Israel, M.A., and Fisher, S.J. (1999). A repertoire of differentially expressed transcription factors that offers insight into mechanisms of human cytotrophoblast differentiation. Dev Genet *25*, 146-157.

Kandel, E.S., and Hay, N. (1999). The regulation and activities of the multifunctional serine/threonine kinase Akt/PKB. Exp Cell Res *253*, 210-229.

Keogh, R.J., Harris, L.K., Freeman, A., Baker, P.N., Aplin, J.D., Whitley, G.S., and Cartwright, J.E. (2007). Fetal-derived trophoblast use the apoptotic cytokine tumor necrosis factor-alpha-related apoptosis-inducing ligand to induce smooth muscle cell death. Circ Res *100*, 834-841.

Knoth, M., and Larsen, J.F. (1972). Ultrastructure of a human implantation site. Acta Obstet Gynecol Scand *51*, 385-393.

Kopan, R., and Ilagan, M.X. (2009). The canonical Notch signaling pathway: unfolding the activation mechanism. Cell *137*, 216-233.

Kovats, S., Main, E.K., Librach, C., Stubblebine, M., Fisher, S.J., and DeMars, R. (1990). A class I antigen, HLA-G, expressed in human trophoblasts. Science *248*, 220-223.

Krebs, L.T., Shutter, J.R., Tanigaki, K., Honjo, T., Stark, K.L., and Gridley, T. (2004). Haploinsufficient lethality and formation of arteriovenous malformations in Notch pathway mutants. Genes Dev *18*, 2469-2473.

Krebs, L.T., Xue, Y., Norton, C.R., Shutter, J.R., Maguire, M., Sundberg, J.P., Gallahan, D., Closson, V., Kitajewski, J., Callahan, R.*, et al.* (2000). Notch signaling is essential for vascular morphogenesis in mice. Genes Dev *14*, 1343-1352.

Krebs, L.T., Xue, Y., Norton, C.R., Sundberg, J.P., Beatus, P., Lendahl, U., Joutel, A., and Gridley, T. (2003). Characterization of Notch3-deficient mice: normal embryonic

development and absence of genetic interactions with a Notch1 mutation. Genesis *37*, 139-143.

Krikun, G., Mor, G., Alvero, A., Guller, S., Schatz, F., Sapi, E., Rahman, M., Caze, R., Qumsiyeh, M., and Lockwood, C.J. (2004). A novel immortalized human endometrial stromal cell line with normal progestational response. Endocrinology *145*, 2291-2296.

Lai, E.C. (2004). Notch signaling: control of cell communication and cell fate. Development *131*, 965-973.

Langbein, M., Strick, R., Strissel, P.L., Vogt, N., Parsch, H., Beckmann, M.W., and Schild, R.L. (2008). Impaired cytotrophoblast cell-cell fusion is associated with reduced Syncytin and increased apoptosis in patients with placental dysfunction. Mol Reprod Dev *75*, 175-183.

Langdon, T., Hayward, P., Brennan, K., Wirtz-Peitz, F., Sanders, P., Zecchini, V., Friday, A., Balayo, T., and Martinez Arias, A. (2006). Notch receptor encodes two structurally separable functions in Drosophila: a genetic analysis. Dev Dyn *235*, 998-1013.

Lawson, N.D., Scheer, N., Pham, V.N., Kim, C.H., Chitnis, A.B., Campos-Ortega, J.A., and Weinstein, B.M. (2001). Notch signaling is required for arterial-venous differentiation during embryonic vascular development. Development *128*, 3675-3683.

Lee, E.J., Baek, M., Gusev, Y., Brackett, D.J., Nuovo, G.J., and Schmittgen, T.D. (2008). Systematic evaluation of microRNA processing patterns in tissues, cell lines, and tumors. Rna *14*, 35-42.

Lescisin, K.R., Varmuza, S., and Rossant, J. (1988). Isolation and characterization of a novel trophoblast-specific cDNA in the mouse. Genes Dev *2*, 1639-1646.

Levine, R.J., Hauth, J.C., Curet, L.B., Sibai, B.M., Catalano, P.M., Morris, C.D., DerSimonian, R., Esterlitz, J.R., Raymond, E.G., Bild, D.E.*, et al.* (1997). Trial of calcium to prevent preeclampsia. N Engl J Med *337*, 69-76.

Li, M., Yee, D., Magnuson, T.R., Smithies, O., and Caron, K.M. (2006). Reduced maternal expression of adrenomedullin disrupts fertility, placentation, and fetal growth in mice. J Clin Invest *116*, 2653-2662.

Librach, C.L., Werb, Z., Fitzgerald, M.L., Chiu, K., Corwin, N.M., Esteves, R.A., Grobelny, D., Galardy, R., Damsky, C.H., and Fisher, S.J. (1991). 92-kD type IV collagenase mediates invasion of human cytotrophoblasts. J Cell Biol *113*, 437-449.

Liu, Z.J., Xiao, M., Balint, K., Smalley, K.S., Brafford, P., Qiu, R., Pinnix, C.C., Li, X., and Herlyn, M. (2006). Notch1 signaling promotes primary melanoma progression by activating mitogen-activated protein kinase/phosphatidylinositol 3-kinase-Akt pathways and up-regulating N-cadherin expression. Cancer Res *66*, 4182-4190.

Louvet, S., Aghion, J., Santa-Maria, A., Mangeat, P., and Maro, B. (1996). Ezrin becomes restricted to outer cells following asymmetrical division in the preimplantation mouse embryo. Dev Biol *177*, 568-579.

MacCalman, C.D., Furth, E.E., Omigbodun, A., Bronner, M., Coutifaris, C., and Strauss, J.F., 3rd (1996). Regulated expression of cadherin-11 in human epithelial cells: a role for cadherin-11 in trophoblast-endometrium interactions? Dev Dyn *206*, 201-211.

MacCalman, C.D., Getsios, S., and Chen, G.T. (1998). Type 2 cadherins in the human endometrium and placenta: their putative roles in human implantation and placentation. Am J Reprod Immunol *39*, 96-107.

Miao, H.Q., Soker, S., Feiner, L., Alonso, J.L., Raper, J.A., and Klagsbrun, M. (1999). Neuropilin-1 mediates collapsin-1/semaphorin III inhibition of endothelial cell motility: functional competition of collapsin-1 and vascular endothelial growth factor-165. The Journal of cell biology *146*, 233-242.

Maltepe, E., Bakardjiev, A.I., and Fisher, S.J. (2010). The placenta: transcriptional, epigenetic, and physiological integration during development. J Clin Invest *PMC Journal-In Process*.

Maltepe, E., Krampitz, G.W., Okazaki, K.M., Red-Horse, K., Mak, W., Simon, M.C., and Fisher, S.J. (2005). Hypoxia-inducible factor-dependent histone deacetylase activity determines stem cell fate in the placenta. Development *132*, 3393-3403.

Maniotis, A.J., Folberg, R., Hess, A., Seftor, E.A., Gardner, L.M., Pe'er, J., Trent, J.M., Meltzer, P.S., and Hendrix, M.J. (1999). Vascular channel formation by human melanoma cells in vivo and in vitro: vasculogenic mimicry. Am J Pathol *155*, 739-752.

Masumura, T., Yamamoto, K., Shimizu, N., Obi, S., and Ando, J. (2009). Shear stress increases expression of the arterial endothelial marker ephrinB2 in murine ES cells via the VEGF-Notch signaling pathways. Arterioscler Thromb Vasc Biol *29*, 2125-2131.

Matijevic, R., and Johnston, T. (1999). In vivo assessment of failed trophoblastic invasion of the spiral arteries in pre-eclampsia. Br J Obstet Gynaecol *106*, 78-82.

Mayhew, T.M. (2009). A stereological perspective on placental morphology in normal and complicated pregnancies. J Anat *215*, 77-90.

Maynard, S., Epstein, F.H., and Karumanchi, S.A. (2008). Preeclampsia and angiogenic imbalance. Annu Rev Med *59*, 61-78.

Maynard, S.E., Min, J.Y., Merchan, J., Lim, K.H., Li, J., Mondal, S., Libermann, T.A., Morgan, J.P., Sellke, F.W., Stillman, I.E.*, et al.* (2003). Excess placental soluble fms-like tyrosine kinase 1 (sFlt1) may contribute to endothelial dysfunction, hypertension, and proteinuria in preeclampsia. J Clin Invest *111*, 649-658.

McCright, B., Gao, X., Shen, L., Lozier, J., Lan, Y., Maguire, M., Herzlinger, D., Weinmaster, G., Jiang, R., and Gridley, T. (2001). Defects in development of the kidney, heart and eye vasculature in mice homozygous for a hypomorphic Notch2 mutation. Development *128*, 491-502.

McCright, B., Lozier, J., and Gridley, T. (2006). Generation of new Notch2 mutant alleles. Genesis *44*, 29-33.

McCune, J.M., Namikawa, R., Kaneshima, H., Shultz, L.D., Lieberman, M., and Weissman, I.L. (1988). The SCID-hu mouse: murine model for the analysis of human hematolymphoid differentiation and function. Science *241*, 1632-1639.

McGill, M.A., Dho, S.E., Weinmaster, G., and McGlade, C.J. (2009). Numb regulates post-endocytic trafficking and degradation of Notch1. J Biol Chem *284*, 26427-26438.

McMaster, M.T., Librach, C.L., Zhou, Y., Lim, K.H., Janatpour, M.J., DeMars, R., Kovats, S., Damsky, C., and Fisher, S.J. (1995). Human placental HLA-G expression is restricted to differentiated cytotrophoblasts. J Immunol *154*, 3771-3778.

Metcalfe, J., Romney, S.L., Ramsey, L.H., Reid, D.E., and Burwell, C.S. (1955). Estimation of uterine blood flow in normal human pregnancy at term. J Clin Invest *34*, 1632-1638.

Miele, L. (2006). Notch signaling. Clin Cancer Res *12*, 1074-1079.
Miller, R.K., Genbacev, O., Turner, M.A., Aplin, J.D., Caniggia, I., and Huppertz, B. (2005). Human placental explants in culture: approaches and assessments. Placenta *26*, 439-448.

Mincheva-Nilsson, L., and Baranov, V. (2010). The role of placental exosomes in reproduction. Am J Reprod Immunol *63*, 520-533.

Molinaro, T.A., and Barnhart, K.T. (2007). Ectopic pregnancies in unusual locations. Semin Reprod Med *25*, 123-130.

Moltzahn, F., Olshen, A.B., Baehner, L., Peek, A., Fong, L., Stoppler, H., Simko, J., Hilton, J.F., Carroll, P., and Blelloch, R. (2011). Microfluidic-based multiplex qRT-PCR identifies diagnostic and prognostic microRNA signatures in the sera of prostate cancer patients. Cancer Res *71*, 550-560.

Morrow, D., Cullen, J.P., Cahill, P.A., and Redmond, E.M. (2007). Cyclic strain regulates the Notch/CBF-1 signaling pathway in endothelial cells: role in angiogenic activity. Arterioscler Thromb Vasc Biol *27*, 1289-1296.

Mullendore, M.E., Koorstra, J.B., Li, Y.M., Offerhaus, G.J., Fan, X., Henderson, C.M., Matsui, W., Eberhart, C.G., Maitra, A., and Feldmann, G. (2009). Ligand-dependent Notch signaling is involved in tumor initiation and tumor maintenance in pancreatic cancer. Clin Cancer Res *15*, 2291-2301.

Naicker, T., Khedun, S.M., Moodley, J., and Pijnenborg, R. (2003). Quantitative analysis of trophoblast invasion in preeclampsia. Acta Obstet Gynecol Scand *82*, 722-729.

Nakayama, H., Liu, Y., Stifani, S., and Cross, J.C. (1997). Developmental restriction of Mash-2 expression in trophoblast correlates with potential activation of the notch-2 pathway. Dev Genet *21*, 21-30.

Niwa, H., Toyooka, Y., Shimosato, D., Strumpf, D., Takahashi, K., Yagi, R., and Rossant, J. (2005). Interaction between Oct3/4 and Cdx2 determines trophectoderm differentiation. Cell *123*, 917-929.

Oberg, C., Li, J., Pauley, A., Wolf, E., Gurney, M., and Lendahl, U. (2001). The Notch intracellular domain is ubiquitinated and negatively regulated by the mammalian Sel-10 homolog. J Biol Chem *276*, 35847-35853.

Odegard, R.A., Vatten, L.J., Nilsen, S.T., Salvesen, K.A., and Austgulen, R. (2000). Risk factors and clinical manifestations of pre-eclampsia. Bjog *107*, 1410-1416.

Passey, R.J., Williams, E., Lichanska, A.M., Wells, C., Hu, S., Geczy, C.L., Little, M.H., and Hume, D.A. (1999). A null mutation in the inflammation-associated S100 protein S100A8 causes early resorption of the mouse embryo. J Immunol *163*, 2209-2216.

Pauken, C.M., and Capco, D.G. (2000). The expression and stage-specific localization of protein kinase C isotypes during mouse preimplantation development. Dev Biol *223*, 411-421.

Pijnenborg, R., Vercruysse, L., and Hanssens, M. (2006). The Uterine Spiral Arteries In Human Pregnancy: Facts and Controversies. Placenta.

Plaks, V., Sapoznik, S., Berkovitz, E., Haffner-Krausz, R., Dekel, N., Harmelin, A., and Neeman, M. (2010). Functional Phenotyping of the Maternal Albumin Turnover in the Mouse Placenta by Dynamic Contrast-Enhanced MRI. Mol Imaging Biol.

Prakobphol, A., Genbacev, O., Gormley, M., Kapidzic, M., and Fisher, S.J. (2006). A role for the L-selectin adhesion system in mediating cytotrophoblast emigration from the placenta. Dev Biol *298*, 107-117.

Psychoyos, A. (1973). Hormonal control of ovoimplantation. Vitam Horm *31*, 201-256.

Qi, R., An, H., Yu, Y., Zhang, M., Liu, S., Xu, H., Guo, Z., Cheng, T., and Cao, X. (2003). Notch1 signaling inhibits growth of human hepatocellular carcinoma through induction of cell cycle arrest and apoptosis. Cancer Res *63*, 8323-8329.

Queenan, J.T., Jr., Kao, L.C., Arboleda, C.E., Ulloa-Aguirre, A., Golos, T.G., Cines, D.B., and Strauss, J.F., 3rd (1987). Regulation of urokinase-type plasminogen activator production by cultured human cytotrophoblasts. J Biol Chem *262*, 10903-10906.

Raab, G., Kover, K., Paria, B.C., Dey, S.K., Ezzell, R.M., and Klagsbrun, M. (1996). Mouse preimplantation blastocysts adhere to cells expressing the transmembrane form of heparin-binding EGF-like growth factor. Development *122*, 637-645.

Ramsey, E.M., Houston, M.L., and Harris, J.W. (1976). Interactions of the trophoblast and maternal tissues in three closely related primate species. Am J Obstet Gynecol *124*, 647-652.

Rebay, I., Fleming, R.J., Fehon, R.G., Cherbas, L., Cherbas, P., and Artavanis-Tsakonas, S. (1991). Specific EGF repeats of Notch mediate interactions with Delta and Serrate: implications for Notch as a multifunctional receptor. Cell *67*, 687-699.

Red-Horse, K., Kapidzic, M., Zhou, Y., Feng, K.T., Singh, H., and Fisher, S.J. (2005). EPHB4 regulates chemokine-evoked trophoblast responses: a mechanism for incorporating the human placenta into the maternal circulation. Development *132*, 4097-4106.

Red-Horse, K., Rivera, J., Schanz, A., Zhou, Y., Winn, V., Kapidzic, M., Maltepe, E., Okazaki, K., Kochman, R., Vo, K.C.*, et al.* (2006). Cytotrophoblast induction of arterial apoptosis and lymphangiogenesis in an in vivo model of human placentation. J Clin Invest *116*, 2643-2652.

Redman, C.W., and Sargent, I.L. (2005). Latest advances in understanding preeclampsia. Science *308*, 1592-1594.

Ricci-Vitiani, L., Pallini, R., Biffoni, M., Todaro, M., Invernici, G., Cenci, T., Maira, G., Parati, E.A., Stassi, G., Larocca, L.M.*, et al.* (2010). Tumour vascularization via endothelial differentiation of glioblastoma stem-like cells. Nature *468*, 824-828.

Roberts, J.M., and Lain, K.Y. (2002). Recent Insights into the pathogenesis of pre-eclampsia. Placenta *23*, 359-372.

Robertson, W.B., Brosens, I.A., and Dixon, H.G. (1973). Placental bed vessels. American journal of obstetrics and gynecology *117*, 294-295.

Roca, C., and Adams, R.H. (2007). Regulation of vascular morphogenesis by Notch signaling. Genes Dev *21*, 2511-2524.

Roth, I., Corry, D.B., Locksley, R.M., Abrams, J.S., Litton, M.J., and Fisher, S.J. (1996). Human placental cytotrophoblasts produce the immunosuppressive cytokine interleukin 10. J Exp Med *184*, 539-548.

Schlafke, S., and Enders, A.C. (1975). Cellular basis of interaction between trophoblast and uterus at implantation. Biol Reprod *12*, 41-65.

Schroeter, E.H., Kisslinger, J.A., and Kopan, R. (1998). Notch-1 signalling requires ligand-induced proteolytic release of intracellular domain. Nature *393*, 382-386.

Screen, M., Dean, W., Cross, J.C., and Hemberger, M. (2008). Cathepsin proteases have distinct roles in trophoblast function and vascular remodelling. Development *135*, 3311-3320.

Shao, L., and Haltiwanger, R.S. (2003). O-fucose modifications of epidermal growth factor-like repeats and thrombospondin type 1 repeats: unusual modifications in unusual places. Cellular and molecular life sciences : CMLS *60*, 241-250.

Shawber, C.J., Das, I., Francisco, E., and Kitajewski, J. (2003). Notch signaling in primary endothelial cells. Annals of the New York Academy of Sciences *995*, 162-170.

Shawber, C.J., and Kitajewski, J. (2004). Notch function in the vasculature: insights from zebrafish, mouse and man. Bioessays *26*, 225-234.

Shih Ie, M., and Kurman, R.J. (2002). Molecular basis of gestational trophoblastic diseases. Curr Mol Med *2*, 1-12.

Shih, I.M., and Kurman, R.J. (1996). Expression of melanoma cell adhesion molecule in intermediate trophoblast. Lab Invest *75*, 377-388.

Shraga-Heled, N., Kessler, O., Prahst, C., Kroll, J., Augustin, H., and Neufeld, G. (2007). Neuropilin-1 and neuropilin-2 enhance VEGF121 stimulated signal transduction by the VEGFR-2 receptor. Faseb J *21*, 915-926.

Sibai, B.M., Ewell, M., Levine, R.J., Klebanoff, M.A., Esterlitz, J., Catalano, P.M., Goldenberg, R.L., and Joffe, G. (1997). Risk factors associated with preeclampsia in healthy nulliparous women. The Calcium for Preeclampsia Prevention (CPEP) Study Group. Am J Obstet Gynecol *177*, 1003-1010.

Simmons, D.G., Fortier, A.L., and Cross, J.C. (2007). Diverse subtypes and developmental origins of trophoblast giant cells in the mouse placenta. Dev Biol *304*, 567-578.

Simmons, D.G., Natale, D.R., Begay, V., Hughes, M., Leutz, A., and Cross, J.C. (2008). Early patterning of the chorion leads to the trilaminar trophoblast cell structure in the placental labyrinth. Development *135*, 2083-2091.

Smith, L.J. (1985). Embryonic axis orientation in the mouse and its correlation with blastocyst relationships to the uterus. II. Relationships from 4 1/4 to 9 1/2 days. J Embryol Exp Morphol *89*, 15-35.

Soker, S., Takashima, S., Miao, H.Q., Neufeld, G., and Klagsbrun, M. (1998). Neuropilin-1 is expressed by endothelial and tumor cells as an isoform-specific receptor for vascular endothelial growth factor. Cell *92*, 735-745.

Starkey, P.M., Sargent, I.L., and Redman, C.W. (1988). Cell populations in human early pregnancy decidua: characterization and isolation of large granular lymphocytes by flow cytometry. Immunology *65*, 129-134.

Stewart, C.L., Kaspar, P., Brunet, L.J., Bhatt, H., Gadi, I., Kontgen, F., and Abbondanzo, S.J. (1992). Blastocyst implantation depends on maternal expression of leukaemia inhibitory factor. Nature *359*, 76-79.

Stoddart, C.A., Liegler, T.J., Mammano, F., Linquist-Stepps, V.D., Hayden, M.S., Deeks, S.G., Grant, R.M., Clavel, F., and McCune, J.M. (2001). Impaired replication of protease inhibitor-resistant HIV-1 in human thymus. Nat Med *7*, 712-718.

Strumpf, D., Mao, C.A., Yamanaka, Y., Ralston, A., Chawengsaksophak, K., Beck, F., and Rossant, J. (2005). Cdx2 is required for correct cell fate specification and differentiation of trophectoderm in the mouse blastocyst. Development *132*, 2093-2102.

Sutherland, A.E., Calarco, P.G., and Damsky, C.H. (1993). Developmental regulation of integrin expression at the time of implantation in the mouse embryo. Development *119*, 1175-1186.

Swift, M.R., and Weinstein, B.M. (2009). Arterial-venous specification during development. Circ Res *104*, 576-588.

Takahashi, T., Nakamura, F., Jin, Z., Kalb, R.G., and Strittmatter, S.M. (1998). Semaphorins A and E act as antagonists of neuropilin-1 and agonists of neuropilin-2 receptors. Nat Neurosci *1*, 487-493.

Tang, F., Hajkova, P., Barton, S.C., O'Carroll, D., Lee, C., Lao, K., and Surani, M.A. (2006). 220-plex microRNA expression profile of a single cell. Nat Protoc *1*, 1154-1159.

Thery, C., Ostrowski, M., and Segura, E. (2009). Membrane vesicles as conveyors of immune responses. Nat Rev Immunol *9*, 581-593.

Tomizawa, Y., Sekido, Y., Kondo, M., Gao, B., Yokota, J., Roche, J., Drabkin, H., Lerman, M.I., Gazdar, A.F., and Minna, J.D. (2001). Inhibition of lung cancer cell growth and induction of apoptosis after reexpression of 3p21.3 candidate tumor suppressor gene SEMA3B. Proc Natl Acad Sci U S A *98*, 13954-13959.

Uyttendaele, H., Ho, J., Rossant, J., and Kitajewski, J. (2001). Vascular patterning defects associated with expression of activated Notch4 in embryonic endothelium. Proc Natl Acad Sci U S A *98*, 5643-5648.

Varanou, A., Withington, S.L., Lakasing, L., Williamson, C., Burton, G.J., and Hemberger, M. (2006). The importance of cysteine cathepsin proteases for placental development. J Mol Med *84*, 305-317.

Venkatesha, S., Toporsian, M., Lam, C., Hanai, J., Mammoto, T., Kim, Y.M., Bdolah, Y., Lim, K.H., Yuan, H.T., Libermann, T.A*., et al.* (2006). Soluble endoglin contributes to the pathogenesis of preeclampsia. Nat Med *12*, 642-649.

Verlohren, S., Geusens, N., Morton, J., Verhaegen, I., Hering, L., Herse, F., Dudenhausen, J.W., Muller, D.N., Luft, F.C., Cartwright, J.E*., et al.* (2010). Inhibition of trophoblast-induced spiral artery remodeling reduces placental perfusion in rat pregnancy. Hypertension *56*, 304-310.

Vicovac, L., Jones, C.J., and Aplin, J.D. (1995). Trophoblast differentiation during formation of anchoring villi in a model of the early human placenta in vitro. Placenta *16*, 41-56.

Villa, N., Walker, L., Lindsell, C.E., Gasson, J., Iruela-Arispe, M.L., and Weinmaster, G. (2001). Vascular expression of Notch pathway receptors and ligands is restricted to arterial vessels. Mech Dev *108*, 161-164.

Vinot, S., Le, T., Ohno, S., Pawson, T., Maro, B., and Louvet-Vallee, S. (2005). Asymmetric distribution of PAR proteins in the mouse embryo begins at the 8-cell stage during compaction. Dev Biol *282*, 307-319.

Wang, C., Qi, R., Li, N., Wang, Z., An, H., Zhang, Q., Yu, Y., and Cao, X. (2009). Notch1 signaling sensitizes tumor necrosis factor-related apoptosis-inducing ligand-induced apoptosis in human hepatocellular carcinoma cells by inhibiting Akt/Hdm2-mediated p53 degradation and up-regulating p53-dependent DR5 expression. J Biol Chem *284*, 16183-16190.

Wang, H.U., Chen, Z.F., and Anderson, D.J. (1998). Molecular distinction and angiogenic interaction between embryonic arteries and veins revealed by ephrin-B2 and its receptor Eph-B4. Cell *93*, 741-753.

Wang, X.L., Fu, A., Raghavakaimal, S., and Lee, H.C. (2007). Proteomic analysis of vascular endothelial cells in response to laminar shear stress. Proteomics *7*, 588-596.

Wang, Z., Banerjee, S., Li, Y., Rahman, K.M., Zhang, Y., and Sarkar, F.H. (2006). Down-regulation of notch-1 inhibits invasion by inactivation of nuclear factor-kappaB, vascular endothelial growth factor, and matrix metalloproteinase-9 in pancreatic cancer cells. Cancer Res *66*, 2778-2784.

Wang, Z., Li, Y., Ahmad, A., Banerjee, S., Azmi, A.S., Kong, D., Wojewoda, C., Miele, L., and Sarkar, F.H. (2010). Down-regulation of Notch-1 is associated with Akt and FoxM1 in inducing cell growth inhibition and apoptosis in prostate cancer cells. J Cell Biochem.

Wang, Z., Li, Y., Banerjee, S., Kong, D., Ahmad, A., Nogueira, V., Hay, N., and Sarkar, F.H. (2010). Down-regulation of Notch-1 and Jagged-1 inhibits prostate cancer cell growth, migration and invasion, and induces apoptosis via inactivation of Akt, mTOR, and NF-kappaB signaling pathways. J Cell Biochem *109*, 726-736.

Weinmaster, G. (1998). Notch signaling: direct or what? Curr Opin Genet Dev *8*, 436-442.

Weng, A.P., Ferrando, A.A., Lee, W., Morris, J.P.t., Silverman, L.B., Sanchez-Irizarry, C., Blacklow, S.C., Look, A.T., and Aster, J.C. (2004). Activating mutations of NOTCH1 in human T cell acute lymphoblastic leukemia. Science *306*, 269-271.

Williams, C.K., Li, J.L., Murga, M., Harris, A.L., and Tosato, G. (2006). Up-regulation of the Notch ligand Delta-like 4 inhibits VEGF-induced endothelial cell function. Blood *107*, 931-939.

Wilson, C., Nikitenko, L.L., Sargent, I.L., and Rees, M.C. (2004). Adrenomedullin: multiple functions in human pregnancy. Angiogenesis *7*, 203-212.

Winn, V.D., Gormley, M., Paquet, A.C., Kjaer-Sorensen, K., Kramer, A., Rumer, K.K., Haimov-Kochman, R., Yeh, R.F., Overgaard, M.T., Varki, A.*, et al.* (2009). Severe preeclampsia-related changes in gene expression at the maternal-fetal interface include sialic acid-binding immunoglobulin-like lectin-6 and pappalysin-2. Endocrinology *150*, 452-462.

Winn, V.D., Haimov-Kochman, R., Paquet, A.C., Yang, Y.J., Madhusudhan, M.S., Gormley, M., Feng, K.T., Bernlohr, D.A., McDonagh, S., Pereira, L.*, et al.* (2007). Gene expression profiling of the human maternal-fetal interface reveals dramatic changes between midgestation and term. Endocrinology *148*, 1059-1079.

Winslow T. Appendix A: Early Development . In *Stem Cell Information* [World Wide Web site]. Bethesda, MD: National Institutes of Health, U.S. Department of Health and Human Services, 2009 [cited Friday, November 19, 2010]. Available at <http://stemcells.nih.gov/info/scireport/appendixa>

Witt, C.M., Won, W.J., Hurez, V., and Klug, C.A. (2003). Notch2 haploinsufficiency results in diminished B1 B cells and a severe reduction in marginal zone B cells. J Immunol *171*, 2783-2788.

Xiang, R.H., Hensel, C.H., Garcia, D.K., Carlson, H.C., Kok, K., Daly, M.C., Kerbacher, K., van den Berg, A., Veldhuis, P., Buys, C.H.*, et al.* (1996). Isolation of the human semaphorin III/F gene (SEMA3F) at chromosome 3p21, a region deleted in lung cancer. Genomics *32*, 39-48.

Xue, Y., Gao, X., Lindsell, C.E., Norton, C.R., Chang, B., Hicks, C., Gendron-Maguire, M., Rand, E.B., Weinmaster, G., and Gridley, T. (1999). Embryonic lethality and vascular defects in mice lacking the Notch ligand Jagged1. Hum Mol Genet *8*, 723-730.

Yamaguchi, S., Asanoma, K., Takao, T., Kato, K., and Wake, N. (2009). Homeobox gene HOPX is epigenetically silenced in human uterine endometrial cancer and suppresses estrogen-stimulated proliferation of cancer cells by inhibiting serum response factor. Int J Cancer *124*, 2577-2588.

Yin, L., Velazquez, O.C., and Liu, Z.J. (2010). Notch signaling: emerging molecular targets for cancer therapy. Biochem Pharmacol *80*, 690-701.

Zdravkovic, T., Genbacev, O., Prakobphol, A., Cvetkovic, M., Schanz, A., McMaster, M., and Fisher, S.J. (2006). Nicotine downregulates the l-selectin system that mediates cytotrophoblast emigration from cell columns and attachment to the uterine wall. Reprod Toxicol *22*, 69-76.

Zheng, Q., Qin, H., Zhang, H., Li, J., Hou, L., Wang, H., Zhang, X., Zhang, S., Feng, L., Liang, Y.*, et al.* (2007). Notch signaling inhibits growth of the human lung adenocarcinoma cell line A549. Oncol Rep *17*, 847-852.

Zhong, T.P., Childs, S., Leu, J.P., and Fishman, M.C. (2001). Gridlock signalling pathway fashions the first embryonic artery. Nature *414*, 216-220.

Zhou, Y., Bianco, K., Huang, L., Nien, J.K., McMaster, M., Romero, R., and Fisher, S.J. (2007). Comparative analysis of maternal-fetal interface in preeclampsia and preterm labor. Cell Tissue Res *329*, 559-569.

Zhou, Y., Damsky, C.H., Chiu, K., Roberts, J.M., and Fisher, S.J. (1993). Preeclampsia is associated with abnormal expression of adhesion molecules by invasive cytotrophoblasts. J Clin Invest *91*, 950-960.

Zhou, Y., Damsky, C.H., and Fisher, S.J. (1997). Preeclampsia is associated with failure of human cytotrophoblasts to mimic a vascular adhesion phenotype. One cause of defective endovascular invasion in this syndrome? J Clin Invest *99*, 2152-2164.

Zhou, Y., Fisher, S.J., Janatpour, M., Genbacev, O., Dejana, E., Wheelock, M., and Damsky, C.H. (1997). Human cytotrophoblasts adopt a vascular phenotype as they differentiate. A strategy for successful endovascular invasion? J Clin Invest *99*, 2139-2151.

Zhou, Y., Genbacev, O., and Fisher, S.J. (2003). The human placenta remodels the uterus by using a combination of molecules that govern vasculogenesis or leukocyte extravasation. Ann N Y Acad Sci *995*, 73-83.

Zhou, Y., McMaster, M., Woo, K., Janatpour, M., Perry, J., Karpanen, T., Alitalo, K., Damsky, C., and Fisher, S.J. (2002). Vascular endothelial growth factor ligands and receptors that regulate human cytotrophoblast survival are dysregulated in severe preeclampsia and hemolysis, elevated liver enzymes, and low platelets syndrome. Am J Pathol *160*, 1405-1423.

Publishing Agreement

It is the policy of the University to encourage the distribution of all theses, dissertations, and manuscripts. Copies of all UCSF theses, dissertations, and manuscripts will be routed to the library via the Graduate Division. The library will make all theses, dissertations, and manuscripts accessible to the public and will preserve these to the best of their abilities, in perpetuity.

I hereby grant permission to the Graduate Division of the University of California, San Francisco to release copies of my thesis, dissertation, or manuscript to the Campus Library to provide access and preservation, in whole or in part, in perpetuity.

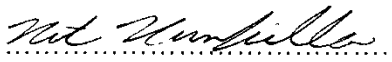

Author Signature

3/4/2011

Date